Advances in Chemical Physics, Volume XXXI
Edited by I. Prigogine, Stuart A. Rice

THEORY AND MOLECULAR MODELS FOR WATER

FRANK H. STILLINGER

Bell Laboratories, Murray Hill, New Jersey

CONTENTS

I. INTRODUCTION

A. Importance of Water

Throughout all the natural sciences, no single other substance approaches water in prominence and indispensibility. This fact obviously derives from the large amount of water present at the earth's surface as vapor, liquid, and solid. It has also meant that phenomena deemed worthy of scientific attention in chemistry, physics, geology, and meteorology have had a decidedly aqueous bias.

Informed opinion holds that life can only arise in, and be supported by, a suitable aqueous medium.[1] It is therefore fitting that high importance has been attached to the detection recently of water on Mars[2] and in galactic clouds.[3] Since it is likely that life exists at many scattered planetary sites throughout the known universe,[4] molecular biology may therefore have to enlarge its scope to literally cosmic proportions, without at the same time foregoing its fundamentally aqueous character.

In view of these matters, it is quite natural to lavish particular attention on water in the form of quantitative theories designed primarily to describe this substance alone. With the possible exception of liquid helium, no other substance deserves such concentrated scrutiny. Thus water historically has elicited frequent, wide-ranging, imaginative, and often mutually contradictory models or theories.[5] Viewing these works in detail and in chronological sequence may eventually provide historians of science with valuable insights into the social dynamics of scientific research.

Only within the last few years (since 1960, roughly) has it become technically feasible to produce quantitative and deductive theory for water without large elements of uncertainty. This period coincides with the general availability of rapid digital computers to the scientific community. These computers have provided essential numerical advances in both the quantum mechanical and statistical mechanical aspects of the fields that underlie present understanding. This should not be interpreted to mean that the future of water theory will remain heavily computational, rather than analytical, but the present era seems to be a natural evolutionary stage of development of the subject with no reasonable alternative.

The scope of this article is neither historical nor comprehensive. The goal instead encompasses a small set of approaches to the subject, each member

of which bears a clearly definable relation to the fundamental principles of statistical mechanics. It is our belief that extensions of these approaches hold the greatest promise for future progress, and considerable attention has been devoted to the ways in which that progress can be realized.

B. Characteristic Properties of Water

Water displays a striking set of physical properties, some apparently unique, which serve to define its unusual "personality." Their existence adds extra zest to the task of developing a viable theory of water, which ultimately is charged with connecting these properties to molecular structure and interactions. We now list a few of the more important attributes.

1. Contraction on melting. At 1 atm pressure, the molar volume decreases from 19.66 cm^3 for ice at 0°C, to 18.0182 cm^3 for liquid water at the same temperature, a loss of 8.3%. This property is relatively rare among all substances but, even considering just the elements, it is shared by germanium and bismuth.

2. Density maximum in the liquid. Subsequent to melting, the liquid at atmospheric pressure continues to contract on further heating until a density maximum is achieved at 3.98°C. The molar volume change for the liquid over this narrow temperature interval is only 0.013%.

No other liquid is known with a corresponding density maximum above its normal melting point. However, fused silica (SiO_2) can be supercooled below its melting point (1610°C) so as to pass through a density maximum.[6]

By increasing the external pressure, the temperature of maximum water density shifts downward, reaching 0°C at 190 bars.

Isotopic substitution exerts significant effects on the temperature of maximum density. For D_2O (m.p. 3.81°C), the maximum occurs at 11.19°C, while for T_2O (m.p. 4.48°C) it occurs at 13.40°C.

3. Numerous ice polmorphs.[7] Hexagonal ice Ih is the familiar form that results from freezing the liquid at atmospheric pressure. Cubic ice Ic is a closely related modification, with virtually the same density, which forms by vapor-phase condensation at very low temperatures. Under elevated pressure, a series of dense ice polymorphs designated ices II, III, V, VI, VII, VIII, and IX has been observed. In addition, Bridgeman has reported ice IV with D_2O, although this has not been subsequently confirmed and may correspond to a special metastable structure.

None of the thermodynamically stable ice polymorphs displays a close-packed arrangement of molecules. It seems likely therefore that further ice polymorphs are yet to be discovered under extremely high pressures (i.e., the megabar range).

The multiplicity of ice crystal structures alone suggests that water molecule interactions must be rather complicated. It is inconceivable that spherical

molecules interacting, say, through the Lennard-Jones 12-6 potential could exhibit anywhere near as many crystal structures.

4. High melting, boiling, and critical temperatures. In contrast with other molecular substances having comparable molecular weight (nitrogen, carbon dioxide, methane, ammonia, hydrogen fluoride, hydrogen cyanide, etc.), these characteristic temperatures are anomalously high. Relatively speaking, water must consequently be a strongly binding many-body system.

5. Compressibility minimum. Normally, liquids become more isothermally compressible as the temperature rises. However, under atmospheric pressure, the isothermal compressibility for water declines with increasing temperature from the melting point to 46°C. This phenomenon disappears at high pressure (above 3 kbars).

6. Large dielectric constant. This results from a complex combination of mutual polarization between neighboring molecules in an external field and their tendency mutually to align their permanent moments. In attempting to understand the nature of water as a dielectric medium (particularly as a solvent for electrolytes), it is valuable to remember that other liquids can have similarly high dielectric constants but very different chemical structure. Some examples are formamide, ethylene carbonate, and *N*-methylacetamide.[8]

7. Negative pressure coefficient of viscosity. Among all liquids for which the relevant measurements are available, water is exceptional. Below 30°C the initial effect of compression is to increase fluidity. Clearly related is the observation that electrolyte conductances increase with pressure in water, unlike the behavior in other solvents.[9]

8. High molar heat capacity.

9. Negative entropies of transfer for many hydrocarbons from nonpolar solvents into water.[10]

10. Curved Arrhenius plots for kinetic properties. For viscosity, dielectric relaxation time, and the self-diffusion constant, all in the liquid, the respective energies of activation increase as temperature declines. The effect is particularly noticeable when results for supercooled water are included in the Arrhenius plots.

C. Suitable Goals for the Theory

Three rather distinct objectives can be posed for the development of a satisfactory theory of water. They are:

a. Reproduce as faithfully as possible all available experiments.

b. Predict novel phenomena, and results of measurements within uncharted territories, to motivate future experimentation.

c. Generate results that aid human comprehension (of water), but which are attainable through no conceivable laboratory experiment.

Owing to the striking nature of the characteristic properties of water listed in Section B, objective *a* becomes indeed pressing. Certainly a theory of water that fails ultimately to reproduce most of those properties qualitatively must be branded a pragmatic failure. However, to insist at this present early stage of the subject that the sole legitimate end of theory lies in numerical precision must surely be an unbalanced view.

Category *b* includes properties under extreme conditions of temperature and pressure, or behavior induced by extremely high electric fields. Theory can aid in sifting out expensive and arduous hypothetical experiments with little chance of adding fundamental knowledge, from those with high promise.

In the long run item *c* is probably the most significant of the three objectives. It is possible in principle to calculate quantities such as face distributions and volume distributions for Voronoi (nearest-neighbor) polyhedra, curvatures and torsions for diffusive paths, three-molecule distribution functions, and the statistical topology of random hydrogen bond networks. Precise data of these kinds have inestimable value in constructing a vivid picture of what water is like at the molecular level. Without a structurally and kinetically detailed description, one can hardly claim to understand water. Yet it is obvious that experiments alone, however precise, will not suffice to bring this elaborate picture into sharp focus. Theory must move to provide that clarification.

Subsequent sections in this exposition reflect our conviction about the absolute importance of developing theory along proper deductive lines. One is first obliged to obtain a well-defined Hamiltonian for the water system, at some level of molecular detail; then one must proceed to apply known principles of statistical mechanics to predict the consequent ensemble behavior. To this end we begin with a description of individual water molecules, pass on to study of their molecular interactions, and then analyze several recent statistical mechanical formalisms based on the knowledge of those interactions.

II. PROPERTIES OF THE WATER MOLECULE

A. Equilibrium Structure

The lowest vertical electronic excitation for the isolated water molecule lies quite high, at 7.49 eV. Consequently, it suffices for the purposes of the present exposition to consider only the ground electronic state.

The ground state is nonlinear, with C_{2v} symmetry. The three nuclei therefore inhabit the vertices of an isosceles triangle, with the apex angle at the oxygen equal to 104.48° and OH bond lengths equal to 0.9576 Å.[11] The center of mass of the molecule is displaced from the oxygen along the bisector

of the HOH apex angle. In the event that the oxygen nucleus is ^{16}O, these displacement distances have the values:

$$\begin{array}{ll} H_2O & 0.06563\ \text{Å} \\ D_2O & 0.1179\ \text{Å} \\ T_2O & 0.1603\ \text{Å} \end{array} \tag{2.1}$$

An important feature of the subsequent theoretical development hinges on the fact that the internal bond angle in the isolated water molecule is only slightly smaller than the ideal tetrahedral angle θ_t:

$$\theta_t = \cos^{-1}(-\tfrac{1}{3}) = 109.4712^\circ \tag{2.2}$$

This is the angle subtended by two vertices of a regular tetrahedron at that tetrahedron's center. Equivalently, it is the angle of intersection between any two principal diagonals of a cube. The relevance of θ_t for structural chemistry of course arises from sp^3 hybridization of atomic orbitals for elements in the first row of the periodic system.[12]

The Hellmann–Feynman theorem[13] requires that the total electrostatic force on each nucleus, due both to other nuclei and to electron distribution, vanish identically. This places an important condition on the electron distribution in the molecule. This distribution cannot be a linear superposition of spherically symmetric components for the three atoms, while maintaining a mechanically stable nonlinear triatomic configuration. Instead, the charge distribution must build up along the OH bonds and within the interior of the isosceles triangle.[14]

B. Electical Properties

The measured value for the water molecule dipole moment is[15]

$$\mu = 1.855 \times 10^{-18}\ \text{esu cm} \tag{2.3}$$

Symmetry requires that the vector moment point along the HOH angle bisector; the oxygen end of the molecule is negative and the hydrogen end is positive. Given μ and the nuclear geometry, it is a trivial exercise to compute the position of the centroid of the electronic charge distribution (total charge $-10e$). This position lies along the symmetry axis 0.07866 Å from the oxygen nucleus. The result should be compared to the corresponding distance 0.1173 Å that would have been implied by a linear superposition of atomic densities and consequently zero net dipole moment for the molecule.

The traceless electrical quadrupole tensor is conventionally defined to have the elements:

$$\Theta_{ij} = \tfrac{1}{2}\int (3x_i x_j - r^2)\rho_e(\mathbf{r})\, d\mathbf{r} \tag{2.4}$$

wherein $\rho_e(\mathbf{r})$ represents the molecular charge density, including both electronic and nuclear contributions. In the case of water, $\boldsymbol{\Theta}$ is diagonal in a Cartesian coordinate system whose axes x_1, x_2, and x_3 are respectively parallel to the symmetry axis (and along the angle bisector), in the molecular plane but perpendicular to the symmetry axis, and perpendicular to the symmetry plane. Figure 1 illustrates this coordinate system.

Since water possesses a permanent dipole moment, the elements of $\boldsymbol{\Theta}$ depend on the origin chosen for the diagonalizing coordinate system. Suppose these tensor elements are known in one coordinate system, with values denoted by $\Theta_{ij}^{(0)}$. If an alternative parallel system with origin at x_1', x_2', x_3' is of interest, the transformed tensor elements become:

$$\begin{aligned}\Theta_{ij} &= \tfrac{1}{2}\int [3(x_i - x_i')(x_j - x_j') - r^2(x_1', x_2', x_3')]\rho_e(\mathbf{r})\, d\mathbf{r} \\ &= \Theta_{ij}^{(0)} + \mu_1 x_1' + \mu_2 x_2' + \mu_3 x_3' - \tfrac{3}{2}(\mu_i x_j' + \mu_j x_i')\end{aligned} \tag{2.5}$$

In particular $\Theta_{ij}^{(0)}$ might represent values relative to the oxygen nucleus; then, if the origin is moved forward along the x_1 direction by distance l (shown in Fig. 1), we have

$$\begin{aligned}\Theta_{11}(l) &= \Theta_{11}^{(0)} - 2\mu l \\ \Theta_{22}(l) &= \Theta_{22}^{(0)} + \mu l \\ \Theta_{33}(l) &= \Theta_{33}^{(0)} + \mu l\end{aligned} \tag{2.6}$$

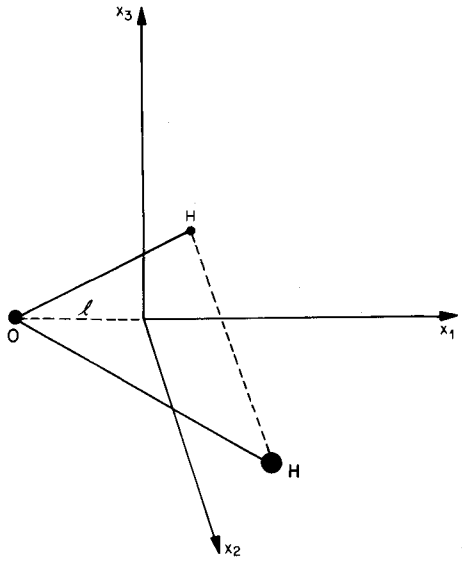

Fig. 1 Cartesian coordinate system for which the electric quadrupole tensor $\boldsymbol{\theta}$ is diagonal. The molecule lies in the x_1x_2 plane.

The most accurate source of quadrupole moments is molecular beam Zeeman spectroscopy. The moments thus determined refer to an origin at the molecular center of mass. A recent application of the method for D_2O has been carried out by Verhoeven and Dymanus,[16] who conclude

$$\begin{aligned}\Theta_{11}(0.1179) &= -0.321 \times 10^{-26} \text{ esu cm}^2 \\ \Theta_{22}(0.1179) &= \ \ 2.724 \times 10^{-26} \text{ esu cm}^2 \\ \Theta_{33}(0.1179) &= -2.402 \times 10^{-26} \text{ esu cm}^2\end{aligned} \tag{2.7}$$

Equation (2.6) permits us to transfer these to the oxygen origin:

$$\begin{aligned}\Theta_{11}(0) &= \Theta_{11}^{(0)} = 0.116 \times 10^{-26} \text{ esu cm}^2 \\ \Theta_{22}(0) &= \Theta_{22}^{(0)} = 2.505 \times 10^{-26} \text{ esu cm}^2 \\ \Theta_{33}(0) &= \Theta_{33}^{(0)} = -2.621 \times 10^{-26} \text{ esu cm}^2\end{aligned} \tag{2.8}$$

Note that the axial quadrupole moment $\Theta_{11}(l)$ has changed sign as a result of this origin shift, passing through zero when

$$l = 0.0313 \text{ Å} \tag{2.9}$$

The water molecule can respond to electric fields at optical frequencies only by polarizing its electron distribution. The resulting linear response may be expressed as a polarizability tensor $\boldsymbol{\alpha}$ which is also diagonal in the coordinate system illustrated in Fig. 1. Separate components of $\boldsymbol{\alpha}$ have not been experimentally established for water, but the mean polarizability $\bar{\alpha}$ can be determined from the Lorenz–Lorentz equation for the refractive index. By this means Moelwyn-Hughes[17] concludes:

$$\begin{aligned}\bar{\alpha} &= \tfrac{1}{3}(\alpha_{11} + \alpha_{22} + \alpha_{33}) \\ &= 1.444 \times 10^{-24} \text{ cm}^3\end{aligned} \tag{2.10}$$

On the basis of accurate Hartree–Fock calculations, Liebmann and Moskowitz[18] find that $\boldsymbol{\alpha}$ manifests modest anisotropy. These investigators report:

$$\begin{aligned}\alpha_{11} &= 1.452 \times 10^{-24} \text{ cm}^3 \\ \alpha_{22} &= 1.651 \times 10^{-24} \text{ cm}^3 \\ \alpha_{33} &= 1.226 \times 10^{-24} \text{ cm}^3\end{aligned} \tag{2.11}$$

The agreement between the mean of these values, 1.443×10^{24} cm^3, and result (2.10) is certainly very good and perhaps somewhat fortuitous. It will be interesting ultimately to see how (2.11) compares with predictions from a more elaborate calculation which carefully accounts for electron correlation.

The dipole moment (2.3) is larger than the critical moment:

$$\mu_c = 1.63 \times 10^{-18} \text{ esu cm} \tag{2.12}$$

above which a molecule automatically binds an extra electron.[19] Thus a stable anion H_2O^- in principle must exist, although doubtless with small ionization potential and a very extended electron cloud. However, there is at present no experimental evidence for this species.

C. Normal Modes of Vibration

Figure 2 illustrates the directions of nuclear motion in each of the three normal modes. Two of the modes preserve the molecular C_{2v} symmetry, and since they act primarily to change bond angle and bond length, the names symmetric bend and symmetric stretch are appropriate.

The third normal mode rigorously involves hydrogen motions along the OH bond directions, but out of phase. Whereas the oxygen moves parallel to the x_1 axis in the two symmetric modes (see Fig. 1), it moves parallel to the x_2 axis in the asymmetric mode.

An increase in hydrogen isotope mass causes a decrease in all three vibrational frequencies. The nine specific frequencies for H_2O, D_2O, and T_2O are shown in Fig. 2 as well, all referring to ^{16}O. Incomplete isotopic

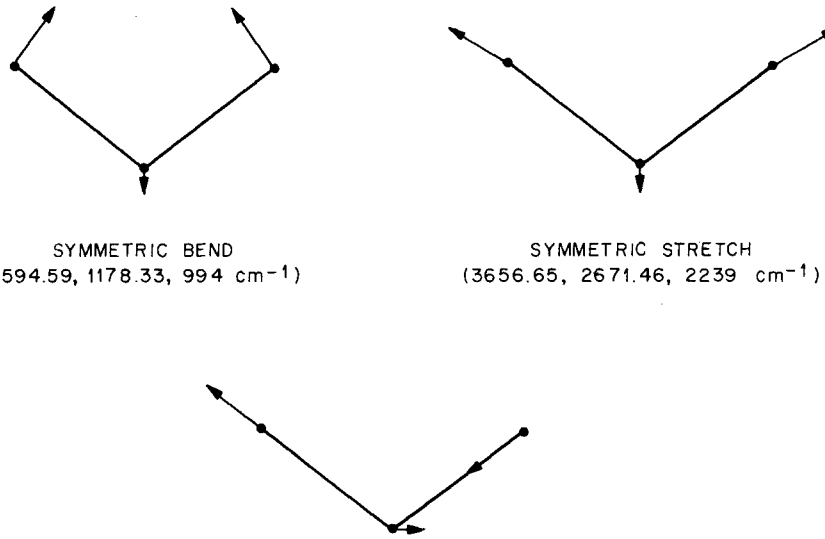

Fig. 2 Directions of nuclear motion for vibrational normal modes. The respective frequencies for H_2O, D_2O, and T_2O (with ^{16}O) are shown in parentheses.

substitution, to form HDO for instance, destroys the symmetry character of each of the modes.

The intramolecular potential energy surface (in the Born–Oppenheimer approximation) that gives rise to the vibrations can be expressed as a function of the changes in bond angle ($\Delta\theta$) and bond lengths (Δr_1 and Δr_2). In the vicinity of the mechanical equilibrium point ($\Delta\theta$, Δr_1, Δr_2 all zero), this potential energy U may be developed as a multiple Taylor series in the displacements:

$$\begin{aligned} U(\Delta r_1, \Delta r_2, \Delta\theta) = U(0,0,0) &+ \tfrac{1}{2}K_r[(\Delta r_1)^2 + (\Delta r_2)^2] \\ &+ \tfrac{1}{2}K_\theta(r_e\Delta\theta)^2 + K_r'\Delta r_1\Delta r_2 \\ &+ K_{r\theta}(r_e\Delta\theta)(\Delta r_1 + \Delta r_2) + \cdots \end{aligned} \tag{2.13}$$

where we have used r_e to denote the equilibrium bond length (0.9576 Å). The four harmonic force constants have the values:[20]

$$\begin{aligned} K_r &= 8.454 \\ K_\theta &= 0.761 \\ K_r' &= -0.101 \\ K_{r\theta} &= 0.228 \end{aligned} \tag{2.14}$$

all in units 10^5 dynes/cm, under the proviso that $\Delta\theta$ is measured in radians. These numbers demonstrate that, by more than an order of magnitude, water molecules more strongly resist bond length changes than they do angular deformation.

Owing to the small mass of the hydrogen isotopes, the quantum mechanical zero point motion is relatively large. The rms amplitudes for H_2O and D_2O are found to be[21]

$$\begin{aligned} H_2O: \quad & \langle(\Delta r_1)^2\rangle^{1/2} = \langle(\Delta r_2)^2\rangle^{1/2} = 0.0677 \text{ Å} \\ & \langle(\Delta\theta)^2\rangle^{1/2} = 8.72^\circ \\ D_2O: \quad & \langle(\Delta r_1)^2\rangle^{1/2} = \langle(\Delta r_2)^2\rangle^{1/2} = 0.0578 \text{ Å} \\ & \langle(\Delta\theta)^2\rangle^{1/2} = 7.49^\circ \end{aligned} \tag{2.15}$$

Anharmonic terms in the Taylor expansion (2.13) for U therefore need explicitly to be taken into account in precise calculations involving vibrations.

At 25°C thermal energy $k_B T$ is the equivalent of 207 cm^{-1} in spectroscopic usage. Thus reference to frequencies in Fig. 2 shows that water molecule vibrations remain virtually always in their ground states in the ordinary temperature range. By contrast, the free-molecule rotational level spacings

are on the order of 20 cm^{-1} for H_2O and 10 cm^{-1} for D_2O, hence free rotations are close to the classical limit at room temperature.

In the asymmetric stretch mode, the molecular dipole moment magnitude should remain constant, although it rocks back and forth with the nuclear motion. If the total molecular moment comprises roughly two vector components directed along the OH bonds, the symmetric bend motion will modulate μ, increasing it when the bond angle decreases. Symmetrically stretching the bonds similarly should increase μ. Unfortunately, the magnitudes of these moment modulations are not known, and would be fitting objects for future careful quantum mechanical study.

Formally, an arbitrarily distorted water molecule can be identified uniquely with a fixed and properly oriented molecule without distortion. The centers of mass and the molecular planes of the two will be coincident. The remanent three-dimensional configuration space is spanned by the three normal mode amplitudes; that is, these amplitudes provide an orthogonal system of coordinates within the distortion subspace.

III. WATER–MOLECULE INTERACTIONS

A. Potential–Energy Resolution

We now turn our attention to a collection of N water molecules arranged arbitrarily in space. For each a set of nine configurational coordinates is required to locate the precise positions of its three nuclei. These nine coordinates for any molecule i ($1 \leq i \leq N$) are simply denoted by $\mathbf{X}_i$.

If the N molecules are sufficiently well separated from one another to be properly regarded as isolated, the potential energy V_N will consist of a sum of single-molecule energies $V^{(1)}$:

$$V_N(\mathbf{X}_1 \cdots \mathbf{X}_N) \to \sum_{i=1}^{N} V^{(1)}(\mathbf{X}_i) \tag{3.1}$$

Except for a possible difference in choice of zero for energy dictated by convenience, $V^{(1)}$ is essentially the potential energy surface function U discussed above [see (2.13)] in connection with vibrational motion. For the present it is not necessary to fix that energy origin.

When any or all of the N molecules form a compact collection, they interact, causing V_N to deviate from the limit (3.1). We wish to resolve V_N in the most general case uniquely into single-molecule, pair, triplet, quadruplet, ..., N-tuplet components:

$$V_N(\mathbf{X}_1 \cdots \mathbf{X}_N) = \sum_{n=1}^{N} \sum_{i_1 < \cdots < i_n = 1}^{N} V^{(n)}(\mathbf{X}_i \cdots \mathbf{X}_{i_n}) \tag{3.2}$$

The component potentials $V^{(n)}$ may be obtained by successive reversion of identity (3.2) for $N = 1, 2, 3, \ldots$.

$$\begin{aligned} V^{(1)}(\mathbf{X}_1) &\equiv V_1(\mathbf{X}_1) \\ V^{(2)}(\mathbf{X}_1, \mathbf{X}_2) &= V_2(\mathbf{X}_1, \mathbf{X}_2) - V^{(1)}(\mathbf{X}_1) - V^{(1)}(\mathbf{X}_2) \\ V^{(3)}(\mathbf{X}_1, \mathbf{X}_2, \mathbf{X}_3) &= V_3(\mathbf{X}_1, \mathbf{X}_2, \mathbf{X}_3) - V^{(1)}(\mathbf{X}_1) - V^{(1)}(\mathbf{X}_2) \\ &\quad - V^{(1)}(\mathbf{X}_3) - V^{(2)}(\mathbf{X}_1, \mathbf{X}_2) - V^{(2)}(\mathbf{X}_1, \mathbf{X}_3) \\ &\quad - V^{(2)}(\mathbf{X}_2, \mathbf{X}_3) \end{aligned} \tag{3.3}$$

The quantity $V^{(n)}$ generally may be written as a remainder left after all possible component potentials of lower order have been subtracted from V_n:

$$V^{(n)}(\mathbf{X}_1 \cdots \mathbf{X}_n) = V_n(\mathbf{X}_1 \cdots \mathbf{X}_n) - \sum_{j=1}^{n-1} \sum_{i_1 < \cdots < i_j = 1}^{n} V^{(j)}(\mathbf{X}_{i_1} \cdots \mathbf{X}_{i_j}) \tag{3.4}$$

The utility of the potential-energy resolution (3.2) hinges on its rapidity of convergence with respect to n. Most of the statistical mechanics of condensed phases has been developed for additive interactions, that is, vanishing $V^{(n)}$ for $n > 2$. This additivity assumption is itself an excellent approximation for nonpolar molecular substances with low polarizability (helium, neon, argon, hydrogen, nitrogen, methane), and for such substances it makes sense to account for nonadditivity via perturbation theory, if at all. Polar substances and ionic materials can generally be expected to possess considerably larger nonadditivity, so special care must be exercised on their behalf. The worst case of all probably is presented by metals (both crystalline and liquid), since the formation of electronic energy bands and a Fermi surface is inevitably a many-nucleus effect. Furthermore, for metals it would not suffice just to consider the ground electronic state potential-energy function V_N, since electron excitation above the Fermi surface is an important phenomenon at any positive absolute temperature.

As we shall see, water belongs to an important class of polar molecular substances that engage in hydrogen bonds. For each of these materials, a special type of nonadditivity connected with the partially covalent (chemical) nature of the hydrogen bond requires careful study.

B. Identification of Molecules and Ions

Thus far we have proceeded under the implicit assumption that N oxygen nuclei and $2N$ hydrogen nuclei are uniquely and completely partitioned into identifiable triads, comprising H_2O molecules. The logical basis for this assumption needs careful scrutiny. In a close encounter between two water molecules, it is quite possible that ambiguity might arise over which two

hydrogens "belong" to each of the two oxygens. In addition, we know that water molecules occasionally dissociate into ions:

$$H_2O \rightleftarrows H^+ + OH^- \tag{3.5}$$

which drift apart, so that subsequent associations change partners. By drawing on a generalization of the formal theory of ion pairing,[22] we can completely remove the ambiguity.

Consider a specific configuration for the $3N$ nuclei. There are exactly $2N^2$ distinct OH pairs, whose distances will be denoted by $l(i, j)$. By convention $1 \leq i \leq N$ will refer to the oxygens, and $1 \leq j \leq 2N$ to the hydrogens. Arrange the $l(i, j)$ in an ascending sequence:

$$\begin{gathered} l(i_1, j_1) < l(i_2, j_2) < \cdots < l(i_M, j_M) \\ M = 2N^2 \end{gathered} \tag{3.6}$$

Since they bear zero measure over the full configuration space, accidental equalities in the ordered list may justifiably be disregarded.

We now proceed to apply the following recursive bonding algorithm.

1. Pair the two nuclei that provide the minimum distance in the list. This OH will henceforth be regarded as bonded.
2. Remove from the list all distances that involve hydrogens previously bonded and/or involve oxygens bonded *twice* previously. This removal leaves a contracted, but still ascending, distance list.
3. Return to step 1 if any distances remain in the list.

The end result of this procedure is that every oxygen is bonded without uncertainty to exactly two hydrogens, and every hydrogen belongs to one and only one oxygen. Furthermore, the procedure is entirely general and can be applied to any initial set of nuclear positions.

If we are to adhere consistently to the bonding algorithm, then it is important to realize that the nine-dimensional vectors $\mathbf{X}_i$ used in Section III.B require constraints. These constraints are necessary to avoid the exchange of hydrogens between neighboring water molecules. This remark is not meant to imply that such exchanges cannot occur; physically, it is clear that they can and often do. Instead it means that certain limits on the $\mathbf{X}_i$ variables must be obeyed to be consistent with the given bonding scheme.

Figure 3*a* and *b* illustrates a pair of water molecules in two relative configurations. In Fig. 3*a*, they are reasonably well separated, and the choice for associating hydrogens with oxygens is entirely clear. However, the molecules have moved closer together in Fig. 3*b* to an extent such that the bonding scheme present in Fig. 3*a* becomes invalid. The bonding algorithm does not permit one of the hydrogens of a neighboring molecule to penetrate

(a) VALID BONDING SCHEME

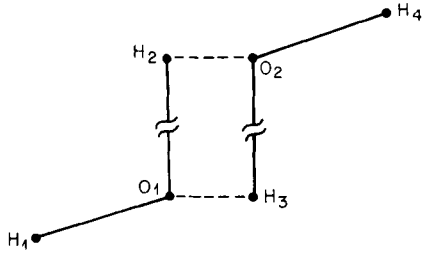

(b) INVALIDATING CLOSE ENCOUNTER

Fig. 3 Necessity for modified association of nuclei into molecules on close encounter. The bonding algorithm that creates molecules ($H_1O_1H_2$) and ($H_3O_2H_4$) in separated configuration (*a*) gives rise to hydrogen exchange and molecules ($H_1O_1H_3$) and ($H_2O_2H_4$) in close encounter (*b*).

more closely to a given molecule's oxygen than the minimum of the four OH bond lengths in both the molecule and its neighbor. Such penetration would automatically force a redrawing of bonds, as in fact Fig. 3*b* explicitly shows.

Conversely, it is easy to see that a set of OH bonds which, for each pair of its H_2O molecules, does *not* lead to a nonbonded oxygen–hydrogen separation smaller than the four OH bonds themselves is precisely the bond set that the algorithm would produce. Therefore, the configurational constraint demanded by a given set of molecules consists of the logical conjunction of constraints just for each of the $N(N-1)/2$ pairs of molecules.

There are precisely

$$\Omega = \frac{(2N)!}{2^N} \tag{3.7}$$

distinct ways of bonding N distinguishable oxygens to $2N$ distinguishable hydrogens so as to form H_2O molecules. The full configuration space for the $3N$ nuclei therefore splits naturally into Ω equivalent, nonoverlapping, and exhaustive regions. It is the interior of such a region to which the collection of nine-vectors $\mathbf{X}_1, \ldots, \mathbf{X}_N$ must be restricted.

The reader will have noticed that, on its completion, the bonding algorithm will by convention have forced into a long-distance marriage pairs of hydroxyl and hydrogen ions produced by dissociation reaction (3.5). They are then simply interpreted as molecules with a very severely stretched bond. Now there is nothing logically to prevent the theory from proceeding on this basis; especially at low temperature, the dissociation could be neglected anyway. But one of the chemically important aims of the theory ought to be a description of the dissociation reaction itself and of the solvated ions that result, so there should be a provision for rendering ions into distinguishable species.

To this end we now propose a natural modification of the bonding algorithm which is convenient for statistical mechanical study of water dissociation. The modification simply prevents the algorithm from going to completion by putting an upper limit L on the length of bonds. This can be implemented by replacing step 1 of the algorithm above by:

1′. If the minimum distance in the ordered list is less than L, pair its two nuclei as a bond. If it is not, stop.

The idea is that any O—H bond stretched to length L by definition breaks at that critical distance. Application of the modified algorithm results in distinct chemical species H_2O, OH^-, H^+, and occasionally O^{2-}.

If the theory were to be developed from this stage without subsequent approximation, predictions for all measurable quantities would have to be strictly independent of L. But to satisfy tradition, as well as chemical and physical intuition, a preferred range of L values deserves to be identified. We therefore suggest that half the distance between neighboring oxygen nuclei in ice (at 0°K and vanishing external pressure)

$$L = 1.375 \text{ Å} \tag{3.8}$$

is a reasonable choice which agrees with the usual notions of dissociation. Note that this choice entails a bond stretch of 0.417 Å from the equilibrium length before breakage can occur.

C. Dimer Interaction

Superficially, the pair potential $V^{(2)}(\mathbf{X}_1, \mathbf{X}_2)$ defined in (3.3) depends on 18 configurational coordinates. But since translational and rotational invariance applies to the complex of six nuclei, $V^{(2)}$ really requires an irreducible

minimum of 12 relative configuration coordinates. These 12 coordinates can, for example, be chosen to be

1. The three vibrational normal mode amplitudes for each molecule.
2. Polar coordinates specifying the displacement between fixed points in the two molecules (such as the oxygen nuclei, or the centers of mass).
3. Euler angles describing the rigid-body rotation relating spatial orientation of the undistorted molecules.

In the case of the noble gases, $V^{(2)}$ depends only on the distance between the centers of the structureless, spherical particles. Consequently, it is possible to determine this function of one variable accurately through a combination of experiments on the second virial coefficient, gas-phase transport coefficients, and differential scattering cross sections. An analogous determination of $V^{(2)}$ for water, however, is not feasible; the 12-dimensional character of the water pair potential introduces insurmountable problems of interpretive nonuniqueness. Direct quantum mechanical calculation of $V^{(2)}(\mathbf{X}_1, \mathbf{X}_2)$ is really the only available technique that is comprehensive, reliable, and unambigous. The various experiments, such as those cited, that involve $V^{(2)}$ at best can provide partial checks on the precision of the quantum mechanical results.

At large separation between molecules 1 and 2, $V^{(2)}$ becomes dominated by the electrostatic interaction of the respective vector dipole moments:

$$\begin{aligned} V^{(2)}(\mathbf{X}_1, \mathbf{X}_2) &\sim \boldsymbol{\mu}(\mathbf{X}_1) \cdot \mathbf{T}_{12} \cdot \boldsymbol{\mu}(\mathbf{X}_2) \\ \mathbf{T}_{12} &= R_{12}^{-3}(\mathbf{1} - 3R_{12}^{-2}\mathbf{R}_{12}\mathbf{R}_{12}) \end{aligned} \tag{3.9}$$

$\mathbf{R}_{12}$ is the vector connecting the centers of the molecules and, to the leading asymptotic order required in (3.9), it is irrelevant which location within the molecule serves as center (oxygen nucleus, center of mass, etc.).The moments $\boldsymbol{\mu}(\mathbf{X}_i)$ are those appropriate for isolated molecules, with a mean value for the ground state given earlier by (2.3).

The asymptotic formula (3.9) can formally be extended to higher orders to account for interactions between higher multipoles for the isolated molecules, and changes in those multipoles due to mutual polarization. A necessary and sufficient condition for convergence of multipole expansions is that the respective charge distributions be confined to the interiors of nonoverlapping spheres. However, this cannot be satisfied strictly for molecules, since their electron densities possess tails of infinite extension. Therefore, the infinite series of which (3.9) represents the leading term must either be divergent for all $R_{12} < \infty$, or else it must converge to a function that differs from $V^{(2)}$ more and more as R_{12} decreases. It is for this reason that higher-order terms in (3.9) have limited value.

The present state of development in computational quantum mechanics is such that high-quality Hartree–Fock calculations can be carried out for small sets of n interacting water molecules, certainly for $n = 1$, 2, 3, and 4. Thus far, extension to $n = 5$ and 6 has required compromises in basis set size with resulting errors which diminish the significance of results.

To date, a large number of Hartree–Fock studies of the water dimer ($n = 2$) has been carried out,[23–29] and as a result a consensus has emerged about the principal characteristics of $V^{(2)}$. Figure 4 displays the structure implied by these studies for the lowest-energy dimer configuration. Two major points become clear, namely, that the individual water molecules suffer little distortion as a result of the interaction, and that an essentially linear hydrogen bond is involved.

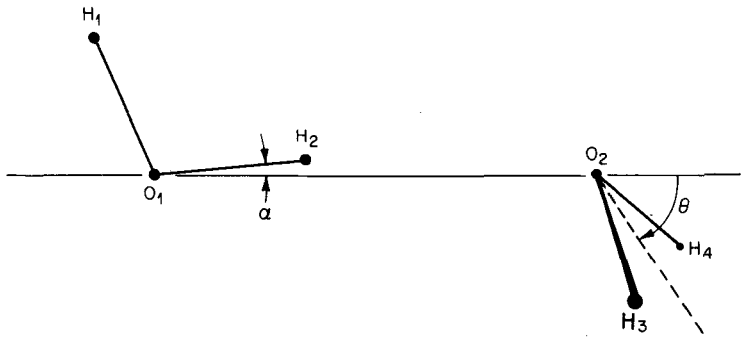

Fig. 4 Lowest-energy dimer structure. The plane containing the proton donor molecule ($H_1O_1H_2$) is a plane of reflection symmetry for the dimer, and as such contains O_2.

Quantitative details vary somewhat from one Hartree–Fock calculation to another, but in all cases the lowest-energy dimer exhibits a phase of symmetry. This plane contains a proton donor molecule ($H_1O_1H_2$ in Fig. 4) which points one of its OH bonds toward the oxygen atom of the proton acceptor molecule ($H_3O_2H_4$ in Fig. 4). The proton acceptor lies in a plane perpendicular to the dimer symmetry plane, with an orientation angle $\theta > 0$ to minimize repulsions between pendant hydrogens. In all calculations the distance $l(O_2H_2)$ is sufficiently large that the bond reconstruction illustrated previously in Fig. 3 is not required—the molecules maintain their individuality.

The specific dimer arrangement shown in Fig. 4 is only one of eight equivalent arrangements leading to an energy minimum. The other seven can be obtained by 180° rotation of the proton acceptor molecule about its

symmetry axis and/or use of one of the other three protons in the linear hydrogen bond.

Table I lists the important parameters for the most stable dimer structure as they have been predicted by the available *ab initio* (all-electron) Hartree–Fock calculations. The entries are arranged roughly in increasing order of precision. The first rows historically were earliest, and employed rather restrictive basis sets; those near the end are more recent, and utilized more nearly complete basis function sets. Proceeding down the list, the trend for the most part is toward smaller binding energy, and greater bond length (R_{OO} is the distance between oxygens). It seems reasonable to suppose by extrapolation that the exact Hartree–Fock limit would produce a binding energy of about 4.50 kcal/mole for a linear hydrogen bond with length $R_{OO} = 3.00$ Å.

Motions of the dimer that tend to change R_{OO} from its optimal value, or to move the donated proton (H_2 in Fig. 4) substantially off the oxygen–oxygen axis, are costly in terms of stabilizing energy. However, rotation of the proton donor molecule about the linear $O_1H_2O_2$ axis is less costly, as is a change in acceptor rotation angle θ.

The covalent chemical bonds holding the individual water molecules together are much stronger and stiffer than the hydrogen bond. Thus the molecules are only slightly perturbed in internal geometry when forming the optimized dimer, in comparison with isolated molecules. The primary change seems to be a small lengthening of the covalent OH bond forming the hydrogen bond, by an order of 0.005 Å (last column in Table I). At the same time, the stretching force constant for this bond decreases substantially when it forms a linear hydrogen bond, according to all the Hartree–Fock calculations for which this has been tested. An additional small effect of the hydrogen bond seems to be an opening up of the HOH angle in the acceptor molecule by about 0.5°, thereby moving it closer to θ_t [see (2.2)].[27]

Popkie, Kistenmacher, and Clementi[29] carried out an extensive set of dimer calculations densely spanning the space of relative configurations, especially in the neighborhood of the stable dimer minimum. The separate water molecules, however, were strictly frozen in their isolated-molecule geometries. These investigators carefully fitted their results to a closed-form expression which constitutes a convenient representation of the Hartree–Fock approximation to $V^{(2)}(\mathbf{X}_1, \mathbf{X}_2)$ within the undistorted molecule subspace. The expression consists of a sum of Coulombic and exponential terms acting between force centers, four in each molecule. These force centers are the three nuclei (with OH bond length 0.957 Å and HOH bond angle 105°), and a fourth center M located 0.2307 Å ahead of the oxygen, along the symmetry axis. The positions and relative charges associated with these centers are shown in Fig. 5.

TABLE I

Parameters Describing Minimum-Energy Dimers Inferred from Various Quantum-Mechanical Calculations[a]

Investigator	Reference	Basis set character	Binding energy (kcal/mole)	R_{OO} (Å)	θ (deg)	α (deg)	$\Delta R_{O_1H_2}$ (Å)
Morokuma, Pedersen	23	G(5, 3|3)	12.6	2.68	18[b]	—	0.012
Del Bene, Pople	24	G[2, 1|1]	6.09	2.73	58	1.0	—
Morokuma, Winick	25	S (minimal)	6.55	2.78	54	—	0.0026
Kollman, Allen	26	G[3, 1|1]	5.27	3.0	25	—	0.010
Hankins, Moskowitz, and Stillinger	27	G[5, 3, 1|2, 1]	5.00	3.00	40	0	<0.01
Diercksen	28	G[5, 4, 1|3, 1]	4.84	3.00	≈ 35	—	0.0040
Popkie, Kistenmacher, and Clementi	29	G[8, 5, 1, 1|4, 1, 1]	4.60	3.00	30	—	—

[a] Angles and distances refer to Fig. 4. G, Gaussian basis; S, Slater basis.

[b] Interpolated.

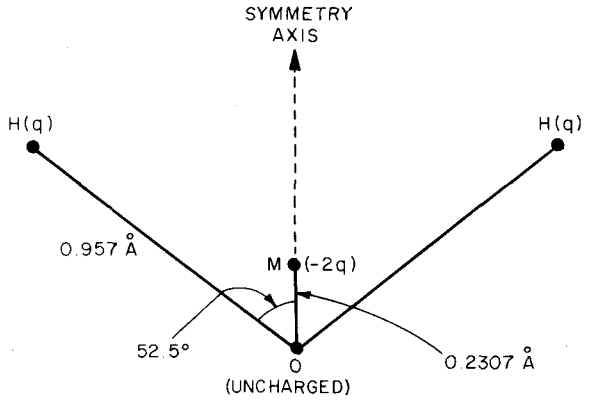

Fig. 5 Four-force-center model of the water molecule used by Popkie, Kistenmacher, and Clementi to fit the Hartree–Fock approximation to $V^{(2)}$.

The Pokie–Kistenmacher–Clementi (PKC) function may be written:

$$V^{(2)}_{\mathrm{PKC}} = a_{\mathrm{OO}} \exp(-b_{\mathrm{OO}} R_{\mathrm{OO}}) + \sum_{(\mathrm{O,H})} a_{\mathrm{OH}} \exp(-b_{\mathrm{OH}} R_{\mathrm{OH}}) + \sum_{(\mathrm{H,H})} \left[a_{\mathrm{HH}} \exp(-b_{\mathrm{HH}} R_{\mathrm{HH}}) + \frac{q^2}{R_{\mathrm{HH}}} \right] - 2q^2 \sum_{(\mathrm{H,M})} \left(\frac{1}{R_{\mathrm{HM}}} \right) + \frac{4q^2}{R_{\mathrm{MM}}} \tag{3.10}$$

q, a's and b's are constants, while the R's are the distances between pairs of force centers (one in each molecule). With distances in angstroms, and energy in kilocalories per mole, the parameters are found to be

$$\begin{aligned} a_{\mathrm{OO}} &= 3.65501 \times 10^5 \text{ kcal/mole} \\ a_{\mathrm{OH}} &= 3.43368 \times 10^3 \text{ kcal/mole} \\ a_{\mathrm{HH}} &= 90.2576 \text{ kcal/mole} \\ b_{\mathrm{OO}} &= 4.76328 \text{ Å}^{-1} \\ b_{\mathrm{OH}} &= 3.65973 \text{ Å}^{-1} \\ b_{\mathrm{HH}} &= 2.30881 \text{ Å}^{-1} \\ q &= 3.21966 \times 10^{-10} \text{ esu} \end{aligned} \tag{3.11}$$

The variation in $V^{(2)}_{\mathrm{PKC}}$ with respect to oxygen–oxygen distance R_{OO} has been plotted in Fig. 6 for the symmetric linear hydrogen bond configuration shown previously in Fig. 4, with $\alpha = 0$ and $\theta = \theta_t/2 = 54.7356°$. Figure 7 presents the θ variation at $R_{\mathrm{OO}} = 3.00$ Å for the same symmetric linear hydrogen bond configuration ($\alpha = 0$).

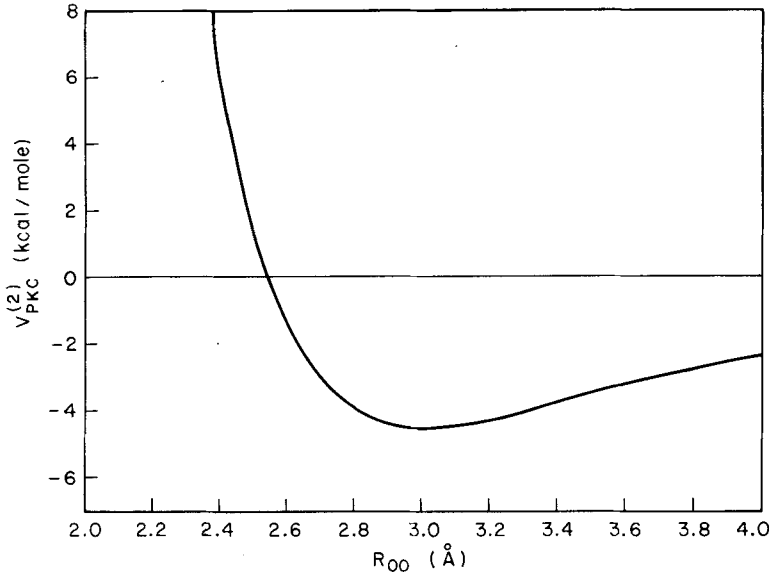

Fig. 6 Distance variation of $V^{(2)}_{PKC}$ in the symmetric linear hydrogen bond configuration shown in Fig. 4 ($\alpha = 0$, $\theta = \theta_t/2$).

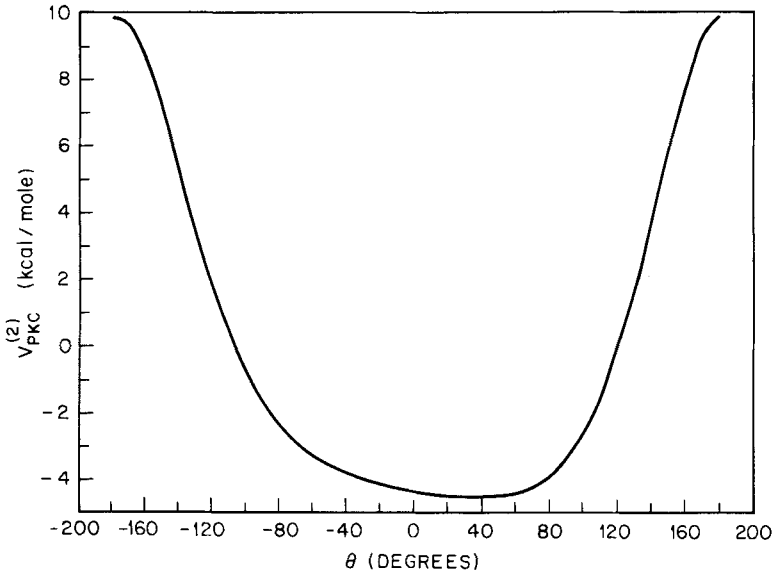

Fig. 7 Acceptor angle variation for $V^{(2)}_{PKC}$ at $R_{OO} = 3.00$ Å. The configuration is the one shown in Fig. 4, with $\alpha = 0$ (linear hydrogen bond).

In the process of forming the linear hydrogen bond, the pair of water molecules experiences a shift in electron density relative to that for isolated molecules. The shift affects the net dipole moment for the interacting dimer, which is no longer the vector sum of the two monomer moments. Hankins, Moskowitz, and Stillinger[27] found that the dimer at its most stable conformation exhibits an 11% enhancement in dipole moment magnitude compared to the magnitude of the isolated-molecule vector sum.

Another measure of the distribution shift is provided by Mullikan atomic population changes relative to isolated monomers. Hankins, Moskowitz, and Stillinger[27] also evaluated these changes for the most stable dimer conformation. In terms of the atomic designations shown in Fig. 4, the changes found are

$$\begin{aligned} \Delta(H_1) &= 0.00963 \\ \Delta(O_1) &= 0.03776 \\ \Delta(H_2) &= -0.03604 \\ \Delta(O_2) &= 0.02212 \\ \Delta(H_3) &= \Delta(H_4) = -0.01674 \end{aligned} \tag{3.12}$$

These numbers represent "fractions of an electron," so $\Delta > 0$ implies more negative charge at the given atom on dimerization. Evidently, the pendant hydrogens on the proton acceptor (H_3 and H_4) have become more positive, while the oxygen of the donor molecule (O_1) has become more negative. These atoms can therefore be expected to act as more acidic, and more basic, respectively, in further hydrogen bond formation in larger water molecule aggregates.

One of the errors inherent in the Hartree–Fock approximation applied to water is that the predicted dipole moment for the single molecule is too large. The dipole moment incorporated in $V^{(2)}_{\mathrm{PKC}}$, arising from the charge distribution illustrated in Fig. 5, is

$$\mu_{\mathrm{PKC}} = 2.27 \times 10^{-18} \text{ esu cm} \tag{3.13}$$

This is 22% larger than the experimental value [see (2.3)]. There is a corresponding modification of $V^{(2)}$ at large separation, in accord with (3.9).

Beside correcting the dipole moment, calculations sufficiently accurate to incorporate the electron correlation neglected by the Hartree–Fock approximation would also begin to account for London dispersion attraction. This attraction arises from correlation between fluctuations in electron distribution for the two molecules, and at large separation it provides for $V^{(2)}$ a negative term proportional to R_{12}^{-6}. Since such correlated-electron calculations are not yet available for the water dimer, it is worthwhile to make a rough estimate of the dispersion attraction.

The neon atom is isoelectronic with the water molecule—both have closed-shell, 10-electron singlet ground states. According to Slater and Kirkwood,[30,31] the respective dispersion attraction at a given distance should be proportional to the three-halves powers of the optical polarizabilities. Using the mean value shown in (2.10) for water, and[32]

$$\alpha(\mathrm{Ne}) = 0.39 \times 10^{-24}\ \mathrm{cm}^3 \tag{3.14}$$

is it possible to scale up the accepted neon dispersion interaction[33] to water. The result is

$$\Delta V^{(2)}_{\mathrm{disp}} \cong -\frac{C}{R_{12}^6}$$
$$C = 98.2\ \text{kcal Å}^6/\text{mole} \tag{3.15}$$

At small separation, the inverse sixth power attractive term is augmented by others which vary as R_{12}^{-8}, R_{12}^{-10}, and so on. In order to incorporate their effect, we can appeal to the same scaling, but applied to the attractive term of an empirical Lennard–Jones 12-6 potential for neon. In particular we draw on Corner's version.[34] At close range it is thereupon suggested that the constant C in (3.15) be empirically modified to

$$C' = 1023\ \text{kcal Å}^6/\text{mole} \tag{3.16}$$

The resulting quantity $-C'/R_{16}^6$ can be appended to $V^{(2)}_{\mathrm{PKC}}$ as a crude estimate of the correlation effect in the hydrogen bond distance range (with R_{12} identified as R_{OO}). The net effect (for $\alpha = 0$, $\theta = \theta_t/2$) is that the linear hydrogen bond compresses from 3.007 to 2.855 Å, while its strength increases from -4.499 to -6.123 kcal/mole.

D. Nonadditivity

Since the linear hydrogen bond already arises at the water molecule pair interaction level, $V^{(2)}$ suffices to explain the gross aspects of water molecule arrangements in aqueous crystals (and perhaps in the liquid as well). But quantitative understanding of water in its condensed phases clearly requires analysis of potential-energy nonadditivity.

In order to hydrogen-bond as a donor to a neighbor, a water molecule uses only one of its OH groups. The other OH group is free to form its own linear hydrogen bond to the back of a second neighbor. Simultaneously, this doubly donating molecule can accommodate two further neighbors at its back (making four neighbors in all), which themselves donate protons in linear hydrogen bonds. Thus fourfold coordination via linear hydrogen

bonds is natural for water molecule aggregates. The most favorable spatial arrangement of these four hydrogen bonds places the five water molecule oxygens at the center and at the vertices of a regular tetrahedron. This pattern is shown in Fig. 8.

The four neighbor molecules in Fig. 8 are available for further hydrogen bonding, so that they too participate in four linear hydrogen bonds emanating in the tetrahedral pattern. Thus a large aggregate of water molecules can form a space-filling network of hydrogen bonds. Since $V^{(2)}$ at least permits relatively free reorientation of the neighbor molecules around the hydrogen bonds shown in Fig. 8, a wide topological variety of three-dimensional networks seems to be possible.

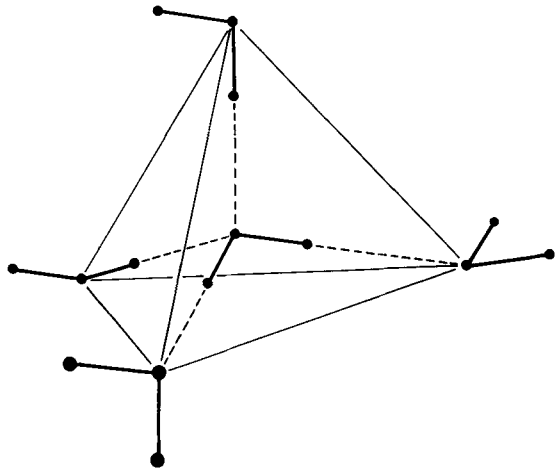

Fig. 8 Fourfold tetrahedral coordination of water molecules via linear hydrogen bonds.

The periodic network structure for hexagonal ice Ih is shown schematically in Fig. 9. This crystal utilizes the tetrahedral hydrogen bonding scheme to form puckered hexagons, of both the chair and boat forms. That the hydrogen atoms do in fact reside along the bonds shown (consistent with the fact that molecular HOH angles are nearly θ_t) has been established by neutron scattering from D_2O ice;[35] furthermore, these hydrogens are nearer one end of the bond than the other, since intact molecules are involved.

Closely related to hexagonal ice is the cubic form which consists exclusively of chair form hexagons. This modification also exhibits ubiquitous fourfold coordination, with linear hydrogen bonds in a tetrahedral pattern about

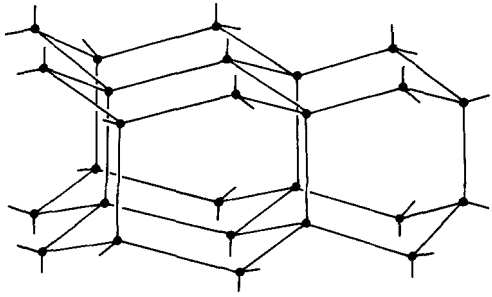

Fig. 9 Hydrogen bond network for ice Ih. The vertices (solid circles) are the positions of the oxygen atoms. The hydrogens are located asymmetrically along the bonds, two near each vertex to form the water molecules.

each oxygen vertex. Significantly, this theme persists with minor distortions throughout high-pressure ice polymorphs,[7] and can be seen clearly in the structure of gas hydrates (clathrates).[36]

The three-molecule nonadditivity function $V^{(3)}(\mathbf{X}_1, \mathbf{X}_2, \mathbf{X}_3)$ in the strict sense depends irreducibly on 21 variables, so its full numerical characterization would be a formidable task. The existence of the hydrogen bond networks just mentioned, however, suggests confining attention largely to those trimer configurations that appear in the networks. Furthermore, one would expect the greatest potential nonadditivity to arise when distances are all small, so additionally restricting attention to hydrogen-bonded trimers seems warranted.

Three topologically distinct types of bonded network trimers exist. They are illustrated in Fig. 10. Each one has a central molecule with two hydrogen bonds, and two end molecules with only one hydrogen bond. In an extended hydrogen bond network such as that shown in Fig. 9 for ice Ih, each molecule acts as the center of six bonded trimers. In terms of the trimer categories defined by Fig. 10, the six consist always of one double donor, one double acceptor, and four sequential trimers.

Hankins, Moskowitz, and Stillinger[27] calculated $V^{(3)}$ for the three trimers shown in Fig. 10, using the Hartree–Fock approximation. For their study the individual molecules were maintained at the stable internal structure established by the one-molecule calculations, and the component bonded dimers in each trimer were of the type shown earlier in Fig. 4, with $\alpha = 0$ and $\theta = -\theta_t/2$. The results are plotted in Fig. 11 versus R_{OO}, the common hydrogen bond length.

On the basis of quite incomplete information, Hankins, Moskowitz, and Stillinger[27] suggested that, for each of the three types of bonded trimers,

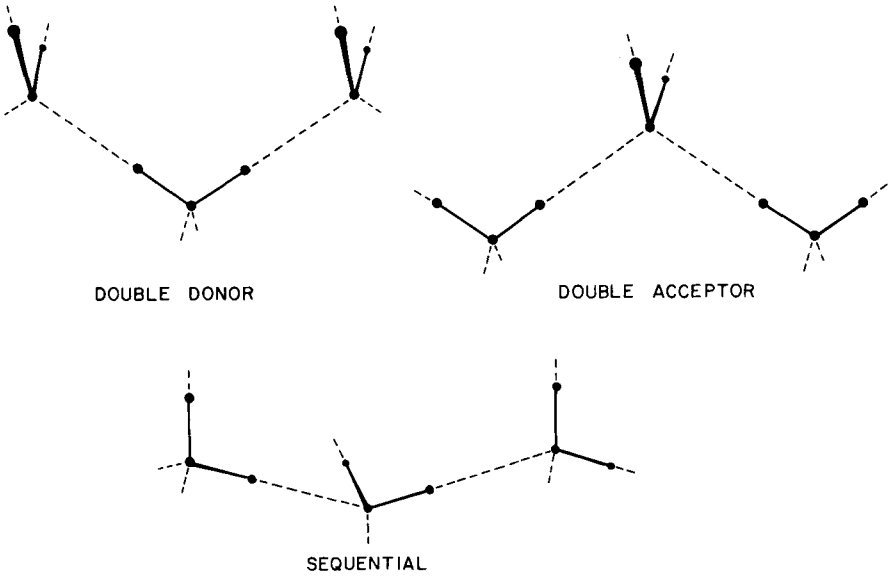

Fig. 10 Topologically distinct hydrogen-bonded trimers.

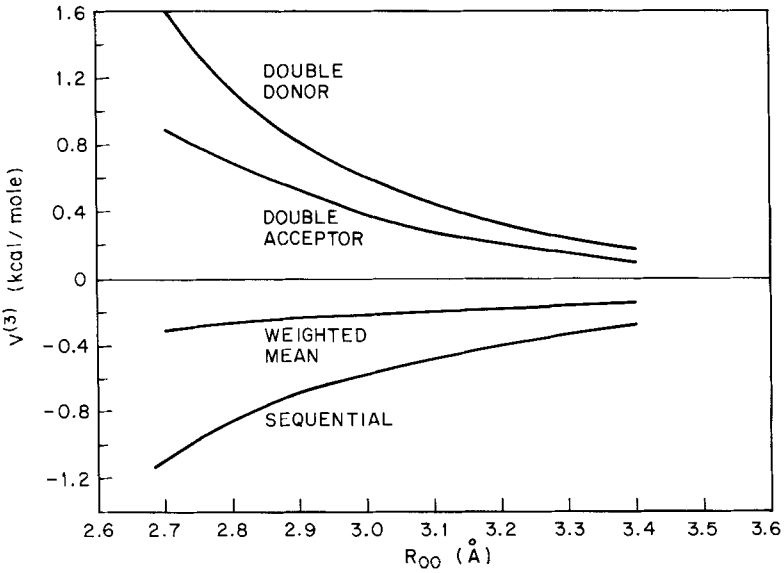

Fig. 11 Trimer nonadditivities for variable common bond length, R_{OO}. The configurations involved are shown in Fig. 10. The weighted mean is $\frac{2}{3}$ (sequential) + $\frac{1}{6}$ (double donor + double acceptor), appropriate for a four-coordinated network.

$V^{(3)}$ is quite insensitive to the rotation of molecules about the linear hydrogen bonds, more insensitive in fact than the separate $V^{(2)}$s involved. This hypothesis has been confirmed by Lentz and Scheraga.[37] It suggests that the $V^{(3)}$ curves shown in Fig. 11 are representative of *all* bonded trimers in an extended network. Because of the invariant ratios of the three types of trimers, it is therefore relevant to examine the weighted mean

$$\langle V^{(3)} \rangle_{\text{net}} = \tfrac{1}{6}[V^{(3)}(\text{double donor}) + V^{(3)}(\text{double acceptor}) + 4V^{(3)}(\text{sequential})] \tag{3.17}$$

The corresponding curve is presented in Fig. 11. It demonstrates that the net effect of $V^{(3)}$, at least for bonded trimers, is to confer extra energetic stability on an extended network. Furthermore, the decrease in $\langle V^{(3)} \rangle_{\text{net}}$ with decreasing R_{OO} constitutes a compressive effect which tends to reduce the hydrogen bond length in the network.

The negative values found for $V^{(3)}$ in the sequential trimer may be interpreted as a strengthening of successive hydrogen bonds in a chain after the first is formed. The possibility of this "hydrogen bond cooperativity" was pointed out several years ago by Frank and Wen,[38,39] who observed that the hydrogen atoms of the acceptor molecule in a dimer (see Fig. 4) should become more positive as a result of the hydrogen bond and, consequently, as stronger Lewis acids, should form stronger successive hydrogen bonds. The Mulliken population shifts quoted earlier for the dimer [see (3.12)] document this idea quantitatively.

Very little systematic study of $V^{(4)}$ has thus far been undertaken. Lentz and Scheraga[37] employed the Hartree–Fock approximation for a cyclic tetramer. This tetramer has S_4 symmetry; the four pendant OH groups around the hydrogen bond square alternate above and below the plane of oxygens. The three bonded trimers included in the tetramer are all sequential. The results show that about 10% of the tetramer binding energy (at the optimal bond length) is attributable to $V^{(3)}$, but only about 1% to $V^{(4)}$ (it is negative for the cyclic tetramer). The broad implication seems to be that, although three-molecule nonadditivity is important for water, the general potential-energy resolution (3.2) is rapidly convergent with order n for physically relevant configurations of water molecule aggregates.

Del Bene and Pople[24] investigated a series of cyclic water polymers, up to and including the cyclic hexamer. Although they interpreted their results to mean that closure of hydrogen bond polygons entails a special cooperative stabilizing phenomenon, the systematic potential-energy resolution (3.2) was not invoked. It seems likely that their polygon stabilities owe their existence primarily to negative $V^{(3)}$s associated with sequential trimers, and not to anomalous $V^{(n)}$s of higher order which come forth under topological closure.

The fractional contribution of potential-energy nonadditivity to the total binding energy of ice Ih is likely typical for all tetrahedrally coordinated networks. The available Hartree–Fock calculations[27,37] imply that about 13% is attributable to nonadditivity.

A clear need exists for further study of nonadditivity in water clusters, and for incorporation of electron correlation into the quantum mechanical computations.

IV. SEMICLASSICAL LIMIT

A. Canonical Partition Function

The connection between the Hamiltonian operator $\mathscr{H}$ for N water molecules (regarded as $2N$ hydrogen nuclei and N oxygen nuclei) and macroscopic thermodynamics can be established through the canonical partition function

$$Q = \mathrm{Tr} \exp(-\beta\mathscr{H}) \qquad \beta = \frac{1}{k_B T} \tag{4.1}$$

where the basis over which the trace is computed includes spin and symmetry as appropriate for the isotopes of interest. The potential energy surface appearing in $\mathscr{H}$ is the quantity $V_N(\mathbf{X}_1 \cdots \mathbf{X}_N)$ whose resolution into singlet, pair, triplet, and so on, components has just been considered:

$$\mathscr{H} = -\tfrac{1}{2}\hbar^2 \sum_{j=1}^{3N} m_j^{-1} \nabla_j^2 + V_N \tag{4.2}$$

The partition function Q yields the Helmholtz free energy F directly:

$$Q = \exp(-\beta F) \tag{4.3}$$

from which other thermodynamic functions may in turn be obtained by standard identities.

For many aspects of the study of water, the full quantum mechanical representation (4.1) for Q is unnecessary. Although the internal normal modes of vibration for the most part remain in their quantum mechanical ground states, it is relevant to examine the rotational and translational degrees of freedom in their classical limits. This point of view is not meant to imply that water (at room temperature, say) achieves this classical limit to high precision. But the required quantum corrections to rotational and translational motion have sufficiently modest magnitudes (H_2O and D_2O differ relatively little)

that eventual calculation of leading quantum corrections to the classical limit makes good physical sense. We return to this matter in Section IX within the context of a model for which quantum corrections can be readily generated.

For the present we therefore confine attention to a collection of classical rigid rotor molecules with quantized internal vibrations. The corresponding semiclassical version of the partition function has the appearance:[40]

$$Q = \frac{1}{N!}\left[\frac{(2\pi k_B T)^3 m^{3/2}(I_1 I_2 I_3)^{1/2} Q_{\text{vib}}}{h^6}\right]^N \times \int d\mathbf{x}_1 \cdots \int d\mathbf{x}_N \exp\left[-\beta \overline{V}_N(\mathbf{x}_1 \cdots \mathbf{x}_N)\right] \tag{4.4}$$

In this expression m stands for the total molecular mass ($m_O + 2m_H$), h is Planck's constant, and the principal moments of inertia are I_1, I_2, and I_3; the vibrational partition function is Q_{vib}. The configuration coordinates for each molecule j have now been reduced to six, symbolized by $\mathbf{x}_j$; these are the Cartesian coordinates of a fixed point in the molecule, and three Euler angles α_j, β_j, and γ_j describing orientation about that fixed point. Unlike the preceding function V_N, the appropriate potential function $\overline{V}_N$ for use in (4.4) employs only these configurational six-vectors $\mathbf{x}_j$ as variables.

Presuming that vibrations are truly harmonic, with angular frequencies ω_α,

$$Q_{\text{vib}} = \prod_{\alpha=1}^{3} \frac{\exp\left(-\frac{1}{2}\beta\hbar\omega_\alpha\right)}{1 - \exp\left(-\beta\hbar\omega_\alpha\right)} \tag{4.5}$$

We noted in Section III.A that molecular vibration force constants are affected by intermolecular interactions, specifically by the formation of hydrogen bonds. We elect to interpret shifts in vibrational energy levels that result from these force-constant changes as a valid part of the interactions $\overline{V}_N$. The frequencies ω_α in (4.5) thus are strictly isolated-molecule frequencies.

The formal prescription for obtaining the rigid-rotor potential-energy functions $\overline{V}_N$ from the more detailed quantities V_N are now specified. First, split nine-vector $\mathbf{X}_j$ into a direct sum of rigid-body coordinates $\mathbf{x}_j$ and a vibration amplitude part $\mathbf{y}_j$:

$$\mathbf{X}_j = \mathbf{x}_j \oplus \mathbf{y}_j \tag{4.6}$$

Then, for an arbitrary collection of n molecules constrained in their rigid body coordinates to $\mathbf{x}_1, \ldots, \mathbf{x}_n$, the remaining amplitudes $\mathbf{y}_1, \ldots, \mathbf{y}_n$ describe vibrations for the complex, which are now collectively determined normal

modes. These $3n$ new normal modes have frequencies shifted from the free-molecule ω_α, but in any event define an n-molecule vibrational partition function:

$$Q_{\text{vib}}^{(n)}(\mathbf{x}_1 \cdots \mathbf{x}_n) = \sum_{\nu=1}^{3n} \frac{\exp\left[-\frac{1}{2}\beta\hbar\omega_\nu(\mathbf{x}_1 \cdots \mathbf{x}_n)\right]}{1 - \exp\left[-\beta\hbar\omega_\nu(\mathbf{x}_1 \cdots \mathbf{x}_n)\right]} \tag{4.7}$$

The vibrationally averaged interaction $\overline{V}_n$ subsequently is defined:

$$\exp\left[-\beta\overline{V}_n(\mathbf{x}_1 \cdots \mathbf{x}_n)\right] = \{\exp\left[-\beta V_n(\mathbf{X}_1 \cdots \mathbf{X}_n)\right]\}_{\mathbf{y}_1 \cdots \mathbf{y}_n = 0} \times \frac{Q_{\text{vib}}^{(n)}(\mathbf{x}_1 \cdots \mathbf{x}_n)}{(Q_{\text{vib}})^n} \tag{4.8}$$

In principle the resulting function $\overline{V}_n$ should depend on temperature. However, under the regime for which normal modes are thermally unexcited, this temperature dependence vanishes.

If the normal modes ω_1, ω_2, and ω_3 were all to shift substantially downward (beside splitting) when molecules came into interaction, the last factor $Q_{\text{vib}}^{(n)}/(Q_{\text{vib}})^n$ would be greater than unity. Consequently $\overline{V}_n$ would be lower than V_n, indicating vibrational stabilization.

A resolution of $\overline{V}_N$ analogous to that shown in (3.2) for V_N is possible. However, the construction definition (4.8) implies that vibrationally averaged pair potentials $\overline{V}^{(2)}$ are the lowest-order components:

$$\overline{V}_N(\mathbf{x}_1 \cdots \mathbf{x}_N) = \sum_{n=2}^{N} \sum_{i_1 < \cdots < i_n = 1}^{N} \overline{V}^{(n)}(\mathbf{x}_{i_1} \cdots \mathbf{x}_{i_n}) \tag{4.9}$$

The inverse relations are

$$\begin{aligned} &\overline{V}^{(2)}(\mathbf{x}_1, \mathbf{x}_2) \equiv \overline{V}_2(\mathbf{x}_1, \mathbf{x}_2) \\ &\overline{V}^{(3)}(\mathbf{x}_1, \mathbf{x}_2, \mathbf{x}_3) = \overline{V}_3(\mathbf{x}_1, \mathbf{x}_2, \mathbf{x}_3) - \overline{V}^{(2)}(\mathbf{x}_1, \mathbf{x}_2) - \overline{V}^{(2)}(\mathbf{x}_1, \mathbf{x}_3) - \overline{V}^{(2)}(\mathbf{x}_2, \mathbf{x}_3) \end{aligned} \tag{4.10}$$

with $\overline{V}^{(n)}$ written in general as $\overline{V}_n$ minus all possible component $\overline{V}^{(j)}$ with $j < n$.

We noted earlier that dispersion attraction is one of the important contributions to $V^{(2)}$, and that it arises from correlation of the electron distributions in the quantum mechanically fluctuating dipole moments. Now $\overline{V}^{(2)}$ includes an extra dispersion attraction due to correlation in fluctuations of molecular dipole moments due to normal mode vibrations.

Although the rigid-rotor potentials $\overline{V}_N$ have been developed in the context of the semiclassical partition function Q, the detailed classical mechanics with $\overline{V}_N$ is itself a valid object for attention. The coupled Newton–Euler

equations of motion provide the time evolution of the system from which linear transport coefficients (viscosity, self-diffusion constant, thermal conductivity, etc.) can be extracted in principle.

B. Molecular Distribution Functions

The Boltzmann factor integrand $\exp(-\beta\bar{V}_N)$ for the semiclassical partition function represents the occurrence probability for any arbitrary configuration of all N molecules. It therefore contains all structural information about the system. But normally N is very large, and for mathematical purposes it is permitted to pass to infinity (with fixed system density—the so-called thermodynamical limit). A more compact way of describing equilibrium molecular arrangements is therefore warranted, one that conveys intensive structural information without suffering the divergences of extensive properties in the large-system limit. The generic molecular distribution functions fulfill this role. They also provide an efficient bridge between molecular configurational correlations and macroscopic thermodynamical properties.

Within the canonical ensemble description of our semiclassical water model, the n-molecule distribution function $\rho^{(n)}$ is obtained through the definition $(1 \leq n \leq N)$:

$$\rho^{(n)}(\mathbf{x}_1 \cdots \mathbf{x}_n) = \frac{N(N-1)\cdots(N-n+1)\int d\mathbf{x}_{n+1}\cdots\int d\mathbf{x}_N \exp(-\beta\bar{V}_N)}{\int d\mathbf{x}_1\cdots\int d\mathbf{x}_N \exp(-\beta\bar{V}_N)} \tag{4.11}$$

where integrations cover orientation, and the volume $\mathcal{V}$ made available to each of the molecules by container walls (or mathematical boundary conditions). Considering a set of infinitesimal six-dimensional volume elements $d\mathbf{x}_1, \ldots, d\mathbf{x}_n$, respectively, surrounding configuration points $\mathbf{x}_1, \ldots, \mathbf{x}_n$, the product

$$\rho^{(n)}(\mathbf{x}_1 \cdots \mathbf{x}_n)\, d\mathbf{x}_1 \cdots d\mathbf{x}_n \tag{4.12}$$

equals the probability that those volume elements simultaneously contain molecules.

If the temperature and density conditions correspond thermodynamically to a single fluid phase, $\rho^{(1)}(\mathbf{x}_1)$ will be independent of $\mathbf{x}_1$:

$$\rho^{(1)}(\mathbf{x}_1) = \frac{N}{8\pi^2\mathcal{V}} \tag{4.13}$$

except in a thin region near a boundary where forces between water molecules and the wall can induce inhomogeneity and orientational anisotropy. The ordinary number density $N/\mathcal{V}$ comprises molecules of all orientations, and

so may be obtained by integrating the homogeneous fluid $\rho^{(1)}$ over Euler angles α_1, β_1, and γ_1:

$$\int_0^{2\pi} d\alpha_1 \int_0^{\pi} \sin\beta_1 \, d\beta_1 \int_0^{2\pi} d\gamma_1 \, \rho^{(1)}(\mathbf{x}_1) = \frac{N}{\mathcal{V}} \tag{4.14}$$

If the temperature and density correspond instead to the existence of one of the ice polymorphs everywhere throughout $\mathcal{V}$, the boundary conditions *may* serve to produce a single essentially fixed crystal. In that event $\rho^{(1)}(\mathbf{x}_1)$ would possess the periodicity and symmetry of the unit cell involved.

Regardless of which state of aggregation prevails (crystalline, liquid, or vapor), provided that just one phase is present, the distribution functions of order $n > 1$ exhibit an asymptotic factorization property. This occurs when the given set of molecular configuration coordinates $\mathbf{x}_1, \ldots, \mathbf{x}_n$ falls into two widely separated subsets, say, $\mathbf{x}_1, \ldots, \mathbf{x}_m$ and $\mathbf{x}_{m+1}, \ldots, \mathbf{x}_n$. In this circumstance the molecular correlations operate only within the subsets, not between them. The resulting asymptotic behavior of $\rho^{(n)}(\mathbf{x}_1, \ldots, \mathbf{x}_n)$ is found to be

$$\rho^{(n)}(\mathbf{x}_1 \cdots \mathbf{x}_n) \to \left[\frac{(N-m)\cdots(N-n+1)}{N\cdots(N-n+m+1)}\right] \rho^{(m)}(\mathbf{x}_1 \cdots \mathbf{x}_m)\rho^{(n-m)}(\mathbf{x}_{m+1} \cdots \mathbf{x}_n) \tag{4.15}$$

The leading numerical factor $[\cdots]$ arises from the normalization inherent in definition (4.11); with fixed n and m it approaches unity as N increases to infinity. By obvious extension, $\rho^{(n)}$ reduces substantially to a product of lower-order functions for any partitioning of $\mathbf{x}_1, \ldots, \mathbf{x}_n$ into any number of widely separated subsets. In any event the rate of approach to factored form is at its slowest with respect to separation distance when the system is at its liquid-vapor critical point.[41]

Apply the six-dimensional gradient operator ∇_1 (corresponding to vector $\mathbf{x}_1$) to both sides of (4.11). After rearrangement, and use of (4.11) itself, the result takes the form

$$\begin{aligned}\nabla_1 W_n(1,\ldots,n) &= \nabla_1 \overline{V}_n(1,\ldots,n) \\ &\quad + \sum_{l=1}^{n} \sum_{m=1}^{N-m} \sum_{i_1 < \cdots < i_l = 1}^{n} \frac{1}{m!} \int d\mathbf{x}_{n+1} \cdots \int d\mathbf{x}_{n+m} \\ &\quad \times [\nabla_1 \overline{V}^{(l+m)}(i_1,\ldots,i_l,n+1,\ldots,n+m)] \frac{\rho^{(n+m)}(1,\ldots,n+m)}{\rho^{(n)}(1,\ldots,n)}\end{aligned} \tag{4.16}$$

where we have set

$$\rho^{(n)}(1\cdots n) = \frac{N\cdots(N-n+1)}{(8\pi^2\mathscr{V})^n}\exp\left[-\beta W_n(1\cdots n)\right] \tag{4.17}$$

Equation (4.16) is a generalized form of the Born–Green–Yvon integro-differential equation that has often been used for the calculation of distribution functions for simple liquids.[42] Its interpretation is straightforward. The first term in the right member of (4.16) is the negative of the generalized force acting on the molecule at $\mathbf{x}_1$ due to those held fixed at $\mathbf{x}_2, \ldots, \mathbf{x}_n$; succeeding terms provide the corresponding effect of the average generalized force at $\mathbf{x}_1$ attributable to the material medium surrounding the fixed set of molecules at $\mathbf{x}_1, \ldots, \mathbf{x}_n$. Thus $-\nabla_1 W_n$ is the total mean force on the molecule at $\mathbf{x}_1$, given that $n-1$ others are present at $\mathbf{x}_2, \ldots, \mathbf{x}_n$. It is therefore appropriate (and traditional) to call the W_n "potentials of mean force."

The singlet potential of mean force $W_1(\mathbf{x}_1)$ vanishes in uniform isotropic fluids, but for crystals it does not vanish if boundary conditions or wall forces serve to clamp the crystal in place. In this case $W_1(\mathbf{x}_1)$ expresses the fact that long-range order in the crystal acts through intermolecular forces to confine and orient any molecule to fit properly into the prevailing lattice. In any event a stoichiometric condition applies to $W^{(1)}$, owing to the fact that the integral of $\rho^{(1)}$ over orientations, and inside a unit cell τ, is fixed by structural parameters:

$$\frac{N}{8\pi^2\mathscr{V}}\int_\tau d\mathbf{x}_1 \exp\left[-\beta W^{(1)}(\mathbf{x}_1)\right] = n_\tau - n_v + n_i \tag{4.18}$$

Here n_τ stands for the number of molecules per unit cell in the perfect crystal, while n_v and n_i, respectively, stand for the average number of vacancies and interstitials per unit cell at the ambient temperature and pressure.

In the large-system limit ($N \to \infty$ with $N/\mathscr{V}$ held constant), the asymptotic factorization property (4.15) for $\rho^{(n)}$ is obviously equivalent to an asymptotic subset additivity reduction for the Ws:

$$W_n(\mathbf{x}_1\cdots\mathbf{x}_n) \to W_m(\mathbf{x}_1\cdots\mathbf{x}_m) + W_{n-m}(\mathbf{x}_{m+1}\cdots\mathbf{x}_n) \tag{4.19}$$

Unlike fluids, crystals are capable of supporting strain fields under the influence of suitable perturbations. For nearly all choices of configurations $\mathbf{x}_1, \ldots, \mathbf{x}_m$ to be inhabited by molecules, a strain field would be expected to arise which would radiate outward from the location of that subset as a slowly diminishing modulation of the normal crystallographic pattern. This strain field is surely capable of carrying correlation to the other subset, provided that the strain field still has a nonnegligible magnitude at its neighborhood. Thus the rate of attainment of the reduction (4.19) with respect to increasing subset separation is controlled by crystal elasticity.

The implied range of correlation should exceed that applicable in fluids, except at the critical point for the latter.

The pair distribution $\rho^{(2)}(\mathbf{x}_1, \mathbf{x}_2)$ conveys useful information about the modes of packing of molecules in the liquid state. In particular it can be used to calculate the mean number of neighbors $\nu(R)$ possessed by any given molecule 1, as a function of the radial distance R out to which neighbors are counted. Specifically,

$$\begin{aligned} \nu(R) &= \frac{8\pi^2\mathscr{V}}{N} \int_{R_{12}<R} \rho^{(2)}(\mathbf{x}_1, \mathbf{x}_2)\, d\mathbf{x}_2 \\ &= \frac{N}{8\pi^2\mathscr{V}} \int_{R_{12}<R} \exp\left[-\beta W_2(\mathbf{x}_1, \mathbf{x}_2)\right] d\mathbf{x}_2 \end{aligned} \tag{4.20}$$

where for the second form we have supposed that N is very large. Although this expression is formally correct for any choice of center for all the molecules, it is most informative in our specific application to choose the oxygen nucleus to play this role. Consequently, the running coordination number $\nu(R)$ counts oxygen nuclei lying within a sphere with radius R drawn about a specific oxygen (although the count excludes the central oxygen).

We know from the generalized Born–Green–Yvon equation [see (4.16)] that an important component of $W_2(\mathbf{x}_1, \mathbf{x}_2)$ is the direct pair interaction $\overline{V}^{(2)}(\mathbf{x}_1, \mathbf{x}_2)$. It is natural to inquire if this is the overwhelmingly predominant contributor to W_2 for near neighbors (those close enough to form an unstrained hydrogen bond), or if indirect contributions from the surrounding medium are important.

Information is available to estimate $\nu(R)$ with W_2 simplified to $\overline{V}^{(2)}$ in (4.20).[40] An absurd conclusion follows from this simplification, namely, that in liquid water near its melting point every molecule has about 10^2 neighbors within 4 Å. Such spontaneous crowding is obviously inconsistent with the strong repulsions operative between molecules closer than 2.5 Å. The problem clearly has its origin in the fact that the pair Boltzmann factor

$$\exp\left[-\beta \overline{V}^{(2)}(\mathbf{x}_1, \mathbf{x}_2)\right] \tag{4.21}$$

at low temperature takes on enormously large values when $\mathbf{x}_1$, $\mathbf{x}_2$ lead to a maximally stabilizing hydrogen bond, and the corresponding approximate $\nu(R)$ picks up a spuriously large contribution.

Evidently, $\overline{V}^{(2)}$ must be largely counterbalanced by indirect medium contributions to W_2. The physical necessity for such repulsive contributions to W_2 is easy to understand. In order that a molecule at $\mathbf{x}_2$ will be able to approach one held fixed at $\mathbf{x}_1$ so as to form the hydrogen bond described by $\overline{V}^{(2)}(\mathbf{x}_1, \mathbf{x}_2)$, it will almost certainly have to expel another molecule in its way. At a low temperature the other molecule is likely enjoying its own

hydrogen bond. Thus one hydrogen bond will have to be broken to form the intended one.

The close balance between direct and indirect interactions in W_2 is particularly crucial in the case of low-temperature ice. As temperature T declines toward absolute zero, Boltzmann factor (4.21) diverges to infinity, although the coordination number remains four precisely, that is, $\nu(R)$ is

$$\lim_{T\to 0} \nu(R) = 4 \qquad 3\ \text{Å} \leq R \leq 4\ \text{Å} \tag{4.22}$$

It is incumbent on any statistical theory of $\rho^{(2)}$ in water to pay particular attention to the competitive balance between W_2 contributions whether the liquid or the solid state is involved.

C. Distribution Function Formulas

Within the regime of applicability of the semiclassical approximation, the average energy per particle

$$\frac{E}{N} = \left[\frac{\partial(\beta F/N)}{\partial\beta}\right]_{\rho} \tag{4.23}$$

consists of:

$$\frac{E}{N} = \frac{E_{\text{vib}} + E_{\text{kin}} + \langle \overline{V}_N \rangle}{N} \tag{4.24}$$

[Here we have assumed that $\overline{V}_N$ is temperature-independent, as will surely be the case at about room temperature. However, at high temperatures where vibrational excitations occur, the last term would have to be replaced by $\langle \partial(\beta \overline{V}_N)/\partial\beta \rangle$.] The vibrational energy may be computed from Q_{vib}, [see (4.5)]:

$$\begin{aligned} \frac{E_{\text{vib}}}{N} &= -\frac{\partial \ln Q_{\text{vib}}}{\partial\beta} \\ &= \sum_{\alpha=1}^{3} \hbar\omega_\alpha \left[\frac{1}{2} + \frac{\exp(-\beta\hbar\omega_\alpha)}{1 - \exp(-\beta\hbar\omega_\alpha)}\right] \end{aligned} \tag{4.25}$$

At about room temperature $\exp(-\beta\hbar\omega_\alpha)$ is negligible for all three normal modes. The kinetic energy E_{kin} consists of classical rotational and translational parts $k_B T/2$ for each degree of freedom, so that

$$E_{\text{kin}} = 3k_B T \tag{4.26}$$

The average intermolecular potential energy

$$\langle \overline{V}_N \rangle = \frac{\int d\mathbf{x}_1 \cdots \int d\mathbf{x}_N \overline{V}_N \exp(-\beta \overline{V}_N)}{\int d\mathbf{x}_1 \cdots \int d\mathbf{x}_N \exp(-\beta \overline{V}_N)} \tag{4.27}$$

may be expressed in terms of molecular distribution functions by inserting relation (4.9) for $\overline{V}_N$ into (4.27), followed by repeated use of the $\rho^{(n)}$ definition (4.11). The final energy formula is found to be

$$\frac{E}{N} = -\frac{\partial \ln Q_{\text{vib}}}{\partial \beta} + 3k_B T + \sum_{n=2}^{N} \frac{1}{n!N} \int \overline{V}^{(n)}(\mathbf{x}_1 \cdots \mathbf{x}_n)\rho^{(n)}(\mathbf{x}_1 \cdots \mathbf{x}_n)\, d\mathbf{x}_1 \cdots d\mathbf{x}_n \tag{4.28}$$

The thermodynamic pressure p can also be put into molecular distribution function form, starting from the identity

$$p = -\left(\frac{\partial F}{\partial \mathscr{V}}\right)_\beta \tag{4.29}$$

In order to carry out the volume derivative of ln Q required by this identity, it is convenient to use a position-coordinate scaling originally devised by Green.[43] The volume is taken to have the shape of a cube. Then the positions $\mathbf{R}_j$ of molecular centers are related to reduced positions $\mathbf{s}_j$ by the transformation ($1 \leq j \leq N$)

$$\mathbf{R}_j = \mathscr{V}^{1/3}\mathbf{s}_j \tag{4.30}$$

The components of each $\mathbf{s}_j$ have limits 0 and 1, so in terms of these new variables the volume dependence of the configuration integral in Q becomes transferred to the arguments of $\overline{V}_N$. After employing the $\overline{V}_N$ expansion (4.9) once again, and carrying out the $\mathscr{V}$ differentiation under the integrals, the "virial" pressure equation of state is obtained in the form

$$p = \frac{N}{\beta\mathscr{V}} - \frac{1}{3\mathscr{V}} \sum_{n=2}^{N} \frac{1}{n!} \int d\mathbf{x}_1 \cdots \int d\mathbf{x}_n \times [(\mathbf{R}_1 \cdot \nabla_{R_1} + \cdots + \mathbf{R}_n \cdot \nabla_{R_n})V^{(n)}(\mathbf{x}_1 \cdots \mathbf{x}_n)]\rho^{(n)}(\mathbf{x}_1 \cdots \mathbf{x}_n) \tag{4.31}$$

Next consider a subvolume $\mathscr{V}_0$ contained entirely within $\mathscr{V}$. The average number of molecules N_0 to be found with centers in $\mathscr{V}_0$ can be calculated by integrating $\rho^{(1)}$ over all orientations, and over positions in this subvolume:

$$\langle N_0 \rangle = \int_{\mathscr{V}_0} \rho^{(1)}(\mathbf{x}_1)\, d\mathbf{x}_1 \tag{4.32}$$

Analogously, the number of pairs of molecules $\frac{1}{2}N_0(N_0 - 1)$ has an average given by a $\rho^{(2)}$ integral over the same region:

$$\langle \tfrac{1}{2}N_0(N_0 - 1) \rangle = \tfrac{1}{2} \int_{\mathscr{V}_0} d\mathbf{x}_1 \int_{\mathscr{V}_0} d\mathbf{x}_2\, \rho^{(2)}(\mathbf{x}_1, \mathbf{x}_2) \tag{4.33}$$

Hence

$$\langle N_0^2 \rangle - \langle N_0 \rangle^2 = \langle N_0 \rangle + \int_{\mathscr{V}_0} d\mathbf{x}_1 \int_{\mathscr{V}_0} d\mathbf{x}_2 \, [\rho^{(2)}(\mathbf{x}_1, \mathbf{x}_2) - \rho^{(1)}(\mathbf{x}_1)\rho^{(1)}(\mathbf{x}_2)] \tag{4.34}$$

Although the last equation is formally exact for any volume $\mathscr{V}$ and subvolume $\mathscr{V}_0$, it is most informative in the $\mathscr{V} \to \infty$ limit, for then the surroundings of $\mathscr{V}_0$ act as an infinite reservoir of particles whose intensive properties are not perturbed by fluctuations in N_0. Furthermore, $\mathscr{V}_0$ may subsequently be presumed to have macroscopic dimensions, and the number fluctuation for $\mathscr{V}_0$ shown in (4.34) must then be related in standard fashion to the isothermal compressibility κ_T:[44]

$$\begin{gathered} \langle N_0^2 \rangle - \langle N_0 \rangle^2 = \frac{\langle N_0 \rangle^2 k_B T \kappa_T}{\mathscr{V}_0} \\ \kappa_T = -\left(\frac{\partial \ln \mathscr{V}}{\partial p} \right)_{N,T} \end{gathered} \tag{4.35}$$

Therefore (4.34) may be cast in the following alternative relation:

$$\rho^2 k_B T \kappa_T = \rho + \mathscr{V}_0^{-1} \int_{\mathscr{V}_0} d\mathbf{x}_1 \int_{\mathscr{V}_0} d\mathbf{x}_2 \, [\rho^{(2)}(\mathbf{x}_1, \mathbf{x}_2) - \rho^{(1)}(\mathbf{x}_1)\rho^{(1)}(\mathbf{x}_2)] \tag{4.36}$$

where we have written ρ for the macroscopic number density $\langle N_0 \rangle / \mathscr{V}_0$. The most striking feature of this result in comparison with the energy and pressure equations (4.28) and (4.31) is that no distribution functions of order greater than two are required, regardless of the nature of $\overline{V}_N$.

In the event that an isotropic liquid or vapor phase inhabits the system, (4.36) may be simplified somewhat:

$$\rho k_B T \kappa_T = 1 + \frac{8\pi^2}{\rho} \int d\mathbf{x}_2 \left[\rho^{(2)}(\mathbf{x}_1, \mathbf{x}_2) - \left(\frac{\rho}{8\pi^2} \right)^2 \right] \tag{4.37}$$

Here we have assumed that $\rho^{(2)}$ is strictly the limit function for an infinite system size and, as a consequence, it has been possible to extend the position part of the $\mathbf{x}_2$ integration to infinity.

Finally, we note that standard techniques are available to expand the molecular distribution functions in a density power series[45] valid for description of the vapor. To leading order $\rho^{(n)}$ is of course proportional to ρ^n. The

specific density series for the infinite system pair distribution function begins with these terms:

$$\rho^{(2)}(\mathbf{x}_1, \mathbf{x}_2) = \left(\frac{\rho}{8\pi^2}\right)^2 \exp\left[-\beta\overline{V}^{(2)}(\mathbf{x}_1, \mathbf{x}_2)\right] \times \left\{1 + \frac{\rho}{8\pi^2}\int d\mathbf{x}_3\, f(\mathbf{x}_1, \mathbf{x}_3) f(\mathbf{x}_3, \mathbf{x}_2) + \frac{\rho}{8\pi^2}\int d\mathbf{x}_3 \exp\left[-\beta\overline{V}^{(2)}(\mathbf{x}_1, \mathbf{x}_3) - \beta\overline{V}^{(2)}(\mathbf{x}_3, \mathbf{x}_2)\right] \times \left[\exp\left(-\beta\overline{V}^{(3)}(\mathbf{x}_1, \mathbf{x}_2, \mathbf{x}_3)\right) - 1\right]\right\} + O(\rho^4) \tag{4.38}$$

where the Mayer f function has been introduced following the normal convention:

$$f(\mathbf{x}_i, \mathbf{x}_j) = \exp\left[-\beta\overline{V}^{(2)}(\mathbf{x}_i, \mathbf{x}_j)\right] - 1 \tag{4.39}$$

By using the density expansion for $\rho^{(2)}$ in the compressibility relationship (4.37), it is possible to generate virial coefficients for the pressure:

$$\frac{\beta p}{\rho} = 1 + B(T)\rho + C(T)\rho^2 + \cdots \tag{4.40}$$

The second and third virial coefficients have the integral expressions

$$B(T) = -\frac{1}{2(8\pi^2)}\int d\mathbf{x}_2\, f(\mathbf{x}_1, \mathbf{x}_2) \tag{4.41}$$

$$C(T) = -\frac{1}{3(8\pi^2)^2}\int d\mathbf{x}_2 \int d\mathbf{x}_3 \{f(\mathbf{x}_1, \mathbf{x}_2) f(\mathbf{x}_1, \mathbf{x}_3) f(\mathbf{x}_2, \mathbf{x}_3) + \exp\left[-\beta\overline{V}_3(\mathbf{x}_1, \mathbf{x}_2, \mathbf{x}_3)\right] - \exp\left[-\beta\overline{V}^{(2)}(\mathbf{x}_1, \mathbf{x}_2) - \beta\overline{V}^{(2)}(\mathbf{x}_1, \mathbf{x}_3) - \beta\overline{V}^{(2)}(\mathbf{x}_2, \mathbf{x}_3)\right]\} \tag{4.42}$$

V. EFFECTIVE PAIR POTENTIALS

A. Variational Principle

Both the conceptual and computational aspects of water theory would become significantly streamlined if the total interaction potential were additive, that is, vanishing trimer, tetramer, pentamer, and so on, component potentials. Of course we know this is not strictly the case, and nonadditive components evidently exert considerable influence on at least the thermo-

dynamic properties of water. Even so, it is a legitimate and interesting question to ask if there exists an "effective pair potential," possibly differing substantially from the real molecular pair potential, which alone faithfully reproduces microscopic structure and thermodynamic properties for the true nonadditive water system. We outline a procedure that answers this question affirmatively.[46,47]

The following analysis can actually be carried out at any of several alternative levels. In the most precise version, a full quantum mechanical description applies, for which the partition function Q has previously been displayed as the trace of a density operator. But for present purposes, it suffices in illustrating the general strategy to work at the level of the semiclassical approximation, with Q given by (4.4).

Consider a pair of arbitrary real functions $h_1(\mathbf{x}_1 \cdots \mathbf{x}_N)$ and $h_2(\mathbf{x}_1 \cdots \mathbf{x}_N)$ of the N molecular six-vectors. We define their inner product to be

$$\{h_1, h_2\} = (8\pi^2 \mathscr{V})^{-N} \int d\mathbf{x}_1 \cdots \int d\mathbf{x}_N \, h_1(\mathbf{x}_1 \cdots \mathbf{x}_N) h_2(\mathbf{x}_1 \cdots \mathbf{x}_N) \quad (5.1)$$

where the $\mathbf{x}_j$ run between the same limits that apply to Q, namely, all orientations and positions within volume $\mathscr{V}$. Equation (5.1) is analogous to the ordinary inner product of two vectors, a sum of products of corresponding vector components, in that the integral sums over all differential elements $d\mathbf{x}_1 \cdots d\mathbf{x}_N$ the product of corresponding function components. In terms of our functional inner product, the semiclassical partition function (4.4) becomes

$$Q(\overline{V}_N) = Q(\overline{V}_N = 0)\left\{\exp\left(\frac{-\beta \overline{V}_N}{2}\right), \exp\left(\frac{-\beta \overline{V}_N}{2}\right)\right\} \quad (5.2)$$

Just as the distance between the end points of two vectors may be calculated in terms of the inner product of their difference with itself, we take the "distance" between the two functions h_1 and h_2, $D(h_1, h_2)$, to be

$$D(h_1, h_2) = \{h_1 - h_2, h_1 - h_2\}^{1/2} \quad (5.3)$$

The effective pair potential is denoted by $v(\mathbf{x}_i, \mathbf{x}_j)$. Following the form of (5.2), the effective pair potential approximation to Q can be expressed as

$$Q(\Sigma v) = Q(\overline{V}_N = 0)\left\{\exp\left[-\tfrac{1}{2}\beta \sum_{i<j=1}^{N} v(i,j)\right], \exp\left[-\tfrac{1}{2}\beta \sum_{i<j=1}^{N} v(i,j)\right]\right\} \quad (5.4)$$

We postulate that the optimal choice for the function v is the one for which

$$D\{\exp(-\tfrac{1}{2}\beta \overline{V}_N), \exp[-\tfrac{1}{2}\beta \Sigma v(i,j)]\} = \text{minimum} \quad (5.5)$$

In other words, we require that the Boltzmann function's square root $\exp(-\frac{1}{2}\beta \overline{V}_N)$ literally be approached to the minimum possible distance by the corresponding effective pair potential version.

The variational criterion (5.5) forces the best possible fit over the entire configuration space for the N molecules. This is important, for beyond Q itself we want the molecular distribution functions $\rho^{(n)}$ in the effective pair potential approximation:

$$\rho^{(n)}(\mathbf{x}_1 \cdots \mathbf{x}_N | \Sigma v) = \frac{N \cdots (N-n+1) \int d\mathbf{x}_{n+1} \cdots \int d\mathbf{x}_N \exp\left[-\beta \Sigma v(i,j)\right]}{\int d\mathbf{x}_1 \cdots \int d\mathbf{x}_N \exp\left[-\beta \Sigma v(i,j)\right]}, \tag{5.6}$$

also to represent properly the detailed microscopic structure present in the system.

By setting the first functional derivative of (5.5) with respect to v equal to zero, we derive an integral equation for the determination of v:

$$\int d\mathbf{x}_3 \cdots \int d\mathbf{x}_N \exp\left\{-\tfrac{1}{2}\beta\left[\overline{V}_N(\mathbf{x}_1 \cdots \mathbf{x}_N) + \sum_{i<j=1}^{N} v(\mathbf{x}_i, \mathbf{x}_j)\right]\right\}$$
$$= \int d\mathbf{x}_3 \cdots \int d\mathbf{x}_N \exp\left\{-\beta \sum_{i<j=1}^{N} v(\mathbf{x}_i, \mathbf{x}_j)\right\} \tag{5.7}$$

On account of the nonlinearity of this equation in the unknown function v, and because of the high-order multiple integrals, one cannot expect generally to extract the exact solution. However, it should be clear that the effective pair potential can vary somewhat with temperature and density.

Integration of both sides of (5.7) over $\mathbf{x}_1$ and $\mathbf{x}_2$ leads to the relation

$$Q(\tfrac{1}{2}\overline{V}_N + \tfrac{1}{2}\Sigma v) = Q(\Sigma v) \tag{5.8}$$

or what amounts to the same thing for the Helmholtz free energy:

$$F(\tfrac{1}{2}\overline{V}_N + \tfrac{1}{2}\Sigma v) = F(\Sigma v) \tag{5.9}$$

Thus the optimally chosen effective pair potential is such that its corresponding free energy is unchanged by the operation of averaging the effective additive interaction with the true nonadditive interaction $\overline{V}_N$. Similar results apply to $\rho^{(1)}$ and $\rho^{(2)}$, which follow directly from (5.7) after dividing by its integral over $\mathbf{x}_1$ and $\mathbf{x}_2$:

$$\rho^{(1)}(\mathbf{x}_1 | \tfrac{1}{2}\overline{V}_N + \tfrac{1}{2}\Sigma v) = \rho^{(1)}(\mathbf{x}_1 | \Sigma v) \tag{5.10}$$

$$\rho^{(2)}(\mathbf{x}_1, \mathbf{x}_2 | \tfrac{1}{2}\overline{V}_N + \tfrac{1}{2}\Sigma v) = \rho^{(2)}(\mathbf{x}_1, \mathbf{x}_2 | \Sigma v) \tag{5.11}$$

However, these identities do not extend to higher-order $\rho^{(n)}$ (although they would if the procedure were applied to the determination of n-molecule effective interactions v_n, with $n > 2$).

The Schwartz inequality[48] implies that

$$Q(\overline{V}_N) Q(\Sigma v) \geq [Q(\tfrac{1}{2}\overline{V}_N + \tfrac{1}{2}\Sigma v)]^2 \tag{5.12}$$

This, in concert with the earlier result (5.8), leads to

$$Q(\overline{V}_N) \geq Q(\Sigma v) \tag{5.13}$$

In terms of free energies, the direction of the inequality is reversed:

$$F(\overline{V}_N) \leq F(\Sigma v) \tag{5.14}$$

Thus the operation of forcing the system of molecules to conform to an effective pair potential never lowers the free energy.

For pedagogical reasons we can write $\overline{V}_N$ as its strictly additive part, plus a perturbation:

$$\overline{V}_N(1 \cdots N) = \sum_{i<j=1}^{N} \overline{V}^{(2)}(i, j) + \lambda V^{\dagger}(1 \cdots N) \tag{5.15}$$

where λ is a formal perturbation parameter destined ultimately to be set equal to unity, and

$$V^{\dagger}(1 \cdots N) = \sum_{n=3}^{N} \sum_{i_1 < \cdots < i_n = 1}^{N} \overline{V}^{(n)}(i_1 \cdots i_n) \tag{5.16}$$

Imagining λ to increase continuously from zero to unity, the free energy F as well as $\rho^{(1)}$ and $\rho^{(2)}$ will display first-order changes with λ. However, (5.9) to (5.11) imply that v changes from $\overline{V}^{(2)}$ during this coupling process in just such a way that $F(\Sigma v)$, $\rho^{(1)}(\mathbf{x}_1 | \Sigma v)$, and $\rho^{(2)}(\mathbf{x}_1, \mathbf{x}_2 | \Sigma v)$ all manifest exactly the correct leading linear behavior in λ. Although one can propose other effective pair potentials which selectively fit thermodynamical properties[49] or pair distribution functions,[50] it is only the variationally defined function v satisfying (5.7) that simultaneously eliminates first-order errors in F, $\rho^{(1)}$, and $\rho^{(2)}$.

It is possible to develop v in a density power series. The manipulations required are tedious, and are not reproduced here. Instead, we state the result through first order in ρ:[47]

$$v(\mathbf{x}_1, \mathbf{x}_2) = \overline{V}^{(2)}(\mathbf{x}_1, \mathbf{x}_2) + \frac{\rho}{8\pi^2\beta} [\varphi_s(\mathbf{x}_1, \mathbf{x}_2) + \varphi_l] + O(\rho^2) \tag{5.17}$$

$$\varphi_s(\mathbf{x}_1, \mathbf{x}_2) = -2 \int d\mathbf{x}_3 \exp [-\beta \overline{V}^{(2)}(\mathbf{x}_1, \mathbf{x}_3) - \beta \overline{V}^{(2)}(\mathbf{x}_2, \mathbf{x}_3)] \times \{\exp [-\tfrac{1}{2}\beta \overline{V}^{(3)}(\mathbf{x}_1, \mathbf{x}_2, \mathbf{x}_3)] - 1\} \tag{5.18}$$

$$\varphi_l = \frac{1}{6\pi^2 \mathscr{V}} \int d\mathbf{x}_3 \int d\mathbf{x}_4 \exp [-\beta \overline{V}^{(2)}(\mathbf{x}_1, \mathbf{x}_3) - \beta \overline{V}^{(2)}(\mathbf{x}_1, \mathbf{x}_4) - \beta \overline{V}^{(2)}(\mathbf{x}_3, \mathbf{x}_4)] \times \{\exp [-\tfrac{1}{2}\beta \overline{V}^{(3)}(\mathbf{x}_1, \mathbf{x}_3, \mathbf{x}_4)] - 1\} \tag{5.19}$$

Only clusters of three or fewer molecules can contribute in this density order, so the only nonadditivity that can be involved is that for trimers. Since $\overline{V}^{(2)}$ and $\overline{V}^{(3)}$ drop to zero with increasing separation, so too will φ_s. However, φ_l is independent of separation; although it is inversely proportional to $\mathscr{V}$ and thus very small for a large system, its effect when summed over all $N(N-1)/2$ pairs of molecules is thermodynamically significant.

Using the effective pair potential, the analog of energy expression (4.28) is

$$\frac{E}{N} = -\frac{\partial \ln Q_{\text{vib}}}{\partial \beta} + 3k_B T + \frac{1}{2N}\int \left\{\frac{\partial[\beta v(\mathbf{x}_1, \mathbf{x}_2)]}{\partial \beta}\right\}_{N,\mathscr{V}} \rho^{(2)}(\mathbf{x}_1, \mathbf{x}_2 | \Sigma v)\, d\mathbf{x}_1\, d\mathbf{x}_2 \tag{5.20}$$

while the virial equation of state (4.31) is modified to

$$\frac{\beta p}{\rho} = 1 - \frac{4\pi^2 \beta}{\rho}\int d\mathbf{x}_2 \left\{\frac{1}{3}\mathbf{R}_{12}\cdot \nabla_{R_{12}} v(\mathbf{x}_1, \mathbf{x}_2) - \rho\left(\frac{\partial v(\mathbf{x}_1, \mathbf{x}_2)}{\partial \rho}\right)\right\} \times \rho^{(2)}(\mathbf{x}_1, \mathbf{x}_2 | \Sigma v) \tag{5.21}$$

In both these expressions it is important to realize that v does not drop quite to zero with increasing separation R_{12}, but retains a constant value proportional to $\mathscr{V}^{-1}$. It is the presence of this "tail" on v of indefinite range that invalidates the compressibility theorem (4.36), except as a description of local fluctuations, although a complicated modification can be derived.[46]

B. Physical Interpretation

In our survey of water molecule interactions (Section III), it was pointed out that the average effect of nonadditive components of the potential $\overline{V}_N$ was to strengthen hydrogen bond networks, while reducing the length of the component hydrogen bonds somewhat. These influences must be felt by the effective pair potential v. It seems hard to escape the conclusion that the absolute minimum of v is lower than that of the bare pair potential $\overline{V}^{(2)}$, and that this v minimum occurs at a smaller separation.

Since nonadditivity contributes extra binding energy to an assembly of water molecules, a hypothetical water model in which the molecules interact only via the strict pair interactions $\overline{V}^{(2)}$ would necessarily possess lower melting and boiling points. Evidently, the increased strength of v compared to $\overline{V}^{(2)}$ would tend to bring these phase-transition temperatures back up again.

The melting and boiling transitions are first order, with a discontinuous change in molar volume going from one homogeneous phase to the other. With fixed N, $\mathscr{V}$ may be chosen so that ρ lies between the values for coexisting

phases (say, liquid and vapor). In this case the system is macroscopically inhomogeneous, for surface tension will cause agglomeration of the phases into large crystals, droplets, or bubbles. The molecular distribution functions $\rho^{(n)}$ will be profoundly affected by this macroscopic inhomogeneity, displaying slow variations with respect to positions over distances comparable to crystal droplet or bubble diameters.

The effective pair potential is permitted full functional freedom within its defining variational principle (5.5). In particular, it can adopt forms with just the proper coupling strength to reproduce the correct phase transitions exhibited by $\overline{V}_N$. Since the distance D involved is always to be minimized, and since it would be expected to be very large if $\overline{V}_N$ caused phase separation and Σv did not (or vice versa), it seems likely that the effective pair potential approximation should reproduce the given first-order phase changes. In fact, we postulate that in a large-system limit $\overline{V}_N$ and Σv will have *exactly* the same phase diagrams in the T, ρ plane. Furthermore, the corresponding crystalline phases should have the same symmetry properties.

It is interesting to note that the liquid-vapor critical point for water ($T = 374.15°C$, $p = 221.2$ bars, $\rho = 0.32$ g/cm^3) experimentally seems to share with other liquids the conventional set of nonclassical critical exponents.[51] This universality of critical exponents implies insensitivity to most details of the underlying molecular interactions. Consequently, replacement of $\overline{V}_N$ by the proper Σv should involve no change in the critical-point temperature and density, and the required v itself should not entail singular temperature and density variations.

The density expansion (5.17) to (5.19) illustrates the fact that generally v separates into two parts:

$$v(\mathbf{x}_1, \mathbf{x}_2) = v_s(\mathbf{x}_1, \mathbf{x}_2) + \frac{v_l}{\mathcal{V}} \tag{5.22}$$

a short-range part v_s which goes to zero with increasing separation, and a weak constant tail inversely proportional to $\mathcal{V}$ at constant T and ρ. Clearly, this tail has no effect on molecular distribution functions, since it has the same value from one configuration to the next. However, the short-range function v_s, which is necessary to give optimal $\rho^{(n)}$s, does not by itself give an optimal free energy. The long-range tail provides the necessary correction.

In a dense liquid or crystalline phase, each molecule is surrounded by a rather closely packed multitude of neighbors. From a numerical viewpoint it would probably be feasible to simulate the free-energy effect of $v_l/\mathcal{V}$ by a spatially slowly decaying component of v_s instead. Because the neighbors are closely spaced, they would respond negligibly to this geometric compression of the truly long-range tail of v into v_s. Thus, as a practical matter, explicit consideration of $v_l/\mathcal{V}$ may be quite unnecessary for condensed

phases. This possibility is especially clear for low-temperature crystals whose structure and vibrational properties would not be changed by constant shifts in v at each of the first few neighbor shell distances, although of course the free energy *would* be correspondingly affected.

An invariant ratio of the different types of bonded trimers was mentioned earlier for all four-coordinated networks, leading to overall stabilization. Temperature rise causes bond breakage in these networks (most notably at the melting point), and at very high temperatures nearly all trimers are disrupted and no enhanced stability for hydrogen bonds applies. But during the course of temperature rise, the ratio of sequential, double-donor, and double-acceptor molecules need not remain fixed. Figure 12 shows how alternative choices for the scission of two hydrogen bonds impinging on a single network molecule can remove different ratios of trimers (although always 11 of all kinds). As a result, we would expect the destabilizing double-donor and double-acceptor trimers to disappear at a greater initial rate than the stabilizing sequential trimers. Just above the melting point, v can in this

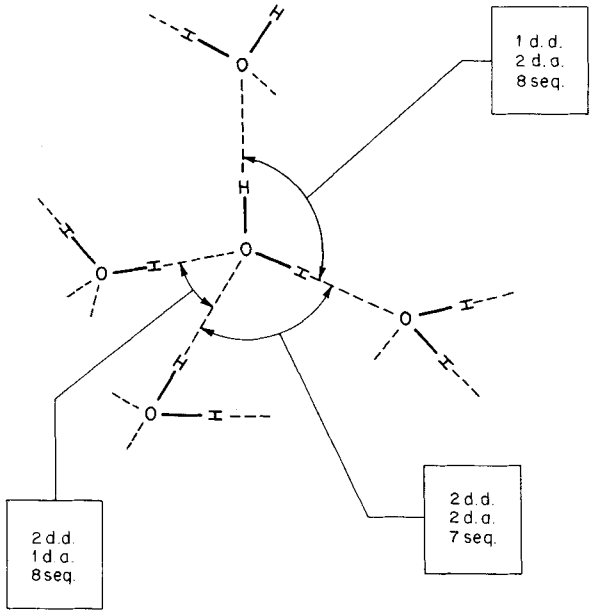

Fig. 12 Trimers disrupted by breaking two hydrogen bonds emanating from the same network molecule. d.d., Double donor; d.a., double acceptor; seq., sequential trimer. In view of the signs of the trimer nonadditivities, it is energetically least costly to break the two bonds if one and only one incorporates a proton of the central molecule.

fashion maintain its greater hydrogen bond strength and shorter length relative to $\overline{V}^{(2)}$; the temperature variation in v may thus be negligible in this range.

VI. LATTICE THEORIES

A. General Formulation

In approximating the definite integral

$$I(a, b) = \int_a^b F(t)\, dt \tag{6.1}$$

by the rectangle rule, the interval $a \leq t \leq b$ is divided into M equal intervals with midpoints

$$t_i = a + \frac{(b - a)(2i - 1)}{2M}, \qquad i = 1, 2, \ldots, M \tag{6.2}$$

and then I is represented by a suitably normalized sum of the integrand over these midpoints:

$$I(a, b) \cong \frac{b - a}{M} \sum_{i=1}^{M} F(t_i) \tag{6.3}$$

The lattice gas partition function Q_l bears the same relationship to the semiclassical partition function Q [see (4.4)] that the rectangle rule approximation (6.3) does to the starting integral (6.1). To establish the relationship for the partition functions, the six-dimensional configuration space available to the rigid-rotor molecules must be divided into equivalent cells whose centers are analogs of the midpoints t_i.

First let the three-dimensional volume $\mathscr{V}$ be uniformly covered by a lattice of $\mathscr{M}$ equivalent points. We shall always want

$$\mathscr{M} > N \tag{6.4}$$

so that the number of discrete locations exceeds the number of molecules and, as a general matter, the limit of $\mathscr{M}$ tending to infinity is ultimately of interest. For the moment we leave open the choice of specific lattice type (simple cubic, body-centered cubic, diamond, face-centered cubic, etc.), but for every lattice there exists a corresponding division of $\mathscr{V}$ into nearest-neighbor polyhedra.[52] These polyhedra are convex and congruent, contain single lattice points at their inversion centers, and are the loci of all positions closer to this central lattice point than to any other lattice point. On account of the last property, they are bounded by midplanes constructed on line segments connecting lattice points.

The volume of each nearest-neighbor polyhedron is denoted by

$$\tau = \frac{\mathscr{V}}{\mathscr{M}} \tag{6.5}$$

By selecting a very anisotropic lattice, it is possible to produce polyhedra that are very long in one or two directions at the expense of the third. For present purposes we specifically avoid this situation, and suppose that the polyhedra are reasonably compact. This criterion will automatically be fulfilled if the basic lattice has cubic symmetry. Now, if $\mathscr{M}$ is sufficiently large, the distance between two molecules with centers confined to the same polyhedron is necessarily small, and $\overline{V}^{(2)}$ will be positive and large. We proceed under the assumption that $\mathscr{M}$ is in a range in which these molecular repulsions prevent multiple occupancy of the polyhedra.

In the same way the lattice affords $\mathscr{M}$ discrete locations with volume $\mathscr{V}$, we must also divide the orientational space $8\pi^2$ into an integer number ν of equal-weight regions. The lattice theory then provides for a coarse-grained description of any arrangement of the N water molecules in space by means of a set of occupation parameters ξ_i $(1 \leq i \leq \mathscr{M})$, one for each nearest-neighbor polyhedron. In particular,

$$\xi_i = 0 \tag{6.6}$$

indicates that polyhedron i is empty, while

$$\xi_i = 1, 2, \ldots, \nu \tag{6.7}$$

indicates that it contains the center of a molecule with orientation falling into region 1, 2, ..., or ν, respectively, of the full $8\pi^2$ orientation space. Among the $\mathscr{M}$ occupation parameters precisely N can be nonzero, but even under this restraint there remain

$$\frac{\mathscr{M}!\,\nu^N}{N!(\mathscr{M}-N)!} \tag{6.8}$$

distinct sets of values $\{\xi\}$ describing distinguishable coarse-grained system configurations.

The total molecular interaction relevant for the lattice approximation is denoted by $\overline{V}_N\{\xi\}$ for simplicity. It is equal to the vibrationally averaged function $\overline{V}_N(\mathbf{x}_1 \cdots \mathbf{x}_N)$ evaluated for molecules placed at the centers of the polyhedra and given orientations central to the rotational regions specified by the parameter set $\{\xi\}$. Figure 13 illustrates in elementary two-dimensional fashion the centered and discretely oriented water molecules, one to each cell, that might be required by $\{\xi\}$.

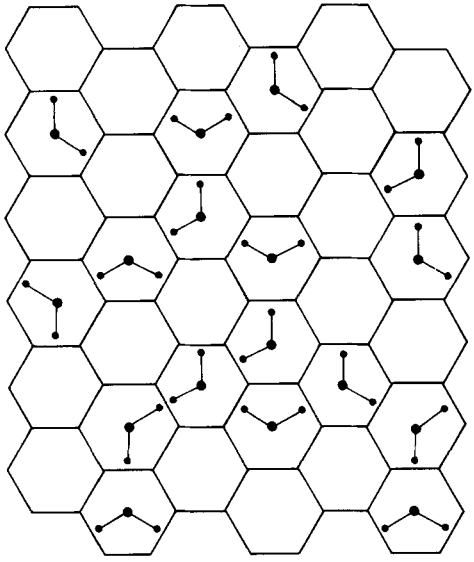

Fig. 13 Centered molecules, with a discrete set of orientations, used to define the lattice model interaction $\bar{V}_N\{\xi\}$. This is a schematic two-dimensional version of the three-dimensional situation.

After accounting for the $N!$ ways in which the water molecules can be distributed among the occupied lattice sites, the partition function Q_l adopts the form

$$Q_1 = \left(\frac{8\pi^2\tau\Lambda}{v}\right)^N \sum_{\{\xi\}} \exp\left[-\beta\bar{V}_N\{\xi\}\right] \tag{6.9}$$

where

$$\Lambda = \frac{(2\pi k_B T)^3 m^{3/2}(I_1 I_2 I_3)^{1/2} Q_{\text{vib}}}{h^6} \tag{6.10}$$

is a factor carried over without change from the semiclassical partition function (4.4). The sum runs over all distinct sets $\{\xi\}$ consistent with the given number of molecules. As $\mathcal{M}$ and v approach infinity, Q_l approaches Q to be sure, but the advantage of the lattice approximation lies in computational simplifications that obtain for certain finite choices of $\mathcal{M}$ and v.

In the coarse-grained lattice representation, the molecular distribution functions $\rho^{(n)}$ are replaced by probability functions $P^{(n)}(i_1 \cdots i_n|\xi_1 \cdots \xi_n)$, giving the chance that simultaneously the lattice sites $i_1, \ldots, i_n$ have the respective occupation parameter values $\xi_1, \ldots, \xi_n$. The defining relations may be written:

$$P^{(n)}(i_1 \cdots i_n|\xi_1 \cdots \xi_n) = \frac{\sum'_{\{\xi\}} \exp\left(-\beta\bar{V}_N\{\xi\}\right)}{\sum'_{\{\xi\}} \exp\left(-\beta\bar{V}_N\{\xi\}\right)} \tag{6.11}$$

The primed numerator summation includes only those sets $\{\xi\}$ displaying the required parameter values at sites $i_1, \ldots, i_n$. By convention we set $P^{(n)} = 0$ if any two i_αs happen to be identical.

Both the mean energy expression (4.28) and the compressibility relation (4.37) can be carried over into the lattice approximation, using the $P^{(n)}$ instead of $\rho^{(n)}$:

$$\frac{E}{N} = -\frac{\partial \ln Q_{\text{vib}}}{\partial \beta} + 3k_B T + \sum_{n=2}^{N} \frac{1}{n!N} \sum_{i_1 \cdots i_n = 1}^{\mathscr{M}} \sum_{\xi_1 \cdots \xi_n = 1}^{\nu} \overline{V}^{(n)}\{\xi_1 \cdots \xi_n\} P^{(n)}(i_1 \cdots i_n | \xi_1 \cdots \xi_n) \tag{6.12}$$

$$\rho k_B T \kappa_T = 1 + \frac{1}{N} \sum_{i_1, i_2 = 1}^{\mathscr{M}} \sum_{\xi_1, \xi_2 = 1}^{\nu} [P^{(2)}(i_1, i_2 | \xi_1, \xi_2) - P^{(1)}(i_1 | \xi_1) P^{(1)}(i_2 | \xi_2)] \tag{6.13}$$

However, there is no way that the virial equation of state (4.31) can be retained in the lattice description, so the pressure must be obtained from another source (such as κ_T) using suitable thermodynamic identities.

Once again it is necessary to emphasize that the theory has been developed without the necessity for specifying a particular molecular center, and in principle any choice serves as well as any other. Nevertheless, a pragmatic element now intrudes for the first time. We have demanded single occupancy of the space-filling polyhedra. This automatically becomes valid as $\mathscr{M} \to \infty$ (N and $\mathscr{V}$ fixed), but the demand must also be met for finite $\mathscr{M} > N$ as well. If the molecular center were taken eccentrically but by convention to be 10 Å from the oxygen nucleus along the symmetry axis, there would be no energetic prevention of double occupancy for any polyhedron, however small, since the molecular electron clouds and nuclei would be well outside the polyhedron. To avoid this difficulty, one is effectively required to embed the center inside the molecular electron distribution to take full advantage of overlap repulsion in avoiding multiple occupancy. The position of the oxygen nucleus qualifies satisfactorily on this count, as Fig. 13 implicitly acknowledges.

The lattice model was originally advocated to study phase transitions for structureless spherical molecules, or for highly symmetric molecules for which free rotation produces an outward appearance of sphericity.[53] The occupation parameters required in that simpler version needed only two values:

$$\begin{aligned} \xi_i &= 0 \quad \text{empty} \\ &= 1 \quad \text{singly occupied} \end{aligned} \tag{6.14}$$

It can easily be shown that this two-state lattice model has an inherent symmetry about the half-filled ($N = \mathcal{M}/2$) state that derives from an isomorphism to the Ising model for magnetic-phase transitions. An important consequence of this "particle-hole" symmetry is that the chemical potential along the critical isochore ($N = \mathcal{M}/2$) is an analytical function of temperature at the critical point. Unfortunately, no analogous symmetry can be identified for the lattice models of water, and it remains an open question whether temperature analyticity of the water chemical potential exists at its critical point, along a suitable symmetry line.[54]

B. Fleming–Gibbs Version

The simplest practical version of the lattice approximation utilizes the body-centered cubic arrangement of sites, with a distance between nearest neighbors corresponding to an unstrained hydrogen bond between two water molecules. Figure 14 shows this lattice structure, for which each site has eight nearest neighbors in a cubical arrangement. The tetrahedral angle between successive hydrogen bonds is realized in a natural way, since four mutually noncontiguous near neighbors (out of the eight) for any given site form vertices of a regular tetrahedron surrounding that site. In fact the fully hydrogen-bonded cubic ice crystal (ice Ic) fits precisely on the

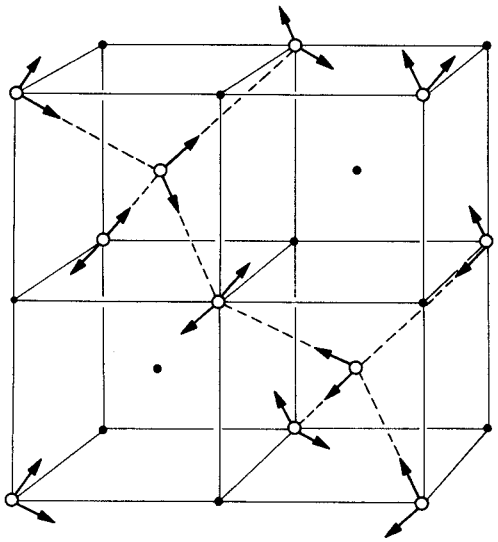

Fig. 14 Body-centered cubic lattice model for water. Dotted lines indicate hydrogen bonds between nearest-neighbor molecules. The molecules shown form a portion of the cubic ice Ic crystal.

body-centered cubic lattice, using every other site. The water molecules shown in Fig. 14 constitute a portion of this ice Ic crystal.

The obvious discrete set of orientations to use should be clear from Fig. 14. The two OH bonds of a given molecule should point toward a pair of nearest-neighbor cube vertices, which are located diagonally across a face of the cube from one another. There are 12 such nearest-neighbor pairs, and therefore 24 discrete orientations for a water molecule with distinguishable hydrogens. Melting of the Ic crystal can occur if molecules frequently reorient from the directions shown in Fig. 14 for the crystal, while also moving at random onto the other sublattice of sites which is totally unoccupied by the crystal.

Two interpenetrating cubic networks can coexist on the body-centered cubic lattice, filling it completely and forming the ice VII structure.[7] Each has fourfold hydrogen bond coordination at each site, but no hydrogen bonds connect the two networks.

Fleming and Gibbs have proposed a way of simplifying the lattice-model interaction $\overline{V}_N\{\xi\}$ to allow explicit statistical calculation to be carried out while retaining the essential features of directional bonding that seem to be characteristic of water.[55,56] Only pair interactions between nearest neighbors are permitted, and the value of the nearest-neighbor interaction depends on the relative orientation in such a way that only three distinct magnitudes are involved:

$$\begin{aligned} \overline{V}^{(2)}\{\xi_1, \xi_2\} &= -E_b && \text{if } \xi_1, \xi_2 \text{ corresponds to a hydrogen bond} \\ &= -\varepsilon_1 && \text{if rotation of one molecule suffices to create a hydrogen bond} \\ &= -\varepsilon_2 && \text{if rotation of both molecules is necessary to create a hydrogen bond} \end{aligned} \tag{6.15}$$

These three energies are treated as adjustable parameters but, clearly, if this simplification is to have meaning, $-E_b$ must be the lowest of the three energies. There are $24^2 = 576$ distinct orientations of a pair of neighboring molecules; of these, 72 lead to interaction $-E_b$, 360 to $-\varepsilon_1$, and 144 to $-\varepsilon_2$. It is important to realize that not all pairs of neighboring molecules, one of which points on OH toward the other, are considered hydrogen-bonded in the Fleming–Gibbs scheme, for it is also necessary that the three pendant OH groups point to other sites of the same ice Ic sublattice (as shown in Fig. 14). In part, pairs with interaction $-\varepsilon_1$ correspond to linear but angularly severely strained hydrogen bonds.

If the lattice is filled with molecules forming ice VII interpenetrating networks, nonbonded nearest neighbors (four of the eight) will always have energy $-\varepsilon_2$. This crystal structure can be thermodynamically destabilized

at low pressure by causing $-\varepsilon_2$ to be the most positive of the three interaction energies, thus simulating the strong repulsions that exist between these unbonded neighbors in the real ice VII crystal.[57] In any event use of the body-centered cubic lattice and nearest-neighbor interactions permits at most two distinct crystalline phases in the Fleming–Gibbs formulation, supplemented by liquid and vapor phases.

The Fleming–Gibbs partition function can be written:

$$Q_l = \left(\frac{\pi^2 \tau \Lambda}{3}\right)^N \sum_{\{\xi\}} \exp\left[\beta(N_b\{\xi\}E_b + N_1\{\xi\}\varepsilon_1 + N_2\{\xi\}\varepsilon_2)\right] \tag{6.16}$$

The numbers of nearest-neighbor pairs of each interaction type have been denoted here by N_b, N_1, and N_2.

Fleming and Gibbs have confined their quantitative studies to the liquid and vapor phases. In order to evaluate the partition function and thermodynamical properties, they have separately used two statistical mechanical approximations, the mean field approximation (MFA),[55] and a more accurate second-order approximation (SOA).[56]

The MFA replaces N_b, N_1, and N_2 in (6.16) by their a priori average values:

$$\begin{aligned} N_b\{\xi\} &\to \tfrac{1}{2}n^2\mathscr{M} \\ N_1\{\xi\} &\to \tfrac{5}{2}n^2\mathscr{M} \\ N_2\{\xi\} &\to n^2\mathscr{M} \end{aligned} \tag{6.17}$$

where n is the lattice-filling fraction $N/\mathscr{M}$. With this assumption all terms in the partition function sum become equal, so

$$Q_l(\text{MFA}) = \frac{\mathscr{M}!}{N!(\mathscr{M}-N)!}\left(\frac{\pi^2\tau\Lambda}{3}\right)^N \exp\left\{\beta n^2 \mathscr{M}\left[\tfrac{1}{2}E_b + \tfrac{5}{2}\varepsilon_1 + \varepsilon_2\right]\right\} \tag{6.18}$$

Taking logarithms, and differentiating with respect to volume, the MFA equation of state for the lattice model is easily found to be

$$\frac{\beta p \mathscr{V}}{\mathscr{M}} = -\ln(1-n) - \beta n^2\left(\tfrac{1}{2}E_b + \tfrac{5}{2}\varepsilon_1 + \varepsilon_2\right) \tag{6.19}$$

The liquid-vapor critical point can be located from the horizontal inflection point of the pressure isotherm family (6.19). At this critical point,

$$\begin{aligned} k_B T_c &= \tfrac{1}{4}(E_b + 5\varepsilon_1 + \varepsilon_2) \\ n_c &= \tfrac{1}{2} \end{aligned} \tag{6.20}$$

Fleming and Gibbs point out that the experimental critical temperature can be reproduced by setting

$$\begin{aligned} E_b &= 4.65 \text{ kcal/mole} \\ \varepsilon_1 = \varepsilon_2 &= 7.2 \times 10^{-2} \text{ kcal/mole} \end{aligned} \tag{6.21}$$

for the MFA. Certainly, the hydrogen bond energy is not unreasonable, in the light of available quantum mechanical information (Section III).

If the experimental critical density is used to assign the nearest-neighbor distance, the result is 3.93 Å, far too large for a well-formed hydrogen bond. As an alternative, Fleming and Gibbs chose to use the nearest-neighbor separation determined by x-ray scattering measurements on liquid water,[58] which increases slightly (and linearly) with increasing temperature but remains within an acceptable distance range for linear hydrogen bonds. In this manner they derived the following critical constants (experimental values in parentheses):

$$\begin{aligned} \rho_c &= 0.688 \text{ g/cm}^3 \\ &\quad (0.325 \text{ g/cm}^3) \\ p_c &= 783 \text{ atm} \\ &\quad (218 \text{ atm}) \end{aligned} \tag{6.22}$$

That the errors in predicted critical constants are very large no doubt stems primarily from a weakness of the MFA, which assumes each molecule is surrounded by a shell of neighbors having the macroscopic distribution of density and orientation. The SOA explicitly removes this weakness by providing for a distribution of nearest neighbors that is correct to leading order in interactions with the central site. The reader should consult the original reference[56] for details. The SOA equation of state extends the MFA result (6.19) to order β^2:

$$\begin{aligned} \frac{\beta p \mathscr{V}}{\mathscr{M}} &= -\ln(1-n) - \beta n^2(\tfrac{1}{2}E_b + \tfrac{5}{2}\varepsilon_1 + \varepsilon_2) \\ &\quad - \beta^2 n^2(\tfrac{1}{4}E_b{}^2 + \tfrac{5}{4}\varepsilon_1{}^2 + \tfrac{1}{2}\varepsilon_2{}^2) \\ &\quad + \beta^2 n^3[(\tfrac{1}{2}E_b + \tfrac{3}{2}\varepsilon_1)^2 + (\varepsilon_1 + \varepsilon_2)^2] \\ &\quad - 6\beta^2 n^4(\tfrac{1}{8}E_b + \tfrac{5}{8}\varepsilon_1 + \tfrac{1}{4}\varepsilon_2)^2 \end{aligned} \tag{6.23}$$

Using the SOA, it was found that the liquid phase would boil at 100°C under 1 atm pressure if

$$\begin{aligned} E_b &= 4.58 \text{ kcal/mole} \\ \varepsilon_1 &= 0.915 \text{ kcal/mole} \\ \varepsilon_2 &= -1.19 \text{ kcal/mole} \end{aligned} \tag{6.24}$$

This set of interactions seems somewhat more reasonable than the MFA set (6.21), in that relative configurations leading to $-\varepsilon_2$ are now energetically very unfavorable. By using the same x-ray measurement assignment for the lattice spacing as before, the liquid density at 100°C and 1 atm is found to be

1.323 g/cm^3, compared to the experimental value 0.958 g/cm^3. Fleming and Gibbs ascribe the discrepancy to remanent correlation error in the SOA, rather than inherent crudeness of the lattice model itself. By implication a more accurate treatment of the statistical mechanical evaluation of Q_l should improve predictions relative to experiment. In any event the SOA improves on the MFA dramatically, for the latter predicts a 30-atm vapor pressure for the liquid at 100°C, using the interaction set (6.24).

The critical parameters obtained for the SOA and energies (6.24) are

$$\begin{aligned} T_c &= 739.1°\text{C} \\ \rho_c &= 0.353\ \text{g/cm}^3 \\ p_c &= 478.5\ \text{atm} \end{aligned} \tag{6.25}$$

somewhat too large in each case.

The most interesting feature of the SOA calculation is that the liquid, in coexistence with its vapor, exhibits a maximum at 61°C in the lattice-filling fraction $n = N/\mathcal{M}$. The actual mass density requires accounting for the temperature variation of lattice spacing, and as a result the density maximum becomes displaced to roughly −50°C. Although one would have liked the mass density to reach a maximum at 4°C to agree with measurements, the significant point to note is that the lattice model evidently possesses the general capacity to produce maxima. No doubt further refinements could achieve better agreement, since it is clear that a delicate balance of opposing influences is present.

Fleming and Gibbs calculated the specific heats C_V and C_p in the SOA, and found the results to be "fairly good." However, the isothermal compressibility κ_T is too large by a factor of 2 for the liquid between 0 and 100°C, and increases with temperature instead of showing a minimum as experiment does at 46°C.

Implicit in the SOA is a specification of the mean number of nearest neighbors of each type to a typical molecule. Throughout the normal liquid range, 0 to 100°C, the total mean number of nearest neighbors is close to 6.8. This is significantly larger than the value 4.5 suggested by x-ray scattering work.[58] It would be informative to know if a more precise statistical treatment than SOA would improve this comparison.

C. Bell's Version

Bell[59] has proposed and analyzed a lattice model for water that is closely related to that of Fleming and Gibbs. It also uses the body-centered cubic array of sites shown in Fig. 14, and each molecule has the same 24 discrete orientations as before. The major difference is that Bell's version incorporates both two *and* three-molecule interactions.

The specific pair interaction used by Bell operates only between nearest neighbors:

$$\begin{aligned} \bar{V}^{(2)}\{\xi_1, \xi_2\} &= -(\varepsilon + w) \qquad \text{if } \xi_1, \xi_2 \text{ corresponds to a hydrogen bond} \\ &= -\varepsilon \qquad\quad \text{if no hydrogen bond exists} \end{aligned} \tag{6.26}$$

(This is identical to the Fleming–Gibbs interaction if $E_b = \varepsilon + w$ and $\varepsilon_1 = \varepsilon_2 = \varepsilon$.) The nonadditive three-molecule interaction operates only between compact triangles of molecules:

$$\bar{V}^{(3)}\{\xi_1, \xi_2, \xi_3\} = \tfrac{1}{3}u \tag{6.27}$$

that is, for three simultaneously occupied sites in a 45°-45°-90° triangle whose legs connect nearest neighbors and whose hypotenuse connects second neighbors. No such compact triangles of molecules exist for the half-filled lattice in an ice Ic configuration, but the completely filled lattice has $12\mathscr{M}$ compact triangles. The incorporation of positive u into the Bell version becomes the mechanism whereby interpenetrating ice VII hydrogen bond networks are thermodynamically relegated to high pressure.

Corresponding to the Fleming–Gibbs expression (6.16), Bell's lattice model partition function has the form

$$Q_l = \left(\frac{\pi^2 \tau \Lambda}{3}\right)^N \sum_{\{\xi\}} \exp\left[\beta(N_b\{\xi\}w + N_p\{\xi\}\varepsilon - \tfrac{1}{3}N_t\{\xi\}u)\right] \tag{6.28}$$

As before, N_b is the number of hydrogen-bonded pairs; N_p stands for the total number of neighboring pairs of water molecules of all types

$$N_p = N_b + N_1 + N_2 \tag{6.29}$$

The total number of compact trimers has been denoted by N_t.

In order to evaluate Q_l for the fluid phases, Bell invokes a cluster-variation method attributed to Guggenheim and McGlashan.[60] For the present case this method self-consistently calculates the distribution of molecules over compact tetrahedral sets of four sites, one of which is shown in Fig. 15. Two of the edges of the tetrahedron connect second-neighbor sites, while the other four connect first neighbors. The body-centered cubic lattice consists of four face-centered cubic sublattices, and each of the tetrahedral clusters has one vertex belonging to each of the four. Considering the nature of the molecular interactions involved in Bell's version of the lattice model, these clusters should be sufficient to describe the most important aspects of short-range order in the fluid phases.

Bell lists 10 fundamentally distinct ways a cluster of sites can be occupied by molecules or left vacant. Each of these has a degeneracy factor $\delta_i (1 \leq i \leq 10)$ expressing the number of ways molecules in a given species of

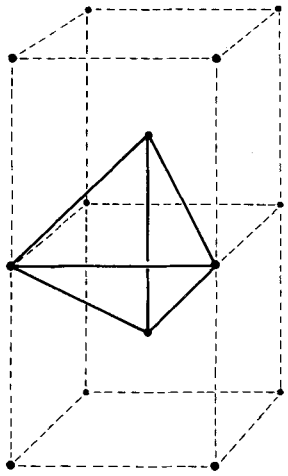

Fig. 15 Tetrahedral cluster of sites (outlined with solid lines) used by Bell to evaluate his lattice model partition function [see (6.28)].

cluster can be reoriented and reassigned to sites. The essence of the Guggenheim–McGlashan technique is its approximation for the number of ways g that cluster species present in fractional concentrations $\Psi_i\delta_i(1 \leq i \leq 10)$ can be realized by placing molecules at the lattice sites:

$$\ln g(\Psi_1 \cdots \Psi_{10}) \cong \ln g_0 - \mathscr{M} \sum_{i=1}^{10} \delta_i \Psi_i \ln \Psi_i \tag{6.30}$$

g_0 is a normalization factor which can be assigned from the known result for random molecular distribution over the lattice:

$$\ln g_0 = 3\mathscr{M}\left[n \ln\left(\frac{n}{12}\right) + (1 - n)\ln(1 - n)\right] \tag{6.31}$$

Associated with each of the cluster species is a characteristic interaction energy e_i, so that the entire system interaction energy is:

$$\mathscr{M} \sum_{i=1}^{10} e_i \delta_i \Psi_i \tag{6.32}$$

The Helmholtz free energy F then can be obtained by maximizing

$$\ln g(\Psi_1 \cdots \Psi_{10}) - \beta\mathscr{M} \sum_{i=1}^{10} e_i \delta_i \Psi_i = -\beta F - N \ln\left(\frac{\pi^2 \tau \Lambda}{3}\right) \tag{6.33}$$

with respect to permissible variations in the Ψ_i (namely, those variations consistent with their normalization, and with fixed n).

Thermodynamic properties were investigated for several choices of the interaction ratios ε/w and u/w. The most significant conclusion drawn from these studies was that the anomalies of liquid-phase density maximum and compressibility minimum could be produced by a rather wide range of assignments of the interaction ratios. Furthermore, these anomalies tended to be suppressed at elevated pressure, just as they are in real water. Table II presents some results taken from Bell's paper which illustrate these features, along with the corresponding experimental numbers. The average number of nearest neighbors is $2\langle N_p \rangle / N$, and has been included in Table II for the temperature of maximum liquid density at the vapor pressure.

TABLE II

Properties Calculated by Bell[59] for His Lattice Model

Interaction ratios		$\frac{p_c \mathcal{V}_c}{k_B T_c}$	$\frac{T(\max \rho)}{T_c}$	$\frac{T(\min \kappa_T)}{T_c}$	$\frac{2\langle N_p(\max \rho)\rangle}{N}$	Ice lattice energy (kcal/mole)
ε/w	u/w					
1/2	1/2	0.197	0.525	0.455	4.07	9.0
1	3/4	0.208	0.477	0.447	4.42	7.2
2	5/4	0.218	0.364	0.381	4.82	5.7
Experiment:		0.243	0.427	0.494	4.4	13.4

The lattice energy of ice in the present model is $2(\varepsilon + w)$ per molecule. In order to fix the energy scale for each of the energy ratio cases considered in Table II, the calculated critical temperatures were fitted to the measured value. The resulting lattice energies (for cubic ice) are given in the last column of the table. Although they are compared with an experimentally determined value for hexagonal ice, the cubic-versus-hexagonal distinction should have little importance since the two polymorphs have such similar bonding geometry and density. The comparison shows that the lattice models tend to have considerably weaker binding than real ice.

The average coordination numbers look very encouraging, and seem to stay small compared to the Fleming–Gibbs result for a wide range of interaction ratios.

The cluster variation technique employed by Bell is probably more accurate at low temperatures than the Fleming–Gibbs SOA. In order to make decisive comparisons of the two lattice model versions, it would be valuable to have available a set of cluster variation calculations for the Fleming–Gibbs case.

D. Possible Extensions

The existing calculations demonstrate that the lattice model approach is a valuable theoretical tool in understanding water. It would also be valuable to have research on this class of models widened in scope. We now list several feasible possibilities.

1. In the body-centered cubic lattice models discussed here, the melting transitions and range of crystal stability should be studied for the ice Ic and ice VII structures permitted by the models. Beside comparing the fluid-phase properties to experiment as has already been done, at least the low-pressure melting temperature of cubic ice should be required to agree roughly with that of real ice Ih. This would put an extra constraint on the interaction energy parameters.

Four long-range order parameters would be necessary in an order-disorder treatment of the crystals, corresponding to the four ways of building complete ice Ic networks on the lattice. Their introduction would complicate each of the statistical treatments somewhat, but not to the point of impossibility.

It hardly needs to be mentioned that prediction of a negative melting volume for ice is one of the attractive goals of this extension.

2. In addition to the interactions employed by Fleming and Gibbs, and by Bell, there are other versions that deserve to be tested. Most obvious is the need to rectify the short-range nature of the pair interactions, and for this purpose dipole–dipole interactions could be introduced for second neighbors at least, or perhaps perturbatively for all distances beyond first neighbors using a reasonable value of the molecular dipole moment.

With respect to nearest-neighbor molecule pairs, neither the Fleming–Gibbs nor the Bell version can be reconciled fully with the known behavior of the pair potential-energy function $V^{(2)}(\mathbf{x}_1, \mathbf{x}_2)$ as discussed in Section III.C. A more realistic alternative would involve distinguishing classes of nearest neighbors as: (*a*) hydrogen-bonded with all relevant angles tetrahedral; (*b*) single, linear hydrogen bond, but with the acceptor molecule twisted out of one of the tetrahedral arrangements; (*c*) unlinked by a linear hydrogen bond. The first two of these would have constant interaction energies $-\varepsilon_a$ and $-\varepsilon_b$, the former being more negative. Pairs in category (*c*) could be treated as interacting via electrostatic dipole moments at their centers.

Bell's three-molecule nonadditive energy [see (6.27)] may indeed be effective in destabilizing interpenetrating networks at low pressure and in holding down the mean coordination number in the liquid. However, it has doubtful validity as a representation of real water molecule interactions. More useful in the long range would be use of trimer nonadditivities only for the three doubly bonded species shown in Fig. 10, with signs and magnitudes agreeing with the available quantum mechanical studies. An inquiry of this

kind could help to resolve the long-standing question how hydrogen bond cooperativity (i.e., nonadditivity) influences the microscopic state of aggregation in the liquid.[38,39]

3. We have viewed the lattice models as analogues for the classical configuration integral of the familiar rectangle rule used for numerical integration with one variable. To improve precision for the lattice models, it is desirable to identify specific ways of achieving a finer grid size than the convenient but coarse body-centered cubic lattice. One suggestion is illustrated in Fig. 16. It amounts to augmenting the body-centered cubic array to form a face-centered cubic array with 16 times as many sites per unit volume. The original pairs of sites that were nearest neighbors have become sixth neighbors under the elaboration, and are $6^{1/2}$ times as far apart as the new nearest-neighbor site distance.

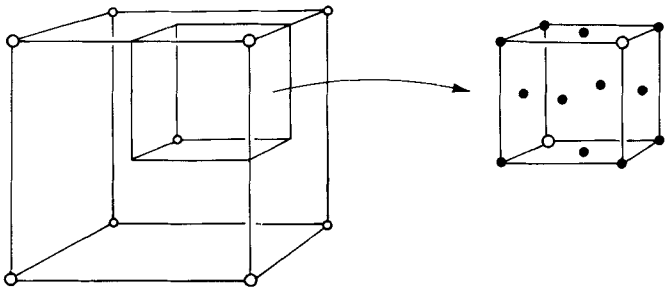

Fig. 16 Conversion of the body-centered cubic array to a face-centered cubic array by adding new sites (solid circles). The new lattice formed in this way has a site density 16 times that of its precursor.

If the old pairs of neighboring sites in the body-centered lattice are retained as the separation for an unstrained hydrogen bond, it is obvious that several other distances are now available in the augmented lattice for describing stretched and compressed hydrogen bonds. It should also be obvious that the orientation space for a single molecule can now be more finely subdivided according to the new set of ways that OH bonds can point toward nearby sites. The greater number of interaction energies that would have to be specified with the finer grid is a conceptual virtue, but a computational vice.

Hydrogen bond polygons on the body-centered cubic lattice can have only even numbers of sides (6, 8, 10, 12, etc.). The denser face-centered lattice affords sufficient configurational flexibility to allow odd polygons (5, 7, 9, 11, etc.) to exist with relatively little bond strain. This may prove to be an

important structural feature for a topologically accurate description of liquid water. In addition, a set of ice polymorphs should become possible larger than that permitted by the coarse body-centered array.

4. The conventional lattice model for simple substances has previously been quantized to provide a description of liquid helium.[61] By introducing creation and annihilation operators for each of the rotational states at a lattice site, with appropriate commutation relations, a quantized lattice model for water could also be constructed. This extension might be a valuable theoretical tool for explaining isotope effects in water and its solutions.

VII. CELL MODELS

A. Cell-Cluster Expansion

The principle behind the lattice model approach to evaluation of the water partition function is that a sequence of finer and finer grids enforces convergence toward the desired continuum description of configurations for the full set of molecules. The rate of convergence may be rather slow, however, since hydrogen bonds are not only strong but also markedly concentrated in small regions of relative distance and angle space for a pair of interacting molecules. That the empirically determined bond strengths are low for lattice calculations [see (6.24) and Table II] doubtless stems from the fact that they are averages over finite regions and therefore necessarily include strained configurations.

An alternative route of convergence to the full continuum representation is available, which offers several attractive advantages. This route defines the so-called cell models which attempt in a direct way to account for rapid variation in intermolecular potentials as molecules move away from regularly spaced lattice sites. As we shall see, this approach can be developed as a formally exact method by introducing a cell-cluster expansion. The general character of the cell models is such that the dynamics of the water system can also be investigated, especially in regard to short-time behavior. Of course, the lattice models do not normally possess this capacity.

The cell-cluster general development begins at the same stage as the lattice theory, by using a regular array of $\mathscr{M}$ sites in volume $\mathscr{V}$, on which molecules can adopt a number of v of discrete orientations. In principle, it does not matter what geometric type of array is used, for the subsequent development is always exact. But for practical reasons one will always want to optimize the rate of convergence of the method, and this demands selection of a starting grid that permits the molecules to adopt energetically "natural" configurations relative to each other. The body-centered cubic lattice discussed at length in Section VI fulfills this requirement, and is probably the most sensible starting point for any serious cell model computations.

The basic cell-cluster identity writes the semiclassical partition function Q first in terms of independent-molecule cell factors $Z^{(1)}$, and then incorporates correction factors $Y^{(n)}$ to account for errors attributable to the correlated motion of each subset of $n > 1$ molecules moving in their cells at the same time. Thus we write:

$$Q = \left(\frac{8\pi^2\tau\Lambda}{v}\right)^N \sum_{\{\xi\}} \left[\prod_{i=1}^{\mathcal{M}} Z_i^{(1)}\{\xi\}\right]\left[\prod_{i<j=1}^{\mathcal{M}} Y_{ij}^{(2)}\{\xi\}\right] \times \left[\prod_{i<j<k=1}^{\mathcal{M}} Y_{ijk}^{(3)}\{\xi\}\right]\cdots\left[\prod_{i_1<\cdots<i_N=1}^{\mathcal{M}} Y_{i_1\cdots i_N}^{(N)}\{\xi\}\right] \tag{7.1}$$

Here we rely on the notation used earlier for the lattice partition function Q_l in (6.9). Subscripts on the Zs and Ys refer to the lattice sites involved and, by convention, if any one of these sites is unoccupied in state $\{\xi\}$, the corresponding factor should be set equal to unity.

The single-molecule cell factors $Z_i^{(1)}\{\xi\}$ are the integrals:

$$Z_i^{(1)}\{\xi\} = \frac{v}{8\pi^2\tau} \exp\left(-\beta\Phi_i^{(0)}\{\xi\}\right) \int_{(\xi_i)} d\mathbf{x}_1 \exp\left[-\beta\Phi_i^{(1)}(\mathbf{x}_1, \{\xi\})\right] \tag{7.2}$$

where $\Phi^{(0)}$ is the potential energy of the molecule (numbered 1) when it is located precisely at the lattice site (configuration $\mathbf{x}_1^{(0)}\{\xi\}$):

$$\Phi_i^{(0)}\{\xi\} = \sum_{n=2}^{N} \frac{1}{n} \sum_{i_2<\cdots<i_n=2}^{N} \overline{V}^{(n)}(\mathbf{x}_1^{(0)}\{\xi\}, \mathbf{x}_{i_2}^{(0)}\{\xi\} \cdots \mathbf{x}_{i_n}^{(0)}\{\xi\}) \tag{7.3}$$

and where $\Phi^{(1)}$ is the *change* in potential energy experienced by molecule 1 as it wanders off of the lattice site and rotates:

$$\Phi_i^{(1)}(\mathbf{x}_1, \{\xi\}) = \overline{V}_N(\mathbf{x}_1, \mathbf{x}_2^{(0)}\{\xi\}, \mathbf{x}_3^{(0)}\{\xi\} \cdots \mathbf{x}_N^{(0)}\{\xi\}) - \overline{V}_N(\mathbf{x}_1^{(0)}\{\zeta\}, \mathbf{x}_2^{(0)}\{\xi\} \cdots \mathbf{x}_N^{(0)}\{\xi\}) \tag{7.4}$$

Although $\Phi_i^{(0)}$ and $\Phi_i^{(1)}$ in the strict sense depend on the status of *all* sites, it is clear that only those close to site i matter substantially. The integration in (7.2) is to be carried out over a six-dimensional cell, denoted by (ξ_i), corresponding to the restriction of the center of molecule 1 to the interior of the nearest-neighbor polyhedron surrounding site i, with orientation restricted to the $8\pi^2/v$ region belonging to the standard orientation decreed by ξ_i. The $Z_i^{(1)}$ have been defined to reduce to unity in the limit of vanishing interactions.

Aside from normalization the $Z_i^{(1)}\{\xi\}$ are classical configurational partition functions for single molecules moving under the influence of the intermolecular forces of fixed neighbors. In a similar way, for every $2 \leq m \leq N$

we can define configuration integrals:

$$Z^{(m)}_{i_1,\ldots,i_m}\{\xi\} = \frac{1}{m!}\left(\frac{v}{8\pi^2\tau}\right)^m \exp\left[-\beta(\Phi^{(0)}_{i_1}\{\xi\} + \cdots + \Phi^{(0)}_{i_m}\{\xi\})\right]$$

$$\times \int_{(\xi i_1)\cdots(\xi i_m)} d\mathbf{x}_1 \cdots d\mathbf{x}_m \exp\left[-\beta\Phi^{(m)}_{i_1,\ldots,i_m}(\mathbf{x}_1 \cdots \mathbf{x}_m, \{\xi\})\right] \quad (7.5)$$

for molecules 1, 2, ..., m formally attached to sites $i_1, \ldots, i_m$ by $\{\xi\}$. The appropriate multiple-cell potential energy is

$$\Phi^{(m)}_{i_1\ldots i_m}(\mathbf{x}_1 \cdots \mathbf{x}_m, \{\xi\}) = \overline{V}_N(\mathbf{x}_1 \cdots \mathbf{x}_m, \mathbf{x}^{(0)}_{m+1}\{\xi\} \cdots \mathbf{x}^{(0)}_N\{\xi\}) - \overline{V}_N(\mathbf{x}^{(0)}_1\{\xi\} \cdots \mathbf{x}^{(0)}_N\{\xi\}) \quad (7.6)$$

It includes interactions within the movable set of m molecules, as well as their interactions with the surrounding $N - m$ rigidly fixed molecules.

The integration limits in (7.5) are such as to allow the center of each molecule $1, \ldots, m$ to inhabit *all* m cells $i_1, \ldots, i_m$. If all surrounding cells are filled, in the noninteracting limit,

$$Z^{(m)}_{i_1\cdots i_m}\{\xi\} \to \frac{m^m}{m!} \quad (7.7)$$

However, if there are vacant sites near $i_1, \ldots, i_m$, we append the restriction that the minimum sum of squares of distances for the m molecules to sites unoccupied by fixed particles be attained *only* with sites $i_1, \ldots, i_m$, and not with the inclusion of local vacant sites.

If sites i and j are widely separated, the motion of molecules in the respective cells will be independent. With cells small enough that multiple occupation is unlikely on energetic grounds, $Z^{(2)}_{ij}$ then factors into $Z^{(1)}$s:

$$Z^{(2)}_{ij}\{\xi\} \sim Z^{(1)}_i\{\xi\}Z^{(1)}_j\{\xi\} \quad (7.8)$$

The cell pair correction term $Y^{(2)}_{ij}$ appearing in the general cell-cluster expansion (7.1) is simply a ratio whose deviation from unity measures the extent to which factorization is inappropriate:

$$Y^{(2)}_{ij}\{\xi\} = \frac{Z^{(2)}_{ij}\{\xi\}}{Z^{(1)}_i\{\xi\}Z^{(1)}_j\{\xi\}} \quad (7.9)$$

Three-cell correction factors are also defined by appropriate ratios of Zs:

$$Y^{(3)}_{ijk}\{\xi\} = \frac{Z^{(3)}_{ijk}\{\xi\}Z^{(1)}_i\{\xi\}Z^{(1)}_j\{\xi\}Z^{(1)}_k\{\xi\}}{Z^{(2)}_{ij}\{\xi\}Z^{(2)}_{ik}\{\xi\}Z^{(2)}_{jk}\{\xi\}}$$

$$\equiv \frac{Z^{(3)}_{ijk}\{\xi\}}{Z^{(1)}_i\{\xi\}Z^{(1)}_j\{\xi\}Z^{(1)}_k\{\xi\}Y^{(2)}_{ij}\{\xi\}Y^{(2)}_{ik}\{\xi\}Y^{(2)}_{jk}\{\xi\}} \quad (7.10)$$

These factors differ from unity only when all three sites i, j, and k are close together, for if one of them (say, k) recedes from the other two,

$$Z_{ijk}^{(3)}\{\xi\} \sim Z_{ij}^{(2)}\{\xi\}Z_{k}^{(1)}\{\xi\} \tag{7.11}$$

The higher-order correction factors $Y^{(m)}$ have a similar structure. In each case $Z^{(m)}$ is divided by Ys of lower order for every proper subset of sites that can be formed out of the full set of m given sites:

$$Y_{i_1\cdots i_m}^{(m)}\{\xi\} = \frac{Z_{i_1\cdots i_m}^{(m)}\{\xi\}}{\prod_{\mu=1}^{m-1}\sum_{\alpha_1\cdots\alpha_\mu\varepsilon i_1\cdots i_m} Y_{\alpha_1\cdots\alpha_\mu}^{(c)}\{\xi\}} \tag{7.12}$$

where for notational convenience we have set

$$Y_i^{(1)}\{\xi\} \equiv Z_i^{(1)}\{\xi\} \tag{7.13}$$

The recursive linear relations between logarithms of the Zs on the one hand, and the logarithms of the Ys on the other hand, are isomorphous to the identities (3.2) to (3.4) relating total potentials V_n to the component potentials $V^{(n)}$. That (7.1) is in fact an identity results from thorough cancelation of factors between the Ys for each term of the occupation state sum (over $\{\xi\}$) in (7.1). In fact, the recursive quotient definitions (7.12) for cell correlation factors reduce (7.1) to the elementary form

$$Q = \left(\frac{8\pi^2\tau\Lambda}{v}\right)^N \sum_{\{\xi\}} Z_{i_1\cdots i_N}^{(N)}\{\xi\} \tag{7.14}$$

which simply resolves Q into separate contributions from distinct modes of occupation of the set of v $\mathscr{M}$ six-dimensional cells by molecules.

Provided the number of lattice sites $\mathscr{M}$ is no less than the number of molecules N, the precise value of $\mathscr{M}$ can in no way affect the validity of cell-cluster expansion (7.1); it is rigorously correct independently of the choice of $\mathscr{M}$. But just as an optimal choice exists for the lattice structure itself from the standpoint of convergence rate, there ought to be a "best" value for $\mathscr{M}$. A reasonable choice would be that $\mathscr{M} = \mathscr{M}_1$, which minimizes the free energy (i.e., maximizes Q) in the single-cell approximation

$$Q \cong \left(\frac{8\pi^2\tau\Lambda}{v}\right)^N \sum_{\{\xi\}} \prod_{i=1}^{\mathscr{M}} Z_i^{(1)}\{\xi\} \tag{7.15}$$

On restoring just the pair factors $Y^{(2)}$, a slightly shifted $\mathscr{M} = \mathscr{M}_2$ would minimize the resulting more accurate free energy. Similarly $\mathscr{M}_3$, $\mathscr{M}_4$, and so on, would give minima after restoring triplet, quadruplet, and so on, correction factors, but it must be the case that the free energy near these successive minima becomes a flatter and flatter function of $\mathscr{M}$. This raises an interesting question, yet to be answered, for the general cell-cluster theory

of the liquid state: Under what conditions (if any) on the underlying lattice structure does the sequence of formal vacancy concentrations

$$\frac{\mathcal{M}_1 - N}{\mathcal{M}_1}, \frac{\mathcal{M}_2 - N}{\mathcal{M}_2}, \frac{\mathcal{M}_3 - N}{\mathcal{M}_3}, \ldots \tag{7.16}$$

converge to a limit with respect to increasing order of included cell correlation? The existence of the limit would define precisely the "holes" in the liquid state.

B. Weres–Rice Cell Theory

For simple fluids and their mixtures, calculations falling under the general heading "cell theory" have had a long history.[62] By contrast, analogous calculations for water are sparse, and a recent phenomenon. Weissmann and Blum[63] have reported single-molecule partition functions for cells in an expanded (but perfect) ice lattice, and have suggested that the results might be relevant to the liquid state. Nevertheless, the only concerted attack on liquid water using cell theory formalism, and including a realistic assessment of local molecular order, has been published by Weres and Rice.[64] This section outlines their work.

Weres and Rice have based their calculations on an approximate effective pair potential for water molecules that was proposed by Ben-Naim and Stillinger[40] (BNS). This BNS potential v utilizes a spherically symmetric short-range part v_{LJ}, plus an angular portion designed to describe formation of linear hydrogen bonds at a small separation:

$$v(\mathbf{x}_1, \mathbf{x}_2) = v_{LJ}(R_{12}) + S(R_{12})v_{el}(\mathbf{x}_1, \mathbf{x}_2) \tag{7.17}$$

The distance R_{12} is measured between the oxygen nuclei. Each water molecule is regarded as a symmetric tetrad of point charges (two are $+q$, and the other two $-q$), as shown in Fig. 17. The positive charges represent

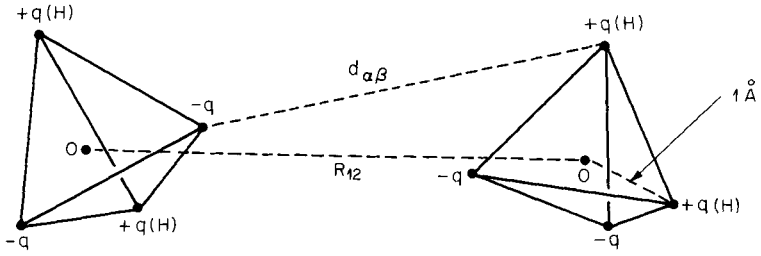

Fig. 17 Molecular charge tetrahedra used in the BNS effective pair potential. The point charges $\pm q$ are symmetrically located 1 Å from the oxygen nucleus. Only one of the 16 charge pair distances $d_{\alpha\beta}$ used in the potential has been shown explicitly.

partially shielded protons, and the negative charges simulate unshared pairs of electrons at the back side of the molecule. All four charges are precisely 1 Å from the oxygen nucleus. The electrostatic interactions of the 16 pairs of point charges, one in each molecule, make up v_{el}:

$$v_{el}(\mathbf{x}_1, \mathbf{x}_2) = q^2 \sum_{\alpha,\beta=1}^{4} \frac{(-1)^{\alpha+\beta}}{d_{\alpha\beta}(\mathbf{x}_1, \mathbf{x}_2)} \tag{7.18}$$

Here α and β index charges (with odd indices belonging to negatives and even indices to positives), and the $d_{\alpha\beta}$ are the appropriate distances. The tendency for tetrahedron vertices with opposite charge signs to align is the mechanism for describing successive linear hydrogen bonds at the tetrahedral angle θ_t. This idea by itself is old, due originally to Bjerrum in his studies of ice,[65] but the BNS application involved for the first time a modulation function $S(R_{12})$ which switches off the electrostatic interactions before the molecules become so close that a charge overlap catastrophe ($d_{\alpha\beta} = 0$) can occur. Specifically, S is a cubic spline function:

$$\begin{aligned} S(R_{12}) &= 0 && 0 \le R_{12} \le R_L \\ &= \frac{(R_{12} - R_L)^2(3R_U - R_L - 2R_{12})}{(R_U - R_L)^3} && R_L \le R_{12} < R_U \\ &= 1 && R_U \le R_{12} \end{aligned} \tag{7.19}$$

with singular points

$$\begin{aligned} R_L &= 2.0379 \text{ Å} \\ R_U &= 3.1877 \text{ Å} \end{aligned} \tag{7.20}$$

The original strength parameterization for the BNS potential required a rough simultaneous fit to both ice and water vapor properties. Subsequent detailed studies using molecular dynamics (see Section VIII) have indicated that a renormalization of the original function with multiplier 1.06 throughout materially improves its overall accuracy.[66,67] After this renormalization the charge q becomes

$$q = 0.19562e = 0.93952 \times 10^{-10} \text{ esu} \tag{7.21}$$

while the Lennard-Jones short-range function

$$v_{LJ}(R_{12}) = 4\varepsilon\left[\left(\frac{\sigma}{R_{12}}\right)^{12} - \left(\frac{\sigma}{R_{12}}\right)^{6}\right] \tag{7.22}$$

requires

$$\begin{aligned} \sigma &= 2.82 \text{ Å} \\ \varepsilon &= 5.3106 \times 10^{-15} \text{ erg} \\ &= 7.6472 \times 10^{-2} \text{ kcal/mole} \end{aligned} \tag{7.23}$$

With these values the minimum of the BNS potential is achieved with a linear hydrogen bond ($R_{12} = 2.760$ Å) at energy -6.887 kcal/mole.

The Weres–Rice calculation has essentially been carried out with approximation (7.15), that is, with neglect of all cell deviation correlation factors $Y^{(n)}$, $n \geq 2$. The single-cell factors $Z^{(1)}$ were distinguished by the occupation state of the octahedral grouping of 14 first- and second-neighbor sites only; the influence of molecules beyond the second-neighbor shell was taken into consideration by means of a dielectric cavity assumption. The cell-model calculation therefore breaks down into three major parts. The first requires classification of the states of the basic 15-site cluster and construction of an entropy expression for a general set of concentrations for these cluster species. The second part involves evaluation of the distinct $Z^{(1)}$, using the BNS interaction. Finally, the third task requires minimization of the free energy with respect to cluster species concentrations to obtain their equilibrium values.

Just as Fleming and Gibbs had done for the lattice model, Weres and Rice varied the nearest-neighbor spacing linearly with temperature to maintain agreement with x-ray scattering experiments.[58] Specifically, the spacing varies from 2.82 Å at 0°C to 2.88 Å at 100°C.

In accord with Stevenson's spectroscopic evidence that the number of water molecules in the liquid with zero or one hydrogen bond must be small,[68] all $Z^{(1)}$ were required to involve two, three, or four hydrogen bonds to nearest neighbors. Even with this restraint there remained 374 distinct "neighbor environments" to be included in the calculations.

A rather elaborate argument is provided in Ref. 64 for the relevant combinatorial factor g, giving the number of ways the cells can be fitted together to form the system. We shall not reproduce that argument here, except to state the result which consists of six contributing factors:

$$g = \prod_{j=1}^{6} g_j \tag{7.24}$$

The first factor gives the number of ways to distribute N molecules over $\mathcal{M}$ sites:

$$g_1 = \frac{\mathcal{M}!}{N!(\mathcal{M} - N)!} \tag{7.25}$$

The second involves the number of hydrogen bonds present in the system, denoted by NP_h, and gives the number of ways that they may be distributed over the $4Nn$ nearest-neighbor molecular pairs expected in a random arrangement of molecules ($n = N/\mathcal{M}$):

$$g_2 = \frac{(4Nn)!}{(NP_h)![N(4n - P_h)]!} \tag{7.26}$$

The next factor is present to account for the fact that a random distribution of hydrogen bonds frequently causes molecules to "have too few or too many hydrogen bonds or incorrect angles between the hydrogen bonds";[64] specifically,

$$g_3 = \left(\frac{P_h}{4}\right)^{2NP_h}\left(\frac{1-n}{1-(P_h/4)}\right)^{N(4-2P_h)} \tag{7.27}$$

Since molecules have two, three, or four hydrogen bonds, with respective fractions P_2, P_3, and P_4 (note that $2P_h = 2P_3 + 3P_3 + 4P_4$), it is necessary to account for the multiplicity of ways that these bonding species may be assigned to the N occupied sites:

$$g_4 = \frac{N!}{(NP_2)!(NP_3)!(NP_4)!} \tag{7.28}$$

Taking into consideration the angularly acceptable arrangements of two, three, or four hydrogen bonds about a given central site (numbering 12, 8, and 2, respectively), it is also necessary to include the factor

$$g_5 = 12^{NP_2}8^{NP_3}2^{NP_4} \tag{7.29}$$

Finally, there is the analog, for the random hydrogen bond network, of Pauling's degeneracy factor for ice,[69] giving the number of ways that protons may be distributed along hydrogen bonds asymmetrically so as to leave molecules intact:

$$g_6 = \left(\frac{6}{2^{P_h}}\right)^N \tag{7.30}$$

Several approximations were used to evaluate the cell factors $Z^{(1)}$. We have already mentioned that neighbors beyond the second-neighbor shell were treated as a dielectric continuum. Most importantly, the cell potentials $\Phi^{(1)}$ were replaced by a quadratic form (calculated using the BNS function) about the stable hydrogen-bonding configuration in such a way that translational and librational motions were dynamically independent harmonic oscillators. Furthermore, the relevant potential-energy second derivatives were averaged over the two relative orientations permitted to hydrogen-bonded neighbors by the body-centered cubic lattice of sites. In this locally harmonic approximation, only that subset of the $v\,(=24)$ standard molecular orientations was considered that led to the maximum number of hydrogen bonds possible with the given arrangement of nearest neighbors.

Neighbors in both the first and second coordination shells that do not hydrogen-bond to the central molecule were treated as linear perturbations (with magnitudes provided by the BNS potential) whose effects could be added, as appropriate, to the cell harmonic oscillator partition functions.

Because linear lattice expansion with temperature was used, the calculated potential-energy curvatures and harmonic oscillator frequencies had to be calculated separately at each temperature of interest.

To compensate partially for neglect of the cell distortion correlation factors $Y^{(2)}$, $Y^{(3)}$, and so on, Weres and Rice elected to include a "communal" entropy of vibrational origin. For the diamond lattice a complete phonon calculation[70] yields 0.391 entropy units more than the comparable Einstein approximation for single-particle motion. To scale this result to a random network in which only a fraction $P_h/2$ of the maximum possible number of hydrogen bonds is present, $0.391(P_h/2)$ entropy units were added to the free energy of the independent cells.

The translational and librational frequencies generated in this calculation were sufficiently high that Weres and Rice felt obliged to use quantum mechanical, rather than classical, partition functions for them. This was done in spite of the fact that the BNS interaction was originally devised within the regime of classical statistical mechanics alone.[40]

When the librational frequencies were calculated for the cubic ice structure, they were found to be considerably higher than librational bands measured for ice Ih (the cubic form should be very similar in this respect). Weres and Rice thus concluded that the BNS interaction was too highly curved in the directions of libration about linear hydrogen bonds, and they suggested that this deficiency could be rectified in an ad hoc fashion simply by scaling the BNS librational curvatures downward with a factor 0.458. Consequently, two parallel sets of calculations were carried out, one set using the BNS interaction directly, and the other set using the "curvature-rescaled BNS" with lower librational frequencies.

The effective pair potential is based on the vibrationally averaged component potentials $\bar{V}^{(n)}$. As (4.8) shows, the latter functions (and thus also the former by implication) include effects arising from shifts in vibrational frequencies due to bonding. However, Weres and Rice felt that, because the BNS effective pair potential was originally derived on a purely classical basis, its use for their quantized cell oscillators should be accompanied by a compensating inclusion of extra binding energy due to intramolecular vibration frequency shifts. Using measured vapor- and liquid-phase frequencies, they calculated an extra 0.900 kcal/mole binding energy for the liquid at its melting point, to be added into the final cell approximation results. At the boiling point 0.694 kcal/mole is the corresponding value.

Minimization of the cell model free energy was carried out by a gradient descent technique in the multidimensional space of species fractions for the various permitted cell neighbor types. A constraint was applied to this minimization, to the effect that the various cell species concentrations should display a ratio of 4:3 for the average number of first to second neighbors.

This is the same as the ratio of numbers of sites in the first and second coordination shells (eight and six, respectively). Unfortunately, this constraint seems to inhibit the proper distribution of vacant sites throughout the system. In particular, this ratio is not applicable for the first and second neighbors in the ice Ic structure.

Over the normal liquid range 0 to 100°C, the computed Gibbs free energy, and its component enthalpy and entropy, showed the proper temperature trends and roughly the correct magnitudes. Use of the librationally rescaled BNS interaction tended to reduce the error in comparison with experiment by a factor of 2 at all temperatures. Table III, from Ref. 64, shows the various contributions to the enthalpy and entropy at 0°C and 100°C, and compares their totals to the respective experimental magnitudes. In this table the standard state for enthalpy is infinitely dilute vapor at absolute zero, while for entropy it is that of ice at absolute zero with frozen-in Pauling disorder $Nk_B \ln \frac{3}{2}$ and with nuclear spins disregarded.

Since empty cells were not explicitly considered in this calculation, the liquid density was assumed to be the same as the average density over the

TABLE III

Thermodynamic Properties Calculated by Weres and Rice for Liquid water, using the Uncorrelated-Distortion cell approximation.[a]

Property	0°C	100°C
Enthalpy (kcal/mole)		
Lattice ($\Phi^{(0)}$)	−8.296	−8.088
Translational	1.729	2.290
Librational	2.517	2.858
Nonbonded neighbors	−1.325	−1.271
Long-range (diel. approximation)	−1.190	−1.166
Intramolecular zero point	−0.900	−0.694
Total	−7.465	−6.071
Experimental total	−8.594	−6.791
Entropy (entropy units)		
Configurational	4.48	4.48
Orientational	1.70	1.69
Translational	7.12	9.28
Librational	2.00	3.44
Nonbonded neighbors	−1.17	−0.95
Vibrational	0.26	0.26
Total	14.39	18.20
Experimental total	15.17	20.79

[a] The librationally rescaled BNS interaction was employed. (This tabulation was copied from Ref. 64, Table II.)

first and second coordination shells. On a per-site basis, this density remains nearly constant throughout the temperature range of the liquid, with a value of 0.587. Taking into account the lattice expansion, this leads to mass densities which agree with observation to 1% or better. The greatest error occurs at the lowest temperature, and the cell calculation has a monotonically decreasing density with temperature with no hint of a density maximum.

The average number of hydrogen bonds per molecule remains equal to about 1.35 from 0 to 100°C, and the mean number of nearest neighbors remains 4.7. The latter result is consistent with x-ray scattering measurements.[58] The respective fractions of doubly, triply, and quadruply hydrogen-bonded molecules stay constant at 0.46, 0.38, and 0.16, respectively. Each of these results concerning local structure in the liquid refers specifically to the rescaled BNS interaction. Taken together they imply that very little structural reorganization (beyond lattice expansion) takes place in the liquid between 0 and 100°C. However, this conclusion might perhaps be regarded with some suspicion, since the structurally sensitive heat capacity C_p comes out of the calculations too low (12 cal/mole deg at 0°C instead of the 18 cal/mole deg measured).

Weres and Rice utilized their rescaled BNS cluster concentrations as input for a calculation of the amorphous-medium translational frequency spectrum, according to a method developed by Weres.[71] Strictly speaking, this goes beyond the scope of cell theory itself, but does test the predicted medium structure. At 10°C the frequency spectrum (i.e., the mode density) has two prominent peaks, at 70 cm^{-1} and at 190 cm^{-1}, which compare well with the broad bands observed in Raman, infrared, and neutron spectroscopy[72] at 60 cm^{-1} and at 170 cm^{-1}.

This cell-model calculation was carried out with a large number of approximations, some of which have uncertain numerical effects. However, the general approach followed seems sound, and at the very least has established that cell-model calculations for water are both feasible and capable of producing nontrivial and interesting results. It would be valuable for the developing field of water theory to exploit cell theory further, using a systematic series of modifications building on the Weres–Rice work. Some possibilities are:

1. The BNS interaction has been superceded by a more accurate effective pair potential (denoted by ST2; see Section VIII). This revised potential has a considerably lower curvature for vibrational motions, and should reduce or eliminate the need for a rescaling operation.

2. The constraint of equal occupation probabilities for first and second coordination shell sites should be removed.

3. A more accurate combinatorial factor g should be sought, perhaps along the lines established by Guggenheim and McGlashan.[60]

4. The equilibrium density should be determined by minimizing free energy with respect to vacancy concentration, rather than by identifying it with the average density over first and second coordination shells. This would be particularly important if the cell model were extended to describe the critical-point region of water, at which local density fluctuations become especially important. Considering the lattice-model results (Section VI), it would not be very surprising if the cell model then produced a liquid-phase density maximum.

5. Since the most frequent number of hydrogen bonds involving the cell molecule turned out to be two, it seems reasonable to expect that singly bonded configurations, and perhaps even unbonded ones, ought to have been permitted at the outset. If Stevenson's[68] ideas are correct, that these species have a low concentration in the liquid, an accurate cell-model calculation should lead to the same conclusion automatically.

6. The assumption of harmonic (and independent) translational and librational motions should be relaxed. Perhaps the requisite cell integrals could be calculated accurately by purely numerical means in the classical limit, and then quantum corrections (as a power series in Planck's constant) explicitly appended.

7. At least a few cell distortion correlation factors $Y^{(2)}$ and $Y^{(3)}$ could be evaluated classically by the Monte Carlo technique[73] to estimate their importance in the full cell cluster development (7.1).

Denley and Rice[74] recently used the configurational results of the Weres–Rice cell theory as a starting point for calculation of the intramolecular frequency spectrum in liquid water. Although they were required to introduce partially untested force-field assumptions, the results seem to account qualitatively for the observed spectra. It will ultimately be rewarding to see if the suggested improvements in the underlying cell theory create major changes in the predicted intramolecular spectra.

VIII. MOLECULAR DYNAMICS SIMULATION

A. Techniques of Computer Simulation

The lattice theory, and the cell theory at the dynamically uncorrelated level, have an attractive appeal due to the simple configurational descriptions of local molecular order that they introduce. If they could be followed through to exact solutions, they would provide compelling and remarkably vivid guides to intuition, thus largely satisfying the human urge to "understand" water.

Unfortunately, it is not possible to solve exactly lattice or cell theories, of the type we have encountered, in three dimensions. The results that have been obtained rest on simplifying statistical mechanical approximations, and

thus inevitably convey uncertainty. This situation also applies to any other analytical approach to understanding liquid water, such as the integral equation method for predicting molecular distribution functions.[75]

It is therefore fortunate that the complementary technique of direct computer simulation affords a viable and fertile alternative. This is not to imply that computer simulation methods are free of difficulty, for they are restricted to relatively small aggregates of molecules (N in the range 10^2 to 10^3), and to classical statistical mechanics at present. However, it is a general rule that the precision and the range of detail available in results of computer simulation for liquids far exceed those of other theoretical methods.

Two distinct simulation techniques have been developed, initially to describe simple liquids. Historically, the Monte Carlo method appeared first.[76] Given the appropriate intermolecular potential, it is designed to generate a large number of system configurations, distributed canonically according to preset values for the temperature and density. The collection of configurations then provides the basis over which arbitrary static properties (energy, virial, fluctuation quantities like C_V and κ_T, etc.) can be computed as suitable averages. Although some Monte Carlo work relevant to liquid water has been published,[29,77,78] its sum total at present is not very extensive, and therefore is not representative of the inherent capacity of the method to characterize the liquid in depth and detail. Consequently, we concentrate attention instead on the other simulation option.

The molecular dynamics method relies on a powerful digital computer to solve the classical equations of motion for the molecular aggregate, subject to suitable initial and boundary conditions. The temporal evolution of the molecular system is recorded in the course of solving these equations and, unlike the Monte Carlo method, this technique permits the calculation of kinetic properties, such as the self-diffusion constant, rotational relaxation, neutron inelastic scattering, and so on. A single molecular dynamics "run" is representative of a microcanonical ensemble, since total energy is a constant of the motion. But since the canonical (Monte Carlo) and microcanonical (molecular dynamics) equilibrium ensembles are equivalent in the large-system limit, barring first-order phase transitions, both are equally valid sources of structural and thermodynamical information. It is in its capacity to describe molecular motions and irreversible phenomena that the molecular dynamics approach enjoys a major advantage over the Monte Carlo approach.

The first use of molecular dynamics, by Alder and Wainwright,[79] involved spherical structureless particles. In this case the dynamical evolution is prescribed by the Newton equations for each of the N particles with mass m

$$\mathbf{F}_j = m\mathbf{a}_j \qquad 1 \leq j \leq N \tag{8.1}$$

which link acceleration $\mathbf{a}_j$ to the total vector force $\mathbf{F}_j$ on each particle j due to all others. In the case of water, the simplest realistic version of molecular dynamics treats each molecule as a rigid asymmetric rotor capable of simultaneous translation and rotation. As a result, it is necessary to supplement (8.1) for the center-of-mass motion by Euler equations[80] for the angular velocities $\boldsymbol{\omega}_j$ in terms of the torques $\mathbf{N}_j$:

$$\begin{aligned} I_1\dot{\omega}_{jx} - \omega_{jy}\omega_{jz}(I_2 - I_3) &= N_{jx} \\ I_2\dot{\omega}_{jy} - \omega_{jz}\omega_{jx}(I_3 - I_1) &= N_{jy} \\ I_3\dot{\omega}_{jz} - \omega_{jx}\omega_{jy}(I_1 - I_2) &= N_{jz} \end{aligned} \tag{8.2}$$

Here the Cartesian coordinates are affixed to molecule j, diagonalizing the inertial moment tensor $\boldsymbol{I}$ so that $I_{xx} = I_1$, and so on.

Normally, molecular dynamics calculations are carried out with periodic boundary conditions, the unit cell having dimensions fixed by the density of interest. The resulting absence of real boundaries produces an optimal situation for observing bulk water properties. However, this choice need not be the case and, in fact, deliberate insertion of "walls" or of crystal surfaces whose forces and torques appear in the dynamical equations (8.1) and (8.2) would be the means for studying interfacial water.

Temperature is implicitly determined by the amount of total energy given to the system as initial momentum and position data. In the long run the translational and rotational kinetic energies are equipartitioned between molecules, with the well-known mean values

$$\langle \tfrac{1}{2}mv_j^2 \rangle = \langle \tfrac{1}{2}\boldsymbol{\omega}_j \cdot \boldsymbol{I}_j \cdot \boldsymbol{\omega}_j \rangle = \tfrac{3}{2}k_B T \tag{8.3}$$

Molecular dynamics calculations must perforce span a limited time interval. The statistics of fluctuations separately for the translational and rotational terms in (8.3) offers one means of monitoring the quasi-ergodicity of the calculation.

In application to liquid argon, accurate and stable numerical integration of the equations of motion is possible using discrete time increments of 10^{-14} sec.[81] This interval is related to the magnitude of the molecular accelerations present in the liquid, and a longer time increment could be used to good practical advantage if the argon atoms interacted more weakly. The situation is quite the opposite in water, however, for the hydrogen-bonding interactions are very strong and highly directional. In conjunction with the small inertial moments possessed by water molecules, this characteristic requires that time increments in the neighborhood of 10^{-16} sec be used,[66] making the simulation of water a significantly more arduous task than that of argon. For a modest number of rigid water molecules, the time-dilation factor for a powerful digital computer between the absolute time interval for the molecules on the one hand, and the much slower running time on the computer on the

other hand, would be about 10^{16}. To carry the water sample forward in time by 1 sec would require 3×10^8 years. Fortunately, most kinetic phenomena of interest in liquid water fall into the picosecond range or shorter, making them fully accessible to the molecular dynamics technique.

Both the Monte Carlo and molecular dynamics simulation methods have frequently been called computer experiments. It is difficult to know if this phrase is offered as a profoundly edifying classification, or as a value judgment. In either event it fails to illuminate. The basic distinction between experiment and theory is that the former manipulates and observes real matter in the laboratory, while the latter constructs algorithms and theorems which may be esthetically pleasing in themselves but which encode numerical operations with varying efficiencies. An exact closed-form solution for the three-dimensional Ising model partition function, for example, would be a remarkable achievement for a variety of reasons, not the least of which would be the rule it gives for high-precision numerical tabulation of the thermodynamical properties for the model at all temperatures. Looked at in this light, it is obvious that the Monte Carlo and molecular dynamics algorithms ought more properly to be classified as computer theory rather than computer experiment.

Only selected portions of the published molecular dynamics work can be covered in this review. The reader may wish to check the cited articles for more detail.

B. ST2 Interaction

The initial studies of liquid water via molecular dynamics[66,67] used the BNS effective pair potential defined earilier in (7.17) to (7.23). This potential assigns specific positions to the oxygen and hydrogen nuclei (bond length 1 Å and bond angle θ_t), so the inertial moments I_1, I_2, and I_3 are determined completely by the atomic masses. The results of those initial molecular dynamics calculations were very encouraging, but suggested that the BNS potential was too tetrahedral, that is, its hydrogen bonds were too directional. This presumption was supported by the Weres and Rice observation[64] that librational frequencies were much too high for the BNS potential.

Consequently, a "second-generation" effective pair potential was devised[82] to mitigate the difficulty. The new interaction is called ST2, and represents a conservative modification of its predecessor. It has the same generic form as before:

$$v(\mathbf{x}_1, \mathbf{x}_2) = v_{LJ}(R_{12}) + S(R_{12})v_{el}(\mathbf{x}_1, \mathbf{x}_2) \tag{7.17}$$

with a short-range Lennard–Jones 12-6 part v_{LJ} and a modulated electrostatic portion Sv_{el} again based on charge tetrads in each molecule. The primary geometric change involved in BNS → ST2 is that the two negative

point charge ($-q$ in Fig. 17) have been drawn inward from 1 to 0.8 Å, measured along the tetrahedral rays from the oxygen nucleus. The charge tetrahedra thus have lower symmetry than before (the OH bond lengths are still 1 Å, and the angles about the O are still θ_t), but remain consistent with the molecular $\mathbf{C}_{2v}$ symmetry.

Changes in the parameters of course were required. For ST2 the Lennard–Jones parameters are

$$\begin{aligned} \sigma &= 3.10 \text{ Å} \\ \varepsilon &= 5.2605 \times 10^{-15} \text{ erg} \\ &= 7.5750 \times 10^{-2} \text{ kcal/mole} \end{aligned} \tag{8.4}$$

while the point charges to be used in (7.18) for v_{el} are

$$q = 0.2357e = 1.13194 \times 10^{-10} \text{ esu} \tag{8.5}$$

The modulation function S has the same cubic spline form (7.19) as before, but now the singular points are

$$\begin{aligned} R_L &= 2.0160 \text{ Å} \\ R_U &= 3.1287 \text{ Å} \end{aligned} \tag{8.6}$$

The absolute minimum of the ST2 potential is achieved in a mirror-symmetric configuration for the dimer as illustrated in Fig. 4. The displacement angle α of the donating OH (see Fig. 4) is only 1.1°, so the hydrogen bond is virtually linear. The separation R_{12} of the oxygens is 2.852 Å, and at this minimum v(ST2) is -6.839 kcal/mole.

It is interesting to trace out the *constrained* minimum for the ST2 potential for fixed oxygen–oxygen separation R_{12}. When this distance exceeds 4.964 Å $= R_c$, the molecular symmetry axes are rigorously collinear (the molecular planes are perpendicular as in Fig. 4 for all R_{12}). This collinearity reflects the predominant influence of dipole–dipole interactions at these large separations. However, the interactions of higher multipoles succeed in producing an instability at R_c, wherein mutual twisting of the molecules at smaller R_{12} leads to configurations more in accord with linear hydrogen bonding. At R_c the dimer can go in either of two ways toward a linear hydrogen bond, depending on which OH bond of the donor molecule begins to rotate toward the acceptor oxygen. Thus R_c is a critical point at which a spontaneous symmetry breaking arises. This point for the constrained energy surface is analogous to the critical point of the free-energy surface (versus magnetization) for a field-free Ising model. In the latter example the spontaneous magnetization also represents a broken symmetry. With respect to water potentials, the existence of a critical separation R_c is not unique with

the ST2 interaction; the BNS interaction has qualitatively the same behavior, and so too should the exact water potentials $V^{(2)}(\mathbf{X}_1, \mathbf{X}_2)$, $\overline{V}^{(2)}(\mathbf{x}_1, \mathbf{x}_2)$, and $v(\mathbf{x}_1, \mathbf{x}_2)$.

C. Nuclear Pair Correlation Functions

Many of the important characteristics of short-range molecular order in liquids are conveniently portrayed in the nuclear pair correlation functions. For water there are three, $g_{OO}(r)$, $g_{OH}(r)$, and $g_{HH}(r)$. They give the probability, relative to random expectation, of the occurrence of distance r as a separation between pairs of nuclei of the subscripted species. The conventional normalization requires (μ, ν = O or H)

$$\lim_{r \to \infty} g_{\mu\nu}(r) = 1 \tag{8.7}$$

in the infinite system limit. These correlation functions obviously represent integral contractions of the pair distribution function $\rho^{(2)}$ introduced earlier; for example,

$$g_{OO}(r) = (32\pi^3\rho^2 r^2)^{-1} \int d\mathbf{x}_2 \, \delta(R_{12} - r)\rho^{(2)}(\mathbf{x}_1, \mathbf{x}_2) \tag{8.8}$$

where R_{12} is the distance between oxygens.

Figure 8 shows the $g_{OO}(r)$ determined by molecular dynamics for a sample of simulated water[82] (using the ST2 potential) at 10°C and mass density 1 g/cm. The calculation involved $N = 216$ molecules confined to a cube with edge length 18.62 Å, to which periodic boundary conditions applied. For comparison, Fig. 18 also shows a $g_{OO}(r)$ result inferred by Narten[83] from x-ray diffraction intensities for water at 4°C (the small temperature difference is negligible for present purposes). The dynamical simulation spanned 8.1 psec, and for convenience was carried out with neglect of molecular interactions for pairs of molecules having their oxygens more than 8.46 Å apart.

The main features of the two curves agree well. The positions at which the prominant first peak occurs differ by no more than 0.01 Å, and the broad successive maxima exhibit nearly equal positions as well. The experimental curves usually show some short-wavelength ripples, and that in Fig. 18 is no exception. If it is justifiable to consider those ripples artifacts of the experimental data processing, the agreement of the molecular dynamics curve with experiment at the first minimum of $g_{OO}(r)$ (near 3.5 Å) may be somewhat better than Fig. 18 seems to indicate.

The most important structural theme carried by these $g_{OO}(r)$ curves is the persistence of tetrahedral icelike order into the liquid phase. Although the second maxima around 4.5 Å are broad, they occur at about the correct multiple (1.633) of the first peak distance to represent second neighbors

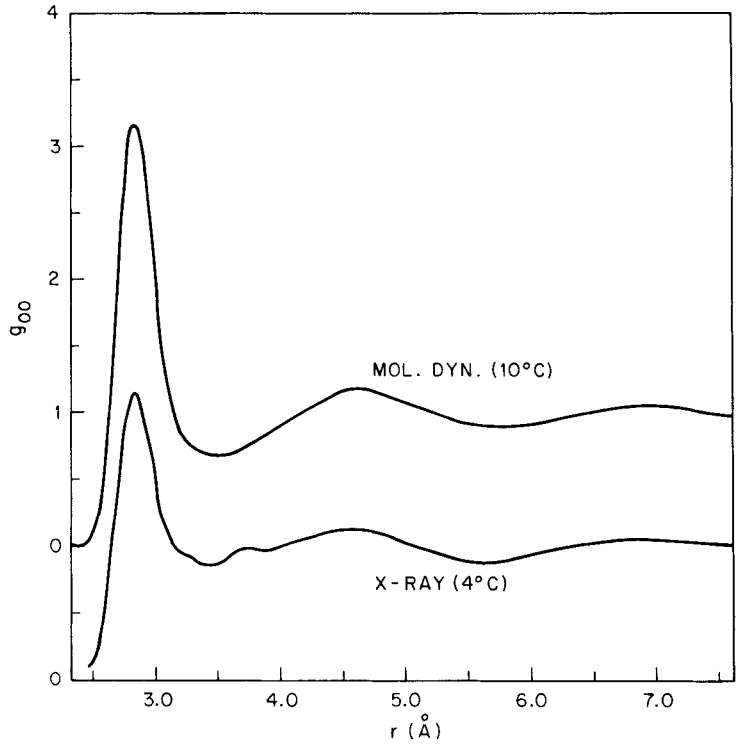

Fig. 18 Comparison of oxygen nucleus pair correlation functions for liquid water. The molecular dynamics result[82] was based on 216 molecules at mass density 1 g/cm^3 interacting through the ST2 effective pair potential. The x-ray diffraction result is due to Narten.[83]

connected along a path of two hydrogen bonds at an angle which on the average is θ_t. In ice Ih or Ic, the second neighbors of course produce a narrow peak; the breadth manifested in the liquid phase indicates frequent and considerable strain.

The molecular dynamics first-neighbor peak is higher and narrower than its experimental counterpart. For the ST2 model the molecular dynamics curve in Fig. 18 is an accurate determination. The experimental curve for real water is probably a less precise determination, considering the interpretive ambiguities one is forced to accept in analyzing the experimental data. Even so, the shape distinction between the respective first peaks is almost certainly real. It probably arises from failure of the molecular dynamics calculations to account for quantum corrections, which tends to delocalize particles somewhat. The same effect on the broader successive g_{OO} maxima is less obvious, and this seems to be the case.

The average number of neighbors computed for the molecular dynamics g_{OO} out to its first minimum is 5.5. The corresponding number for the experimental curve is 5.3, nearly the same. (Note that the average coordination number 4.4 reported by Narten, Danford, and Levy[58] was based on a different definition of "first neighbor.")

ST2 molecular dynamics runs at temperatures both above and below 10°C have also been carried out.[82] The trend observed for g_{OO} agrees with that found by x-ray diffraction,[83] namely, that the amplitude of oscillation of this function about unity diminishes with increasing temperature, while the average coordination number increases somewhat. At least on the basis of g_{OO} evidence, one can conclude that the molecular dynamics approach with the ST2 potential gives a moderately good structural representation of real liquid water.

Some of the characteristic macroscopic anomalies exhibited by water are also qualitatively obtained in the ST2 simulation.[82] It has been found that the liquid density (at the vapour–liquid coexistence line) passes through a

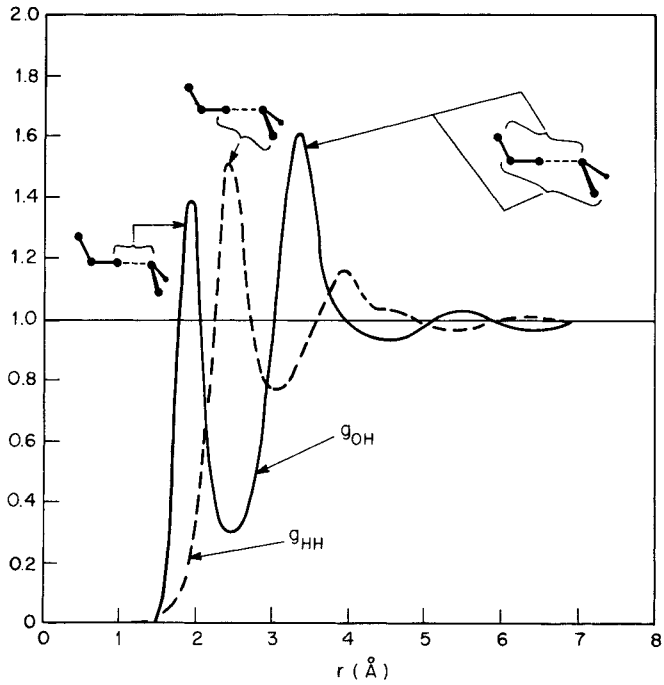

Fig. 19 Nuclear pair correlation functions g_{OH} and g_{HH} for ST2 water model at 10°C, 1 g/cm^3. The intramolecular pairs are not included. The main contributing structures for the prominent peaks are shown.

maximum at 27°C, at which the mass density reaches 1.0047 g/cm^3. Furthermore, the isothermal compressibility passes through a shallow minimum at about 20°C. No doubt these phenomena are related to the remanent tetrahedral order observed in g_{OO}, which slowly disappears as the temperature rises.

In principle it should be possible to combine results from x-ray and neutron diffraction experiments (the latter using distinct isotopically substituted waters) to determine all three functions g_{OO}, g_{OH}, and g_{HH}. But in practice this demanding project has not been yet attempted. The molecular dynamics simulations have preceded experiments by calculating g_{OH} and g_{HH} separately and (for the model) precisely. Figure 19 shows these functions determined by the 10°C, 1 g/cm^3 run on which the g_{OO} curve in Fig. 18 was based. The prominent peak in both functions at a small distance can be identified as shown in terms of hydrogen bonding between neighbors. As expected, these features diminish in distinctiveness as the temperature rises.

By invoking a plausible assumption about the nature of local order in water, Narten produced tentative g_{OH} and g_{HH} functions from available x-ray and neutron diffraction data.[84] Their shapes are qualitatively similar to those shown in Fig. 19, with the same prominent peaks. These peaks are substantially broader than the molecular dynamics versions, perhaps in part because of quantum fluctuations present in the real water.

D. Hydrogen Bond Patterns

The existence of a hydrogen bond between two molecules is not fundamentally a yes-or-no proposition. Analogous to the case for conventional covalent chemical bonds, the hydrogen bond phenomenon is connected with continuous spatial variation in interaction energies, and does not discontinuously "click on" at an unique distance. However, this observation should in no way be interpreted as minimizing the importance for chemistry of the hydrogen bond concept, since this concept conveys specific quantitative information about potential surfaces and serves to motivate extremely important correlations of diverse experimental data.[85]

In connection with computer simulation of water, one is obliged to establish a convention for hydrogen bonds, which can be applied to an arbitrary given configuration of N molecules, that states what pattern of hydrogen bonds exists. In particular, the application of this criterion to ice should automatically have each water molecule hydrogen-bonded to all its four nearest neighbors and to no other molecules. Although such a criterion necessarily must involve some element of arbitrariness, it can serve to legitimize an important class of questions about the topological patterns of hydrogen bonds existing in liquid water and aqueous solutions.

Since the primary attribute of hydrogen bonding is the energy of stabiliza-

tion involved, it is convenient to base the hydrogen bond convention on potential energy alone. For models using an effective pair potential v, one decides whether a pair i, and j of molecules is bonded or not depending on how $v(i, j)$ compares with a preassigned negative cutoff energy V_{HB}:

$$\begin{aligned} v(\mathbf{x}_i, \mathbf{x}_j) &\leq V_{HB} \qquad i \text{ and } j \text{ hydrogen-bonded} \\ &> V_{HB} \qquad i \text{ and } j \text{ not hydrogen-bonded} \end{aligned} \tag{8.9}$$

The element of arbitariness of course is the magnitude of V_{HB}, but once it is assigned the criterion is mathematically unambiguous. A study of the ST2 potential shows that, if V_{HB} lies between -1.7 and -4.5 kcal/mole, the conventional hydrogen bond pattern in ice will be reproduced.[86]

Having selected V_{HB}, it is possible to classify molecules according to the number of hydrogen bonds in which they simultaneously participate. Relative concentrations of nonbonded, single-bonded, double-bonded, and so on, water molecules have been calculated both for BNS[67] and ST2[87] water simulations for a wide variety of V_{HB} choices. For all temperatures and densities investigated to date, the distributions obtained for the liquid have a single maximum. Consequently, one can rule out of serious consideration earlier suggestions[88–91] that liquid water consists of a fully bonded framework heavily invaded by unbonded interstitials for, if that were true, a bimodal distribution would arise for *some* V_{HB} choice. The two maxima of this required bimodal distribution would occur at zero hydrogen bonds (interstitials) and at four hydrogen bonds (framework molecules), with virtually no molecules with one, two, or three hydrogen bonds. Evidently, a more accurate description of liquid water would be "defective, strained, random network," to be consistent with the observed hydrogen bond distributions.

Fixing the concentrations of molecules with different numbers of hydrogen bonds still leaves a wide range of possible topological connections between these bonds. Further specification of the network topology can be achieved by examining the polygons formed by the hydrogen bonds. If it were true, for example, that the liquid networks were equivalent to ice Ih or Ic in which a certain fraction of the nearest-neighbor bonds had been randomly broken, the remaining polygons would have 6, 8, 10, 12, and so on, sides, but no polygons with odd numbers of sides could occur.

Table IV shows polygon counts carried out by computer on the 10°C, 1 g/cm^3 sample of water simulated with the ST2 potential.[86] Four alternate values of V_{HB} were employed to illustrate dependence on this arbitrary parameter, from a rather permissive value (-2.121 kcal/mole) to a very stringent value (-4.848 kcal/mole). Only "non-short-circuited polygons" are included; these are primitive polygons having no hydrogen bond cross-links tending to split them into smaller polygons. For practical reasons it

TABLE IV

Parameters Characterizing the hydrogen bond patterns in Liquid Water at 10°C and Mass Density 1 g/cm^3.[a]

Parameter	I	II	III	IV
V_{HB} (kcal/mole)	−2.121	−3.030	−3.939	−4.848
$\langle b \rangle$	3.88	3.14	2.26	1.18
n_0	0	0.00331	0.0410	0.249
n_1	0.0026	0.029	0.180	0.415
C_3	0.05952	0.002976	0	0
C_4	0.1564	0.04663	0.007606	0
C_5	0.3459	0.1362	0.03406	0.001323
C_6	0.3548	0.1306	0.02447	0.0006614
C_7	0.3320	0.1280	0.01687	0
C_8	0.2715	0.1045	0.01224	0
C_9	0.1971	0.09854	0.01224	0
C_{10}	0.1118	0.09292	0.01422	0
C_{11}	0.07573	0.08664	0.005952	0

[a] The mean number of hydrogen bonds terminating at a molecule is $\langle b \rangle$; n_0 is the fraction of unbonded molecules, and n_1 is the fraction with precisely one bond; C_j stands for the number of non-short-circuited polygons per molecule of the liquid with j sides. (Results from Ref. 86, Table II.)

was necessary to terminate the search-and-count routine after 11-bond polygons.

The entries in Table IV show no preference for either even or odd numbers of sides. Furthermore, by extrapolating the results shown, it is clear that polygons with more than 11 sides exist in nonnegligible concentrations, except when a very strict definition of hydrogen bonds (low V_{HB}) is applied. These observations are inconsistent with published opinions[38,92] to the effect that liquid water consists of unconnected, bulky, icelike clusters suspended in a medium of unbonded water molecules. Instead, further support seems to be given to the random, space-filling, hydrogen bond network view, without any large-scale inhomogeneities, that was first developed for the molecular dynamics simulations by examining stereoscopic photographs of molecular positions.[66,67]

When aqueous solutions are eventually studied by computer simulation, it will be interesting to see what characteristic hydrogen bond structures tend to form around chemically different types of solutes, in comparison with those in pure bulk water. Particular importance attaches to those nonpolar functional groups that engage in hydrophobic bonding.[93]

Up to the present only time-average properties have been calculated for the hydrogen bond network present in liquid water. However, there

are analogous kinetic properties that could also be probed with the available simulation apparatus, whose understanding would unquestionably enrich our comprehension of the molecular nature of water. Using the same definition of hydrogen bonds as before in terms of a preassigned cutoff energy V_{HB}, we mention three distinct lifetime queries:

1. Identify the molecular pairs bonded at time $t = 0$. Define $P_1(t)$ to be the average fraction of pairs that remain bonded *without interruption* over the entire interval from 0 to t.
2. In terms of the same set of $t = 0$ pairs, let $P_2(t)$ be those that are bonded at later time t, *irrespective of intervening interruptions.*
3. Denote the total number of hydrogen bonds present in the system at time t by $N_b(t)$, and set

$$P_3(t) = \frac{\langle [N_b(0) - \langle N_b \rangle][N_b(t) - \langle N_b \rangle] \rangle}{\langle [N_b - \langle N_b \rangle]^2 \rangle} \tag{8.10}$$

P_1, P_2, and P_3 are each equal to unity at $t = 0$, and in the infinite system limit they all approach zero as t increases. Their long time behaviors ought to be roughly exponential with characteristic decay times τ_1, τ_2, and τ_3. Naive considerations lead one to expect

$$\tau_1 < \tau_2 < \tau_3 \tag{8.11}$$

which could be checked for the molecular dynamics simulations.

The ability to pose and answer quantitative questions of the sort mentioned here illustrates the dramatic power of the simulation methods. No experimental techniques are known, or are ever likely to be developed, to determine the topological properties of the hydrogen bond network in liquid water and its solutions. Thus computer simulation has the dual tasks of reproducing experimental results as well as complementing them.

E. Effect of Pressure

The crystallographic structures of the ice polymorphs[7] demonstrate that in the solid phases the response to increasing pressure involves the use of more and more efficient packing with little change in length of hydrogen bonds. In some of the ices, packings denser than ice Ih and Ic are achieved by deformation of angles between successive hydrogen bonds from the ideal θ_t, so as to move second- and higher-order neighbors of any given molecule inward. But interpenetration of networks also accomplishes the same end and, as we have previously noted, the interpenetration of two equivalent ice Ic networks appears in the very-high-pressure ices VII and VIII, with the effect of doubling density and number of nearest neighbors (from four to eight).

One would expect similar considerations to apply in the liquid state. Although experiments to determine structure in very highly compressed liquid water, such as x-ray and neutron diffraction, are probably impractical to execute, molecular dynamics or Monte Carlo simulations are no more difficult to perform with extremes of temperature and pressure than under ordinary conditions.

Figure 20 shows an oxygen–oxygen pair correlation function $g_{OO}(r)$ computed for 97°C and mass density 1.346 g/cm^3. This is the liquid density that exists at the experimental triple point (81.6°C, 22.0 kbars) for liquid, ice VI, and ice VII. Once again the ST2 interaction was employed for the molecular dynamics simulation.

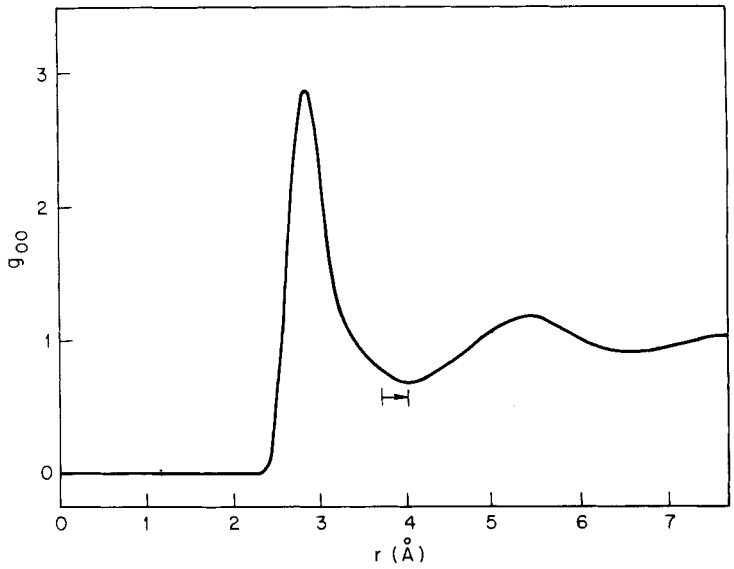

Fig. 20 Oxygen-oxygen pair correlation function for 97°C, 1.346 g/cm^3, based on the ST2 molecular dynamics simulation. The horizontal arrow shows how far the minimum displaces outward as a result of isothermal compression from 1 g/cm^3.

The first maximum of $g_{OO}(r)$ occurs at 2.81 Å, only slightly less than its position at 1 g/cm^3, namely, 2.86 Å. However, the subsequent minimum shifts outward to 4.00 Å, from the 1-g/cm^3 distance 3.68 Å, as shown explicitly in Fig. 20. The mean number of neighbors out to the 4.00-Å minimum is 11.8. In order to make a fair comparison with the low-density number (5.8 neighbors at 97°C), the distance 3.68 Å should instead be used as the upper cutoff, and in this event the high-compression structure possesses

10.0 neighbors. From any point of view, the packing of molecules has been dramatically altered by compressing the liquid from 1 to 1.346 g/cm^3.

The four tetrahedrally disposed directions pointing from the oxygen nucleus to point charges $\pm q$ in definition of the ST2 potential bear an intimate geometric relation to the regular octahedron. In particular, by placing the oxygen at the center of the octahedron, the four tetrahedral directions may be oriented so as simultaneously to pierce the centers of four of the eight triangular faces which share vertices but not edges. This relationship is shown in Fig. 21.

The four pierced octahedron faces in Fig. 21 are faces through which first-neighbor oxygens in an unstrained hydrogen bond network would be seen from the position of the central oxygen, as in the ice crystal. The solid angles described by the unpierced triangular faces would be devoid of first neighbors. The octahedron thus provides a useful way to resolve $g_{OO}(r)$ into angular components:

$$g_{OO}(r) = g_{IV}(r) + g_{V}(r) \tag{8.12}$$

where the established convention[67] denotes pierced and unpierced faces by subscripts IV and V, respectively. The extent to which ice rules on first neighbors are violated in the liquid indicates either angular strains in the local network structure, or interstitial molecules (due possibly to network interpenetration).

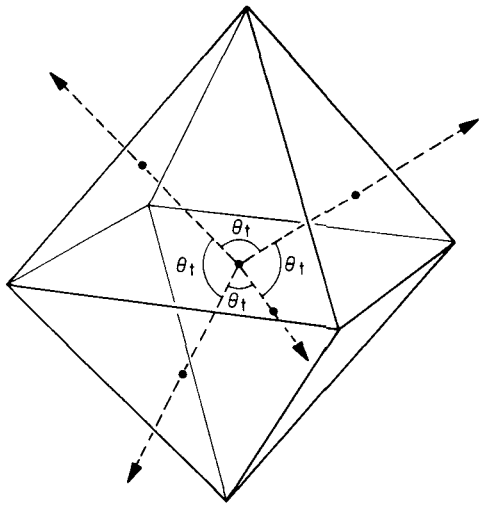

Fig. 21 Tetrahedral directions piercing centers of alternate octahedron faces.

In the low-pressure case (1 g/cm^3), most of the nearest neighbors are known to occur in g_{IV}.[67] But when g_{IV} and g_V are evaluated for high-compression molecular dynamics runs (1.346 g/cm^3), nearly equal numbers of nearest neighbors appear in g_{IV} and g_V, undoubtedly indicating substantial network penetration.

The interpenetrating cubic ice networks forming ice VII place four nearest neighbors in each of g_{IV} and g_V, not enough to make up the observed 10 to 12 in the compressed liquid simulation. Furthermore, the neighbor distance[7] in ice VII is 2.86 Å, significantly larger than the 2.81 Å found in the simulation for the liquid. Finally, the second maximum of g_{OO} in Fig. 20 is too far out compared to the first maximum to be consistent with successive hydrogen bonds at an average angle θ_t. Evidently, it cannot be valid to view the highly compressed liquid as dominated by ice VII structures.

Similar considerations seem to rule out ice VI as a major contributor to the liquid structure. In particular, a well resolved second-neighbor peak[7] would have to appear around 3.51 Å; clearly, it does not in Fig. 20.

The situation concerning the highly compressed liquid is similar to the liquid at atmospheric pressure. A much more diverse set of local structures is represented than can reasonably be generated by slight deformations of the crystal forms present at the respective pressures.

F. Molecular Motions

One aspect of molecular motion in liquids is revealed by the magnitude of the self-diffusion constant D. In an infinite system D may be written in the alternative forms

$$D = \lim_{t\to\infty} \left\{ \frac{\langle [\Delta \mathbf{R}_j(t)]^2 \rangle}{6t} \right\}$$

$$= \tfrac{1}{3} \int_0^\infty \langle \mathbf{v}_j(0) \cdot \mathbf{v}_j(t) \rangle \, dt \tag{8.13}$$

in terms of equilibrium ensemble averages. The former involves the mean-square displacement $\Delta \mathbf{R}_j$ of the center of molecule j over time t, while the second utilizes the velocity $\mathbf{v}_j$ of this molecule's center. For molecules that do not dissociate, it does not matter what fixed point is used as the center.

Neither infinite systems nor infinite periods are available in simulations by molecular dynamics. Nevertheless, (8.13) is still useful. In the first case $\langle [\Delta \mathbf{R}_j]^2 \rangle$ versus t tends to approach a limiting slope quite rapidly, and this slope can be identified with $6D$. In the second case the velocity autocorrelation function decays towards zero sufficiently quickly that the time integral may normally be cut off at an upper limit considerably shorter than the dynamical run interval.

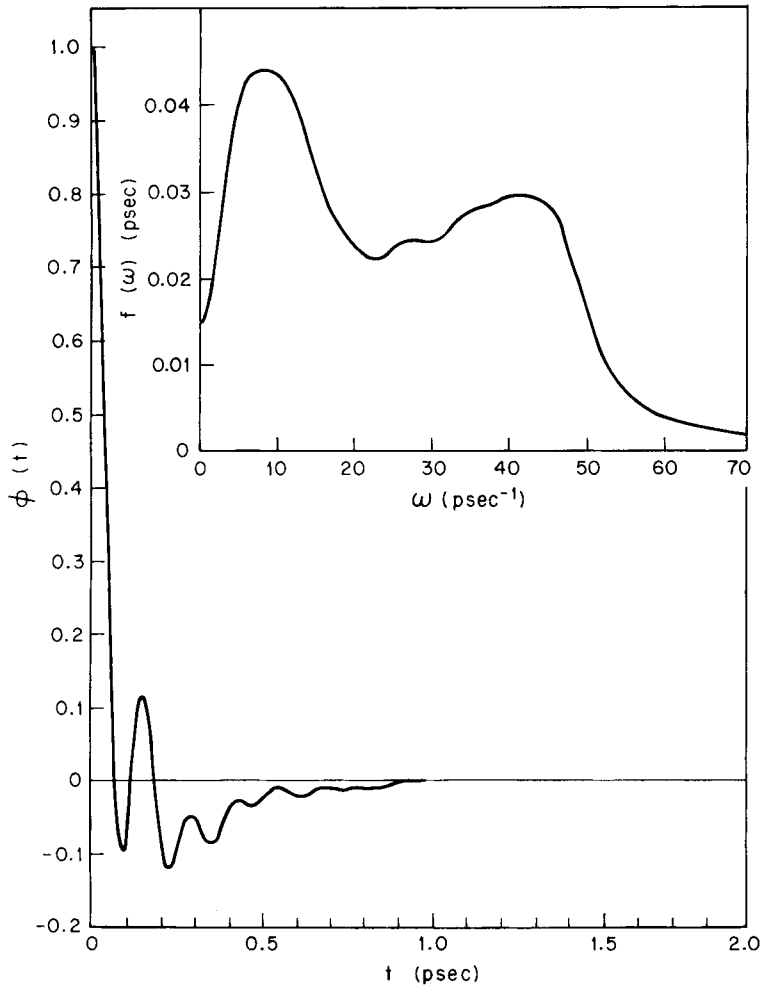

Fig. 22 Normalized center-of-mass velocity autocorrelation function for the ST2 simulation of liquid water at 10°C, 1 g/cm^3.

Figure 22 exhibits a normalized velocity autocorrelation function for center-of-mass motion:

$$\varphi(t) = \frac{\langle \mathbf{v}_j(0) \cdot \mathbf{v}_j(t) \rangle}{\langle v_j^2 \rangle}$$
$$\langle \mathbf{v}_j^2 \rangle = \frac{3k_B T}{m} \tag{8.14}$$

It was calculated for the ST2 simulation of a 10°C, 1-g/cm^3 liquid. The inset shows the power spectrum:

$$f(\omega) = \int_0^\infty \varphi(t) \cos(\omega t)\, dt \tag{8.15}$$

Evidently, $\varphi(t)$ is essentially zero for times larger than a picosecond, whereas the dynamical run from which Fig. 22 was prepared lasted more than 8 psec.

The marked oscillatory nature of $\varphi(t)$ arises from the strong hydrogen bonding present in the liquid. A typical molecule tends to vibrate back and forth several times in the force field of its neighbors before it breaks free or the neighbors shift positions to modify the force field. Velocity autocorrelation functions computed by molecular dynamics for liquid argon[81] approach zero from below as does the water case, but without the distinctive oscillations.

The two broad maxima in $f(\omega)$ are centered at 44 and 215 cm^{-1}. These can probably be identified with broad bands observed experimentally[94] by infrared, Raman, and inelastic neutron-scattering spectroscopy to occur at about 60 cm^{-1}, and in the region 150 to 200 cm^{-1}.

As might have been expected, raising the temperature causes the oscillatory nature of $\varphi(t)$ to diminish. At the same time, the two broad maxima in $f(\omega)$ lose their distinctiveness, while drifting somewhat to lower frequencies.[82]

In principle the velocity autocorrelation function must have an asymptotic tail, of hydrodynamical origin, behaving at $t^{-3/2}$ at long times.[95,96] However, none of the molecular dynamics investigations for water has succeeded in identifying this tail. It is likely that the strong hydrogen bonds present in the liquid create a rigidity toward high-frequency stress, which tends to quench the hydrodynamical tail compared to simple liquids.

The values of D found in the ST2 simulations for water at 1 g/cm^3 show the proper rapid increase with temperature. However, they are uniformly higher than experimental values by about 30% between the melting point and about 40°C.[82] Comparisons are not yet available beyond this temperature range. Although much better agreement could be obtained by increasing the strength of the ST2 interaction (by a simply multiplicative renormalization), such tampering would cause undesirable damage to other properties. Until quantum corrections can be appended to the manifestly classical simulation, it would be misdirected effort to insist on very precise agreement between predicted and measured D.

Rotational diffusion of water molecules has also been studied by the simulation method. Autocorrelation functions for angular momentum components about the three principal axes separately exhibit strong oscillatory character, showing that the molecules execute rapid librational motion

under the directional hydrogen bond forces of neighbors. The quantities

$$\Gamma_n(t) = \langle P_n[\cos \theta(t)] \rangle \tag{8.16}$$

measuring the distribution of angles $\theta(t)$ through which the dipole axis of a molecule turns in time t have also been computed for $n = 1, 2$. The initial behavior of the Γ_n reflects the high-frequency librational motion, but at long times the decay seems to involve a single dominant exponential function of time. Analogous to the center-of-mass velocity autocorrelation function, the presumed hydrodynamical nonexponential tails on the Γ_n are not visible.[97] The decay time exhibited by Γ_1 is closely connected to the macroscopic dielectric relaxation time, and indeed compares reasonably well in magnitude with measured values. However, the exact connection between the microscopic and macroscopic rates is still controversial,[98] so that a decisive comparison cannot yet be made.

The ST2 simulation has also provided the basis for a molecular dynamics calculation of neutron inelastic scattering from liquid water.[99] Protons act as strong incoherent scatterers for neutrons, so observed scattering cross sections yield information about proton motions. In particular, the cross section for scattering with momentum change $\hbar\mathbf{k}$ and energy change $\hbar\omega$ gives the function

$$S_{\text{inc}}(k, \omega) = \int_0^\infty dt \cos(\omega t) \langle \exp[i\mathbf{k} \cdot \Delta\mathbf{r}_j(t)] \rangle \tag{8.17}$$

where $\Delta\mathbf{r}_j(t)$ is the displacement of a typical proton j over time interval t. It is known that

$$\lim_{k \to 0} \frac{\omega^2}{k^2} S_{\text{inc}}(k, \omega) = h(\omega) \tag{8.18}$$

is, aside from trivial factors, the power spectrum of the proton velocity autocorrelation function. The molecular dynamics calculations explicitly show that for all intents and purposes the limiting behavior shown in (8.18) is achieved for $\omega^2 S_{\text{inc}}/k^2$ at $k = 1$ Å^{-1}, which ought to be directly obtainable in real experiments.

Careful studies of both proton and center-of-mass motions by molecular dynamics give no support to quasi-crystalline "jump-and-wait" descriptions for molecular motions in liquid water.[100]

IX. WEAK-ELECTROLYTE MODEL

A. Central Interactions

None of the statistical models mentioned above (lattice models, cell model, molecular dynamics simulations) has permitted water molecules to dissociate. Yet in real water this occurs to produce the chemically important

hydrated H^+ and OH^- ions. Unless it can eventually describe the structure and kinetics of these species in water, the theory of this liquid must be regarded as partial failure. To help avoid this shortcoming, Lemberg and Stillinger have proposed a weak-electrolyte model for water[101] in which the separate H and O particles become the basic dynamical entities, and H_2O molecules spontaneously form as "ion triplets" on account of the specific forces attributed to these particles. The dissociation process thus becomes a natural thermally activated process in the model.

At the heart of the weak-electrolyte model is the selection of three central potentials $V_{HH}(r)$, $V_{OH}(r)$, and $V_{OO}(r)$ which must adequately represent in additive form, for all pairs of nuclei, the totality of interactions in an arbitrary collection of molecules and ions. The first two of these functions are constrained by the requirement that the energy minimum they give for an isolated H_2O possesses the accurately known nonlinear triatomic geometry discussed in Section II. Furthermore, V_{HH}, V_{OH}, and V_{OO} should each have Coulombic forms at large r characteristic of electrostatic charges on Hs and Os which produce the correct dipole moment for the isolated molecules.

Beyond the capacity to describe dissociation and the nature of the resulting solvated ions, the weak-electrolyte model presents other attractive features. Owing to the fact that only central forces are used, it is much easier than otherwise to construct formal expressions for quantum corrections to the classical limit formulas both for equilibrium and for transport properties. Also, it is important that the three normal vibrations have been restored to each molecule,with frequencies determined by the curvatures of V_{HH} and V_{OH}. As a result, it should be possible to examine the broadening of vibrational bands in condensed phases due to interactions between molecules which are themselves described by the three potential functions V_{HH}, V_{OH}, and V_{OO}. Finally, the use of only central pair interactions makes it feasible to examine binary mixture versions of standard integral equations (e.g., BGY, PY, CHNC equations[42]) for prediction of the three nuclear pair correlation functions $g_{OO}(r)$, $g_{OH}(r)$, and $g_{HH}(r)$, which is not possible with rigid-molecule models generally.

Continuing study of the weak-electrolyte model will be necessary to identify the optimal set of central interactions; however, we can display a tentative set which clearly illustrates the main ideas involved. First, the effective charges on the hydrogens (Q^*) and the oxygens ($-2Q^*$) must be

$$\begin{aligned} Q^* &= 0.32983e \\ &= 1.5841 \times 10^{-10} \text{ esu} \end{aligned} \tag{9.1}$$

to conform to the known molecular dipole moment. We then demand that $V_{OH}(r)$ consist just of two inverse power terms, $-2Q^{*2}/r$ for the Coulombic

attraction between the O and H, plus a strong repulsion at short range ($n > 1$):

$$V_{OH}(r) = \frac{2(Q^*)^2}{r_e}\left[\frac{1}{n}\left(\frac{r_e}{r}\right)^n - \frac{r_e}{r}\right] \tag{9.2}$$

This function passes through its minimum when $r = r_e$, the equilibrium bond length in the water molecule. In the present central force context, the asymmetric stretch normal mode frequency depends only on the curvature of V_{OH} at r_e, so n was determined to be

$$n = 14.9797 \tag{9.3}$$

from the observed D_2O frequency. In terms of the convenient units angstroms for length and kilocalories per mole for energy, V_{OH} has the specific expression

$$V_{OH}(r) = \frac{2.66366}{r^{14.9797}} - \frac{72.269}{r} \tag{9.4}$$

Two protons simultaneously present in the minimum of V_{OH} at r_e can be constrained to form a nonlinear triatomic molecule only if V_{HH} possesses a relative minimum at the correct proton–proton distance $r_p = 1.5151$ Å. Energetic stability of the H_2O molecule of course requires

$$2V_{OH}(r_e) + V_{HH}(r_p) < 0 \tag{9.5}$$

but $V_{HH}(r_p)$ can be positive. The symmetric stretch and symmetric bend normal mode frequencies are determined by both curvatures $V''_{OH}(r_e)$ and $V''_{HH}(r_p)$ but, since the first has already been fixed, the second must be chosen to achieve the best simultaneous fit to the symmetric mode frequencies. With this understanding the following specific function was constructed for V_{HH} (in angstroms and kilocalories per mole):

$$V_{HH}(r) = \frac{36.1345}{r} + \frac{30}{1 + \exp[21.9722(r - 2.125)]} - 26.51983 \exp[-4.728281(r - 1.4511)^2] \tag{9.6}$$

With this potential, and that shown for V_{OH} in Eq. (9.4), the symmetric bend frequency is 14.4 % too low and the symmetric stretch frequency is 14.4 % too high, compared to observed values, all for D_2O.

The primary task assigned to V_{OO} is to keep oxygens in different molecules apart. Otherwise the strong attraction between oxygen and hydrogen leads to linear hydrogen bonds of length about $2r_e$, with the bridging hydrogen

half way between. One function found to produce proper asymmetric linear hydrogen bonds with the correct length and strength is

$$V_{OO}(r) = \frac{1697116}{r^{12}} - \frac{4039.394}{r^6} + \frac{144.538}{r} \tag{9.7}$$

expressed as before in angstroms and kilocalories per mole. This and the other two potentials (9.4) and (9.6) are plotted in Fig. 23.

The mechanically stable structure for the hydronium cation H_3O^+ is pyramidal, with all three OH bonds having length r_e, and the apex angles at the oxygen the same as the bond angle in the water molecule. This arises because of the possibility that all six pairs of particles in H_3O^+ can exist simultaneously at the minima of their respective central potentials. It is relevant to note in this connection that the real H_3O^+ is also pyramidal, with apex angles and bond lengths only slightly larger than those predicted by the weak-electrolyte model.[102]

The disproportionation reaction

$$H_2O + H_2O \rightarrow H_3O^+ + OH^- \tag{9.8}$$

with widely separated reactants and products all at their respective mechanical equilibria, is energetically unfavorable. Counting pairs, it becomes clear that the energy must increase by $V_{HH}(r_p)$ to produce the ionic products, which

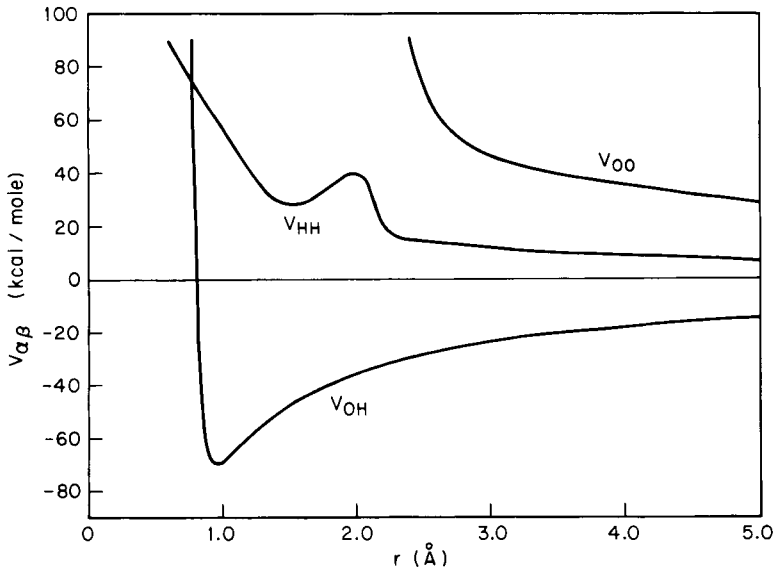

Fig. 23 Central potentials for the weak electrolyte model of water.

Fig. 23 shows to be about 28 kcal/mole. A positive energy of this magnitude is necessary to prevent gross ionization in water molecule aggregates.

Although it is true that the weak-electrolyte model utilizes only interactions for pairs of ionic particles, the molecules out of which they are composed do not necessarily behave as though they have experienced additive *molecular* interactions. Neighboring molecules tend to perturb one another's normal models of vibration, and (4.7) to (4.10) show that vibrationally averaged component potentials $\overline{V}^{(n)}$ of all orders should in principle arise. The automatic incorporation of these many-molecule effects ought to be listed as one of the weak-electrolyte model's virtues.

The H^+ and OH^- ions in the present model do not carry the full charges $\pm e$, but only the partial charges $\pm 0.32983e$. However, the electric fields of the real ions in liquid water are diminished, or shielded, by the electronic polarizability of neighboring molecules. This form of polarizability is not present in the weak-electrolyte model, but the reduced ionic charges offer partial compensation for this omission.

B. Some Classical Formulas

At sufficiently high temperatures the partition function Q for the weak-electrolyte model (with N oxygens and $2N$ hydrogens) takes the classical form:

$$Q = \frac{1}{N!(2N)!\lambda_O^{3N}\lambda_H^{6N}} \int d\mathbf{r}_1 \cdots \int d\mathbf{r}_{3N} \left\{ \exp\left[-\beta \sum_{i<j=1}^{N} V_{OO}(r_{ij}) + \sum_{i=1}^{N} \sum_{j=N+1}^{3N} V_{OH}(r_{ij}) + \sum_{i<j=N+1}^{3N} V_{HH}(r_{ij}) \right] \right\} \tag{9.9}$$

where $\mathbf{r}_1, \ldots, \mathbf{r}_N$ locate oxygens, and $\mathbf{r}_{N+1}, \ldots, \mathbf{r}_{3N}$ locate hydrogens. The integrations span the allowed volume $\mathscr{V}$, and

$$\lambda_\alpha = h(2\pi m_\alpha k_B T)^{-1/2}, \qquad \alpha = O, H \tag{9.10}$$

are the mean thermal de Broglie wavelengths. Denoting the potential energy in (9.9) by $V_{N,2N}$ for compactness, the correlation functions in this classical limit may next be introduced:

$$g_{OO}(r_{12}) = \frac{\mathscr{V}^2 \int d\mathbf{r}_3 \cdots \int d\mathbf{r}_{3N} \exp\left[-\beta V_{N,2N}(\mathbf{r}_1 \cdots \mathbf{r}_{3N})\right]}{\int d\mathbf{r}_1 \cdots \int d\mathbf{r}_{3N} \exp\left[-\beta V_{N,2N}(\mathbf{r}_1 \cdots \mathbf{r}_{3N})\right]}$$

$$g_{OH}(r_{1,N+1}) = \frac{\mathscr{V}^2 \int d\mathbf{r}_2 \cdots \int d\mathbf{r}_N \int d\mathbf{r}_{N+2} \cdots \int d\mathbf{r}_{3N} \exp\left[-\beta V_{N,2N}(\mathbf{r}_1 \cdots \mathbf{r}_{3N})\right]}{\int d\mathbf{r}_1 \cdots \int d\mathbf{r}_{3N} \exp\left[-\beta V_{N,2N}(\mathbf{r}_1 \cdots \mathbf{r}_{3N})\right]}$$

$$g_{HH}(r_{N+1,N+2}) = \frac{\mathscr{V}^2 \int d\mathbf{r}_1 \cdots \int d\mathbf{r}_N \int d\mathbf{r}_{N+3} \cdots \int d\mathbf{r}_{3N} \exp\left[-\beta V_{N,2N}(\mathbf{r}_1 \cdots \mathbf{r}_{3N})\right]}{\int d\mathbf{r}_1 \cdots \int d\mathbf{r}_{3N} \exp\left[-\beta V_{N,2N}(\mathbf{r}_1 \cdots \mathbf{r}_{3N})\right]} \tag{9.11}$$

In the infinite system limit, with fixed ionic densities, these correlation functions each approach unity at a large separation. g_{OH} and g_{HH} have sharp peaks at r_e and r_p, respectively, corresponding to the intramolecular pairs.

Setting $\rho = N/\mathcal{V}$, the local electroneutrality conditions on the infinite system limit correlation functions may be written

$$\rho \int [g_{OH}(r) - g_{OO}(r)]\, d\mathbf{r} = 1 \tag{9.12}$$

and

$$2\rho \int [g_{OH}(r) - g_{HH}(r)]\, d\mathbf{r} = 1 \tag{9.13}$$

These can be supplemented by a "second moment condition" which must always exist for an ionic fluid:[103]

$$\int [2g_{OH}(r) - g_{OO}(r) - g_{HH}(r)]r^2\, d\mathbf{r} = \frac{3k_B T}{8\pi\rho^2(Q^*)^2} \tag{9.14}$$

The fact that interactions in the weak-electrolyte model are central and additive allows the thermodynamic energy E to have an especially simple form:

$$\frac{E}{N} = \frac{9k_B T}{2} + \rho \int d\mathbf{r}\, [\tfrac{1}{2}V_{OO}(r)g_{OO}(r) + 2V_{OH}(r)g_{OH}(r) + 2V_{HH}(r)g_{HH}(r)] \tag{9.15}$$

The virial equation of state undergoes analogous simplifications:

$$\beta p = 3\rho - \frac{\beta\rho^2}{6} \int d\mathbf{r}\, \mathbf{r} \cdot [g_{OO}(r)\nabla V_{OO}(r) + 4g_{OH}(r)\nabla V_{OH}(r) + 4g_{HH}(r)\nabla V_{HH}(r)] \tag{9.16}$$

Although the ideal gas term 3ρ corresponds to $3N$ independent particles, one can show for the dilute vapor of undissociated molecules that the integral term equals -2ρ, leaving

$$\beta p = \rho \tag{9.17}$$

the appropriate ideal gas form for N independent (but composite) particles.

The isothermal compressibility κ_T may be expressed in terms of the oxygen–oxygen pair correlation function:

$$\rho k_B T \kappa_T = 1 + \rho \int d\mathbf{r}\, [g_{OO}(r) - 1] \tag{9.18}$$

The local electroneutrality conditions (9.12) and (9.13) allow this to be converted to the alternate forms

$$2\rho k_B T \kappa_T = 1 + 2\rho \int d\mathbf{r}\, [g_{HH}(r) - 1] \tag{9.19}$$

and

$$k_B T \kappa_T = \int d\mathbf{r}\, [g_{OH}(r) - 1] \tag{9.20}$$

Since large-scale charge separation is not possible in the collection of O and H ions forming the weak-electrolyte model, these two species are forced to execute density fluctuations of long wavelength together, thus producing the variety (9.18) to (9.20) of fluctuation-compressibility theorems. It should be stressed that their validity depends in no way on the extent of water molecule dissociation being small.

By using standard methods of statistical mechanics, one can easily express the static linear response of the ionic fluid to application of an external electrostatic potential in terms of g_{OO}, g_{OH}, and g_{HH}. We consider just a single Fourier component, for which the applied potential is

$$\Psi_{ap}(\mathbf{r}) = \Psi_0 \sin(\mathbf{k} \cdot \mathbf{r}) \tag{9.21}$$

with Ψ_0 small. The H and O ions will rearrange under the influence of Ψ_{ap} so as partially to shield it. The average potential $\overline{\Psi}$ will also be spatially sinusoidal, and we write it:

$$\overline{\Psi}(\mathbf{r}) = \frac{\Psi_0}{\varepsilon(k)} \sin(\mathbf{k} \cdot \mathbf{r}) \tag{9.22}$$

thereby defining the wavelength-dependent dielectric constant $\varepsilon(k)$.[22] The requisite calculation yields the formula

$$\frac{1}{\varepsilon(k)} = 1 - \frac{16\pi\beta\rho(Q^*)^2}{k^2}\left\{\frac{3}{2} + \rho \int d\mathbf{r} \left[\frac{\sin(kr)}{kr}\right][g_{OO}(r) - 2g_{OH}(r) + g_{HH}(r)]\right\} \tag{9.23}$$

At any finite temperature some of the water molecules will have dissociated, rendering the pure liquid slightly conducting. Because it is a conductor, the water will be able to shield very long-wavelength external fields completely:

$$\lim_{k \to 0} \frac{1}{\varepsilon(k)} = 0 \tag{9.24}$$

The electroneutrality and second moment conditions (9.12) to (9.14), when applied to (9.23), assure that this limit is obeyed. However, with a very small

degree of dissociation, it is only for very small k (comparable to, or less than, Debye's κ for the dilute ionic solution) that $\varepsilon(k)$ begins to rise to infinity. For k larger than these tiny values, but still reasonably small, $\varepsilon(k)$ should equal the static dielectric constant (≈ 80 at room temperature) normally quoted for water. At very large k, one sees from (9.23) that $\varepsilon(k)$ approaches unity. Figure 24 schematically illustrates the expected behavior.

Amplitudes $\sigma(\mathbf{k})$ for fluctuating charge density waves may be introduced by the definition

$$\sigma(\mathbf{k}) = \frac{Q^*}{\sqrt{N}} \left\{ -2 \sum_{j=1}^{N} \exp(i\mathbf{k} \cdot \mathbf{r}_j) + \sum_{j=N+1}^{3N} \exp(i\mathbf{k} \cdot \mathbf{r}_j) \right\} \tag{9.25}$$

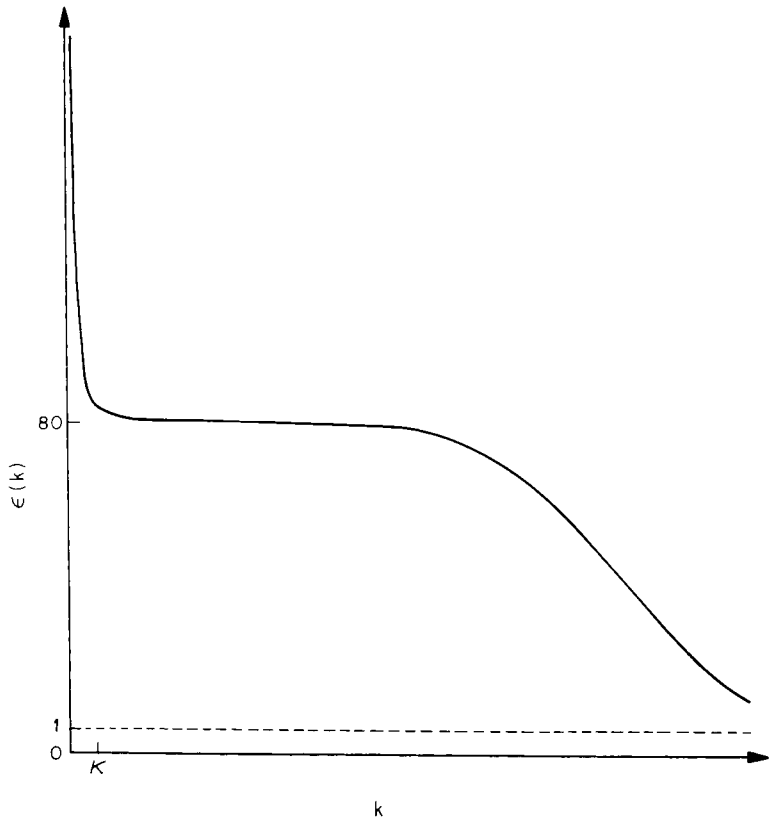

Fig. 24 Schematic graph for $\varepsilon(k)$ in liquid water at room temperature. The Debye κ refers to the very dilute solution of ions formed by molecule dissociation.

It is straightforward to compute the equal-time quadratic fluctuation average for the σs, with the result

$$\langle \sigma^*(\mathbf{k})\sigma(\mathbf{k})\rangle = 4(Q^*)^2\left\{\frac{3}{2} + \rho \int d\mathbf{r}\left[\frac{\sin(kr)}{kr}\right][g_{OO}(r) - 2g_{OH}(r) + g_{HH}(r)]\right\} \tag{9.26}$$

By comparing this expression (9.23), one obtains an alternate $\varepsilon(k)$ formula:

$$\frac{1}{\varepsilon(k)} = 1 - \frac{4\pi\beta\rho}{k^2}\langle \sigma^*(\mathbf{k})\sigma(\mathbf{k})\rangle \tag{9.27}$$

The quadratic fluctuation is always positive for finite k, so $\varepsilon(k)$ cannot be unity or less, thus

$$-\frac{3}{2\rho} < \int d\mathbf{r}\left[\frac{\sin(kr)}{kr}\right][g_{OO}(r) - 2g_{OH}(r) + g_{HH}(r)] \tag{9.28}$$

for all k, irrespective of temperature and density.

Whereas equal-time fluctuations in σs suffice to give static dielectric response, unequal-time correlation functions are related to dielectric response at a finite frequency ω. Yet another advantage of the weak-electrolyte model for water therefore resides in its capacity to describe dielectric relaxation and conduction by providing a means to evaluate real and imaginary parts of $\varepsilon(k, \omega)$.

C. Quantum Corrections

In applying the weak-electrolyte model to water at about room temperature, quantum corrections to the classical statistical mechanics just outlined are unavoidable. Fortunately, there is a simple prescription for generating leading quantum corrections to

$$\rho^{(3N)}(\mathbf{r}_1 \cdots \mathbf{r}_{3N}|\mathbf{r}_1 \cdots \mathbf{r}_{3N}) = \langle \mathbf{r}_1 \cdots \mathbf{r}_{3N}|\exp(-\beta\mathscr{H})|\mathbf{r}_1 \cdots \mathbf{r}_{3N}\rangle \tag{9.29}$$

the diagonal elements of the density matrix for the $3N$ ionic particles. This permits one in principle to calculate corrected averages for operators involving position only, specific examples being the correlation functions g_{OO}, g_{OH}, and g_{HH}.

This simple prescription disregards spin and statistics, which should be valid for condensed phases. It states that the classical format applies, provided

that the potential is replaced by a temperature-dependent apparent potential.[104] For the weak-electrolyte model, $V_{N,2N}$ is replaced by

$$W_{N,2N}(\mathbf{r}_1 \cdots \mathbf{r}_{3N}) = \sum_{i<j=1}^{N} W_{OO}(r_{ij}, \beta) + \sum_{i=1}^{N} \sum_{j=N+1}^{3N} W_{OH}(r_{ij}, \beta) + \sum_{i<j=N+1}^{3N} W_{HH}(r_{ij}, \beta) \tag{9.30}$$

where (γ, δ = O, H).

$$W_{\gamma\delta}(r) = V_{\gamma\delta}(r) + \frac{\hbar^2}{m_{\gamma\delta}} \left\{ \frac{1}{12} \nabla^2 \beta V_{\gamma\delta}(r) - \frac{1}{24} [\nabla \beta V_{\gamma\delta}(r)]^2 \right\} + O(\hbar^4) \tag{9.31}$$

$m_{\gamma\delta}$ is the reduced mass:

$$\frac{1}{m_{\gamma\delta}} = \frac{1}{m_\gamma} + \frac{1}{m_\delta} \tag{9.32}$$

In particular this result assures that computer simulations (Monte Carlo or molecular dynamics) can be carried out as usual, using $W_{N,2N}$ in place of $V_{N,2N}$, to produce corrected static correlation functions.

It is easy to see from (9.31) that the leading quantum corrections (order $\hbar^2$ terms) have the following shape-changing effects on $V_{\gamma\delta}(r)$.

1. Regions of positive curvature (as in the vicinity of minima) are raised, while regions of negative curvature (such as maxima) are lowered, to produce diminished variation.
2. Minima are broadened; maxima are narrowed.

The net effect of these modifications at a given temperature is that the potential energy is less effective in localizing particles relative to one another. Consequently, the correlation function peaks should be somewhat broader and less distinct than if $V_{N,2N}$ alone were used.

Off-diagonal elements of the density matrix can also be displayed in a systematic expansion about the classical limit.[101] However, the results are more elaborate in appearance and interpretation. They are nevertheless required to calculate a wide variety of interesting equilibrium properties, such as the momentum distributions for the two types of atoms present.

Although a molecular dynamics simulation formally carried out with $W_{N,2N}$ in place of the interaction $V_{N,2N}$ is a valid procedure for generating equilibrium structural properties through order $\hbar^2$, one must be careful

not to overinterpret the apparent transport properties emanating from such a simulation. As an example, the quantity

$$\tfrac{1}{3}\int_0^\infty \langle \mathbf{v}_j(0)\cdot\mathbf{v}_j(t)\rangle_W\, dt \tag{9.33}$$

involving the classical velocity autocorrelation function for molecule j in the presence of potential W is not necessarily the correct expression for the self-diffusion constant D through order $\hbar^2$. Instead, one would generally expect additional quantum corrections as well. The development of such quantum corrections for each of the transport coefficients (self-diffusion constant, shear and bulk viscosities, thermal conductivity, complex dielectric constant at arbitrary frequency) to be appended to the classical W-dynamics expression is an important problem whose solution would dramatically extend the power of the molecular dynamics technique.

X. CONCLUSION

The major topics covered in this article show that the theory of water now has a well-established rational basis. Yet it is clear that considerable work remains to be done both on the quantum theory of water molecule interactions and on statistical mechanical techniques for utilizing these interactions in many-body calculations. Presuming that the present high level of interest in the subject persists, the prognosis nevertheless is good for rapid maturing of the field. Furthermore, the special techniques and insights developed for water should encourage similar activity for other polyatomic liquids.

Aqueous solutions have purposely been excluded from this article. However, each of the four statistical mechanical approaches discussed (lattice and cell theories, computer simulation, weak-electrolyte model) has obvious application to solutions. Quantum mechanical studies of solute–water and solute–solute potential energy functions are necessary prerequisites to quantitative statistical theory, and fortunately these calculations have been initiated for noble gases,[105,106] monatomic ions,[107,108] and small organic molecules.[109,110] Certainly, far more needs to be done, especially in examining characteristic functional groups which are included in large molecules of biological interest. A systematic study of the interactions between water molecules and hydrocarbons needs to be carried out, so that realistic models for hydrophobic bonding[93] can be constructed and investigated by the available statistical methods. With aggressive effort along these lines, it is possible within the foreseeable future that conformational kinetics of biopolymers will be simulated via computer, with full accounting of biopolymer

intramolecular degrees of freedom, of ambient water molecule motions, and of interactions between them.

The theoretical study of chemical reactions in aqueous solution is another extremely important subject to which research attention needs to be directed. Fast reactions involving hydrogen ions[111] could probably be simulated by an extension of the weak-electrolyte model described in Section IX, since it already incorporates dissociation and proton transfer. In any case suitable energy surfaces would have to be constructed to describe the interaction of reactants. Furthermore, the precise distinction between reactants and products in terms of separate regions of configuration space leads to the same situation encountered above in defining hydrogen bonds. An element of arbitrariness intrudes, but prediction of measurable properties for the chemically reacting solution must be demonstrably independent of the criterion used to define reactants and products.

The importance of these extensions for a deeper understanding of chemistry cannot be ignored.

References

1. G. Wald, *Proc. Natl. Acad. Sci. U.S.*, **52**, 595 (1964).
2. R. J. Curran, B. J. Conrath, R. A. Hanel, V. G. Kunde, and J. C. Pearl, *Science*, **182**, 381 (1973).
3. A. C. Cheung, D. M. Rank, C. H. Townes, D. D. Thornton, and W. J. Welch, *Nature*, **221**, 626 (1969).
4. I. S. Shklovskii and C. Sagan, *Intelligent Life in the Universe*, Holden–Day, San Francisco, 1966.
5. J. L. Kavenau, *Water and Solute-Water Interactions*, Holden–Day, San Francisco, 1964.
6. R. Brückner, *J. Non-Cryst. Solids*, **5**, 123 (1970).
7. D. Eisenberg and W, Kauzmann, *The Structure and Properties of Water*, Oxford University Press, New York, 1969, Chap. 3.
8. J. Padova, in R. A. Horne, Ed., *Water and Aqueous Solutions*, Wiley-Interscience, New York, 1972, Chap. 4.
9. S. B. Brummer and A. B. Gancy, Ref. 8, Chap. 19.
10. W. Kauzmann, *Advan. Protein Chem.*, **14**, 1 (Table III) (1959).
11. W. S. Benedict, N. Gailar, and E. K. Plyler, *J. Chem. Phys.*, **24**, 1139 (1956).
12. C. A. Coulson, *Valence*, 2nd ed., Oxford University Press, New York, 1961, Chap. VIII.
13. R. P. Feynman, *Phys. Rev.*, **56**, 340 (1939).
14. R. F. W. Bader, *J. Am. Chem. Soc.*, **86**, 5070 (1964).
15. T. R. Dyke and J. S. Muenter, *J. Chem. Phys.*, **59**, 3125 (1973).
16. J. Verhoeven and A. Dymanus, *J. Chem. Phys.*, **52**, 3222 (1970).
17. E. A. Moelwyn-Hughes, *Physical Chemistry*, 2nd ed. Pergamon, New York, 1961, p. 383.
18. S. P. Liebmann and J. W. Moskowitz, *J. Chem. Phys.*, **54**, 3622 (1971).
19. O. Crawford and A. Dalgarno, *Chem. Phys. Lett.*, **1**, 23 (1967).
20. K. Kuchitsu and Y. Morino, *Bull. Chem. Soc. Jap.*, **38**, 814 (1965).
21. C. W. Kern and M. Karplus, in F. Franks, Ed., *Water, A Comprehensive Treatise*, Vol. 1, Plenum, New York, 1972, p. 67.
22. F. H. Stillinger and R. Lovett, *J. Chem. Phys.*, **48**, 3858 (1968).

23. K. Morokuma and L. Pedersen, *J. Chem. Phys.*, **48**, 3275 (1968).
24. J. Del Bene and J. A. Pople, *J. Chem. Phys.*, **52**, 4858 (1970).
25. K. Morokuma and J. R. Winick, *J. Chem. Phys.*, **52**, 1301 (1970).
26. P. A. Kollman and L. C. Allen, *J. Chem. Phys.*, **51**, 3286 (1969).
27. D. Hankins, J. W. Moskowitz, and F. H. Stillinger, *J. Chem. Phys.*, **53**, 4544 (1970); Erratum, **59**, 995 (1973).
28. G. H. F. Diercksen, *Theor. Chim. Acta*, **21**, 335 (1971).
29. H. Popkie, H. Kistenmacher, and E. Clementi, *J. Chem. Phys.*, **59**, 1325 (1973).
30. J. C. Slater and J. G. Kirkwood, *Phys. Rev.*, **37**, 682 (1931).
31. J. G. Kirkwood, *Phys. Z.* **33**, 57 (1932).
32. E. U. Condon and H. Odishaw, Eds., *Handbook of Physics*, McGraw-Hill, New York, York, 1967, p. 7–40.
33. A. Dalgarno, *Advan. Chem. Phys.* **12**, 164 (1967).
34. J. Corner, *Trans. Faraday Soc.*, **44**, 914 (1948).
35. S. W. Peterson and H. A. Levy, *Acta Crystallogr.*, **10**, 70 (1957).
36. L. Pauling, *The Nature of the Chemical Bond* 3rd ed., Cornell University Press, Ithaca, 1960, p. 469.
37. B. R. Lentz and H. A. Scheraga, *J. Chem. Phys.*, **58**, 5296 (1973).
38. H. S. Frank and W. Y. Wen, *Discuss. Faraday Soc.*, **24**, 133 (1957).
39. H. S. Frank, *Proc. Roy. Soc.*, **A247**, 481 (1958).
40. A. Ben-Naim and F. H. Stillinger, in R. A. Horne, Ed., *Water and Aqueous* Solutions, Wiley-Interscience, New York, 1972, Chap. 8.
41. M. E. Fisher, *Rep. Prog. Phys.*, **XXX (II)**, 615 (1967).
42. S. A. Rice and P. Gray, *The Statistical Mechanics of Simple Liquids*, Wiley-Interscience, New York, 1965, Sect. 2.6.
43. H. S. Green, *Proc. Roy. Soc.*, **A189**, 103 (1947).
44. T. L. Hill, *Statistical Mechanics*, McGraw-Hill, New York, 1956, p. 105.
45. W. G. McMillan, Jr., and J. E. Mayer, *J. Chem. Phys.*, **13**, 276 (1945).
46. F. H. Stillinger, *J. Phys. Chem.*, **74**, 3677 (1970).
47. F. H. Stillinger, *J. Chem. Phys.*, **57**, 1780 (1972).
48. F. Riesz and B. Sz.-Nagy, *Functional Analysis*, Frederick Ungar, New York, 1955, p. 40.
49. T. Halcioğlu and O. Sinanoğlu, *J. Chem. Phys.*, **49**, 996 (1968).
50. G. S. Rushbrooke and M. Silbert, *Mol. Phys.*, **12**, 505 (1967).
51. J. M. Levelt Sengers and S. C. Greer, *Int. J. Heat Mass Transfer*, **15**, 1865 (1972).
52. C. A. Rogers, *Packing and Covering*, Cambridge University Press, Cambridge, 1964, p. 74.
53. T. D. Lee and C. N. Yang, *Phys. Rev.*, **87**, 410 (1952).
54. B. Widom and F. H. Stillinger, *J. Chem. Phys.*, **58**, 616 (1973).
55. P. D. Fleming, III, and J. H. Gibbs, *J. Stat. Phys.*, **10**, 157 (1974).
56. P. D. Fleming, III, and J. H. Gibbs, *J. Stat. Phys.*, **10**, 351 (1974).
57. B. Kamb, *J. Chem. Phys.*, **43**, 3917 (1965).
58. A. H. Narten, M. D. Danford, and H. A. Levy, *Discuss. Faraday Soc.*, **43**, 97 (1967).
59. G. M. Bell, *J. Phys. C: Solid State Phys.*, **5**, 889 (1972).
60. E. A. Guggenheim and M. C. McGlashan, *Proc. Roy. Soc.*, **A206**, 335 (1951).
61. R. T. Whitlock and P. R. Zilsel, *Phys. Rev.*, **131**, 2409 (1963).
62. I. Prigogine, *The Molecular Theory of Solutions*, North-Holland, Amsterdam, 1957, Chaps. VII–X.
63. M. Weissmann and L. Blum, *Trans. Faraday Soc.*, **64**, 2605 (1968).
64. O. Weres and S. A. Rice, *J. Am. Chem. Soc.*, **94**, 8984 (1972).
65. N. Bjerrum, *Science*, **115**, 385 (1952).
66. A. Rahman and F. H. Stillinger, *J. Chem. Phys.*, **55**, 3336 (1971).

67. F. H. Stillinger and A. Rahman, *J. Chem. Phys.*, **57**, 1281 (1972).
68. D. P. Stevenson, *J. Phys. Chem.*, **69**, 2145 (1965).
69. L. Pauling, *J. Am. Chem. Soc.*, **57**, 2680 (1935).
70. H. M. J. Smith, *Phil. Trans. Roy. Soc.*, **241**, 105 (1948).
71. O. Weres, *Chem. Phys. Lett.*, **14**, 155 (1972).
72. G. E. Walrafen, in F. Franks, Ed., *Water, A Comprehensive Treatise*, Vol. 1, Plenum, New York, 1972, p. 170.
73. J. M. Hammersley and D. C. Handscomb, *Monte Carlo Methods*, Methuen-Wiley, New York, 1964.
74. D. Denley and S. A. Rice, *J. Am. Chem. Soc.*, **96**, 4369 (1974).
75. A. Ben-Naim, *J. Chem. Phys.*, **52**, 5531 (1970).
76. N. Metropolis, A. W. Rosenbluth, M. N. Rosenbluth, A. H. Teller, and E. Teller, *J. Chem. Phys.*, **21**, 1087 (1953).
77. J. A. Barker and R. O. Watts, *Chem. Phys. Lett.*, **3**, 144 (1969).
78. J. A. Barker and R. O. Watts, *Mol. Phys.*, **26**, 789 (1973).
79. B. J. Alder and T. Wainwright in I. Prigogine, Ed., *Transport Processes in Statistical Mechanics*, Interscience, New York, 1958, p. 97.
80. H. Goldstein, *Classical Mechanics*, Addison-Wesley, Reading, Mass., 1953, p. 158.
81. A. Rahman, *Phys. Rev.*, **136**, A405 (1964).
82. F. H. Stillinger and A. Rahman, *J. Chem. Phys.*, **60**, 1545 (1974).
83. A. H. Narten, *X-ray Diffraction Data on Liquid Water in the Temperature Range 4°C–200°C*, Oak Ridge National Laboratory Technical Report ONRL-4578, July 1970.
84. A. H. Narten, *J. Chem. Phys.*, **56**, 5681 (1972).
85. S. N. Vinogradov and R. H. Linnell, *Hydrogen Bonding*, Van Nostrand Reinhold, New York, 1971.
86. A. Rahman and F. H. Stillinger, *J. Am. Chem. Soc.*, **95**, 7943 (1973).
87. F. H. Stillinger and A. Rahman, *J. Chem. Phys.*, **61**, 4973 (1974).
88. L. Pauling, in D. Hadzi and H. W. Thompson, Eds., *Hydrogen Bonding*, Pergamon, New York, 1959, pp. 1–5.
89. M. D. Danford and H. A. Levy, *J. Am. Chem. Soc.*, **84**, 3965 (1962).
90. O. Ya. Samoilov, *Structure of Aqueous Electrolyte Solutions and the Hydration of Ions*, Consultants Bureau, New York, 1965.
91. J. W. Perram, *Mol. Phys.*, **20**, 1077 (1971).
92. G. Némethy and H. A. Scheraga, *J. Chem. Phys.*, **36**, 3382 (1962).
93. W. Kauzmann, *Advan. Protein Chem.*, **14**, 1 (1959).
94. Ref. 7, Table 4.10.
95. B. J. Alder and T. E. Wainwright, *Phys. Rev.*, **A1**, 18 (1970).
96. M. H. Ernst, E. H. Hauge, and J. M. J. van Leeuwen, *Phys. Rev. Lett.*, **25**, 1254 (1970).
97. N. K. Ailawadi and B. J. Berne, *J. Chem. Phys.*, **54**, 3569 (1971).
98. J. M. Deutch, *Ann. Rev. Phys. Chem.* **24**, 319–22 (1973).
99. F. H. Stillinger and A. Rahman, in *Molecular Motion in Liquids, Proceedings of the 24th Annual Meeting*, Paris, July 3–6, 1973, Société de Chimie Physique, 1974, pp. 479–492.
100. K. S. Singwi and A. Sjölander, *Phys. Rev.*, **119**, 863 (1960).
101. H. L. Lemberg and F. H. Stillinger, *J. Chem. Phys.*, **62**, 1677 (1975).
102. P. A. Kollman and C. F. Bender, *Chem. Phys. Lett.*, **21**, 271 (1973).
103. F. H. Stillinger and R. Lovett, *J. Chem. Phys.*, **49**, 1991 (1968).
104. L. D. Landau and E. M. Lifshitz, *Statistical Physics*, Addison-Wesley, Reading, Mass., 1958, p. 103.
105. M. Losonczy, J. W. Moskowitz, and F. H. Stillinger, *J. Chem. Phys.*, **59**, 3264 (1973).
106. H. Lischka, *Chem. Phys. Lett.*, **20**, 448 (1973).

107. G. H. F. Diercksen and W. P. Kraemer, *Theor. Chim. Acta*, **23**, 387 (1972).
108. W. P. Kraemer and G. H. F. Diercksen, *Theor. Chim. Acta*, **27**, 265 (1972).
109. J. E. Del Bene, *J. Chem. Phys.*, **55**, 4633 (1971).
110. K. Morokuma, *J. Chem. Phys.*, **55**, 1236 (1971).
111. M. Eigen, in S. Claesson, Ed., *Fast Reactions and Primary Processes in Chemical Kinetics, Proceedings of the 5th Nobel Symposium*, Interscience-Wiley, New York, 1967, p. 245.